AD-A078 607 INTERMETRICS INC CAMBRIDGE MASS F/G 17/7
GPS AND EAR/GEANS SOFTWARE SUPPORT.(U)
AUG 79 N A CARLSON , W S WIDNALL , P K SINHA F33615-77-C-1044
UNCLASSIFIED IR-397 AFAL-TR-79-1127 NL

1 OF 2
AD A078607

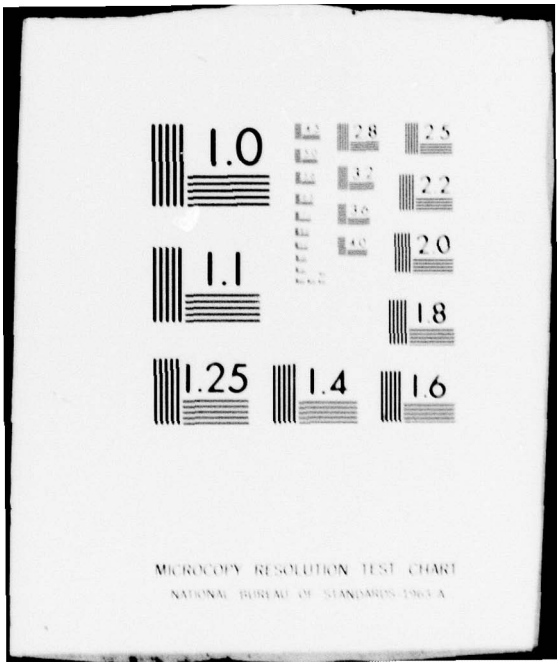
1.0
1.1
1.25
1.4
1.6
2.8
3.2
3.6
4.0
2.5
2.2
2.0
1.8
MICROCOPY RESOLUTION TEST CHART
NATIONAL BUREAU OF STANDARDS-1963-A

AD A078607

LEVEL II

AFAL-TR-79-1127

GPS AND EAR/GEANS SOFTWARE SUPPORT

Intermetrics, Incorporated
701 Concord Avenue
Cambridge, MA 02138

August 1979

TECHNICAL REPORT AFAL-TR-79-1127

Final Report for Period December 1976 - June 1979

DDC FILE COPY

Approved for public release; distribution unlimited

DDC
RECEIVED
DEC 18 1979
A

AIR FORCE AVIONICS LABORATORY
AIR FORCE WRIGHT AERONAUTICAL LABORATORIES
AIR FORCE SYSTEMS COMMAND
WRIGHT-PATTERSON AIR FORCE BASE, OHIO 45433

79 12 18 100

NOTICE

When Government drawings, specifications, or other data are used for any purpose other than in connection with a definitely related Government procurement operation, the United States Government thereby incurs no responsibility nor any obligation whatsoever; and the fact that the government may have formulated, furnished, or in any way supplied the said drawings, specifications, or other data, is not to be regarded by implication or otherwise as in any manner licensing the holder or any other person or corporation, or conveying any rights or permission to manufacture, use, or sell any patented invention that may in any way be related thereto.

This report has been reviewed by the Information Office (OI) and is releasable to the National Technical Information Service (NTIS). At NTIS, it will be available to the general public, including foreign nations.

This technical report has been reviewed and is approved for publication.

Stanton H. Musick

PROJECT ENGINEER

Ronald L. Ringo

RONALD L. RINGO, Chief
Reference Systems Branch
Reconn & Weapon Delivery Division

FOR THE COMMANDER

Richard M. Roberds

RICHARD M. ROBERDS, Colonel, USAF
Chief, Reconnaissance and Weapon
Delivery Division

"If your address has changed, if you wish to be removed from our mailing list, or if the addressee is no longer employed by your organization please notify AFAL/RWA, W-PAFB, OH 45433 to help us maintain a current mailing list".

Copies of this report should not be returned unless return is required by security considerations, contractual obligations, or notice on a specific document.

AIR FORCE/86780/6 December 1979 — 100

UNCLASSIFIED

SECURITY CLASSIFICATION OF THIS PAGE (When Data Entered)

REPORT DOCUMENTATION PAGE

READ INSTRUCTIONS BEFORE COMPLETING FORM

1. REPORT NUMBER: AFAL-TR-79-1127	2. GOVT ACCESSION NO.
3. RECIPIENT'S CATALOG NUMBER	
4. TITLE (and Subtitle): GPS AND EAR/GEANS SOFTWARE SUPPORT	5. TYPE OF REPORT & PERIOD COVERED: Final Report. December 76 — June 79
6. PERFORMING ORG. REPORT NUMBER: IR-397	
7. AUTHOR(s): N.A. Carlson, W.S. Widnall, P.K. Sinha, P.A. Grundy, L.F. Wiederholt, G.J. Geier	8. CONTRACT OR GRANT NUMBER(s): F33615-77-C-1044
9. PERFORMING ORGANIZATION NAME AND ADDRESS: Intermetrics, Inc. 701 Concord Avenue Cambridge, MA 02138	10. PROGRAM ELEMENT, PROJECT, TASK AREA & WORK UNIT NUMBERS: 666A-06-09 / 06
11. CONTROLLING OFFICE NAME AND ADDRESS: Air Force Avionics Laboratory Air Force Wright Aeronautical Laboratories Air Force Systems Command, WPAFB, Ohio 45433	12. REPORT DATE: August 1979
	13. NUMBER OF PAGES: 157 / 166
14. MONITORING AGENCY NAME & ADDRESS (if different from Controlling Office) 63203F	15. SECURITY CLASS. (of this report): Unclassified
	15a. DECLASSIFICATION DOWNGRADING SCHEDULE

16. DISTRIBUTION STATEMENT (of this Report)

Approved for public release, distribution unlimited.

17. DISTRIBUTION STATEMENT (of the abstract entered in Block 20, if different from Report)

18. SUPPLEMENTARY NOTES

19. KEY WORDS (Continue on reverse side if necessary and identify by block number)

Global Positioning System (GPS)	Receiver Aiding
EAR/GEANS Navigator	Vertical channel
Inertial Navigation	Kalman filter/smoother
Radar navigation	Error modeling

20. ABSTRACT (Continue on reverse side if necessary and identify by block number)

The Air Force Avionics Laboratory is sponsoring development of both the Generalized Development Model (GDM) of GPS User equipment, and the EAR/GEANS radar/inertial navigator. This report documents results of analysis and software support for both of these programs. GPS-related analysis has been performed in the area of GDM software support, particularly, stability analysis of alternate designs for rate-aiding of non-coherent mode of GPS receiver; vertical channel analysis and simulation; improved GPS/Inertial

DD FORM 1 JAN 73 1473 EDITION OF 1 NOV 65 IS OBSOLETE

UNCLASSIFIED

SECURITY CLASSIFICATION OF THIS PAGE (When Data Entered)

388 863

JOB

Block 20 (Contd.)

Simulator model implementation; and integrated GPS/strapdown performance studies. EAR/GEANS-related analysis has been performed in the areas of Error Isolation Filter (EIF) development planning; vertical channel error modeling; error modeling for GEANS space-stable baro-inertial navigator; EAR radar measurement modeling; EAR/GEANS flight test data recording; gravity perturbation modeling; EAR/GEANS Error Isolation Filter synthesis; onboard feedback correction compensation in the EIF; and EIF optimal filter/smoother mechanization equations selection.

PREFACE

This work has been sponsored by the Air Force Avionics Laboratory (AFAL) of the Air Force Systems Command, wrignt Patterson Air Force Base, Ohio, under contract F33615-77-C-1044.

The principal technical contributors to this effort for Intermetrics, Inc., have been Dr. William S. Widnall, Dr. Prasun K. Sinha, Mr. Peter A. Grundy, Dr. Lawrence F. Wiederholt, Dr. Neal A. Carlson, and Mr. G. Jeffrey Geier. Dr. Widnall acted as program manager during the first half of the effort, as did Dr. Carlson during the second half. Dr. Carlson compiled and edited this final report.

The original contract technical monitor for AFAL was Major Kenneth A. Myers, followed by Captain David P. Payne, Captain Ronald R. Butler, and finally Mr. Stanton H. Musick.

Accession For
NTIS GRA&I
DDC TAB
Unannounced
Justification
By
Distribution/
Availability Codes
Dist. | Avail and/or special
A

TABLE OF CONTENTS

SECTION		PAGE
I.	INTRODUCTION AND SUMMARY	1-1
	1.1 Background	1-1
	1.2 Objectives	1-1
	1.3 Scope of Effort	1-2
	1.4 Overview of Report	1-3
	1.5 Summary of Results	1-3
II.	GDM SOFTWARE SUPPORT	2-1
	2.1 Chapter Summary	2-1
	2.2 Clock Frequency	2-2
	2.3 Azimuth Gyro G-Sensitivity Calibration and Compensation	2-4
	2.4 Continuity of Kalman Filter Feedback to Receiver Aiding	2-6
	2.5 Stability of Receiver Aiding in Non-Coherent Mode	2-11
	2.6 Stability of Alternate Designs for Rate-Aiding of Non-Coherent Mode of GPS Receiver	2-20
III.	VERTICAL CHANNEL ANALYSIS AND SIMULATION	3-1
	3.1 Chapter Summary	3-1
	3.2 C5A GPS/Inertial Simulation Results	3-1
	3.3 Comparison of Three Vertical Channel Filter Designs	3-11
IV.	IMPROVED IGI SIMULATION MODELS	4-1
	4.1 Chapter Summary	4-1
	4.2 Revised IGI Simulator Computer Program	4-1
V.	INTEGRATED GPS/STRAPDOWN PERFORMANCE	5-1
	5.1 Chapter Summary	5-1
	5.2 Strapdown Inertial Navigation Systems	5-1
	5.3 Integrated GPS/Strapdown Inertial Simulator	5-2
	5.4 Strapdown Inertial Navigation System Performance	5-3

PRECEDING PAGE BLANK

TABLE OF CONTENTS (CONTD.)

SECTION		PAGE
VI.	EAR/GEANS ERROR ISOLATION FILTER SUPPORT	6-1
6.1	Chapter Summary	6-1
6.2	EAR/GEANS EIF Development Plan	6-1
6.3	Vertical Channel Error Model for EAR/GEANS	6-3
6.4	Fundamental Error Dynamics for a Space-Stable Navigator	6-8
6.5	Error Model for the Baro-Damped GEANS Inertial Navigator	6-9
6.6	Radar Measurements and Measurement Matrices for EAR	6-15
6.7	EAR Flight Test Data Recording Requirements	6-16
6.8	Geodetic Error Models for Simulating and Estimating INS Error Behavior	6-17
6.9	Synthesis of EAR/GEANS Error Isolation Filter	6-40
6.10	Feedback Correction Equations for EAR/GEANS EIF	6-72
6.11	Filter/Smoother Mechanization Equations	6-85
APPENDICES:		
A:	Coordinate Rotation Matrices, Vectors, and Errors	A-1
B:	Householder Triangularization Procedure	B-1
REFERENCES		R-1

LIST OF ILLUSTRATIONS

FIGURE		PAGE
1	Rate-Aided Receiver Tracking Loops of the GDM	2-7
2	Generalized Information Flow Diagram	2-12
3	Possible Limit Cycle of Non-Coherent Mode with Feedback Limiter	2-14
4	Unaided INS Position Errors	3-4
5	Unaided INS Velocity Errors	3-5
6	Position Estimation Errors	3-6
7	Velocity Estimation Errors	3-7
8	Attitude Estimation Errors	3-8
9	Clock Phase & Frequency Estimation Errors	3-9
10	Altimeter Scale Factor Estimation Error	3-10
11	Basic Structure of IGI Simulator	4-3
12	Elliptical Cross-Section	6-12
13	Normalized Frequency ω_N	6-31
14	RMS Value of Deflection Process	6-35
15	RMS Value of Position Measurement Noise	6-35
16	True d_0	6-35
17	Fundamental Matrix for Second-Order Altitude-Aided Space Stable System Component Form	6-41

LIST OF TABLES

TABLE		PAGE
1	Vertical Deflection Space-Domain Correlation Functions	6-23
2	Time-Domain Correlation Functions for Random Heading Maneuvers	6-25
3	Time-Domain Correlation Functions for Constant Heading Maneuver	6-26
4	Suboptimal State Vector	6-60
5	Definition of EAR/GEANS Feedback Correction States	6-76
6	Definition of EAR/GEANS Error Isolation Filter States	6-77

SECTION I
INTRODUCTION AND SUMMARY

1.1 Background

The Air Force Avionics Laboratory (AFAL) is participating in the DoD Global Positioning System (GPS) program with the development of a Generalized Development Model (GDM) of GPS User Equipment under Contract No. F33615-75-C-1289 to Collins Radio Group of Rockwell International. The GDM is being developed to demonstrate the performance capability of GPS User Equipment in a hostile electromagnetic environment and to broaden the technology base for GPS User Equipment (UE). In support of this program, the AFAL has developed in-house a linear, direct simulation computer program for an integrated GPS/inertial aircraft navigation system. This program, known as the Integrated GPS/Inertial (IGI) Simulator, has been used in a variety of GPS UE design trade-off studies and mission analyses.

AFAL is also funding the Westinghouse Corporation to develop the Electronically Agile Radar (EAR). This radar is integrated with the GEANS inertial navigation system (INS) to form a complete radar/inertial navigation system known as EAR/GEANS. GEANS provides a continuous time history of position, velocity and attitude while EAR periodically measures position and velocity. The EAR measurements are blended with those of GEANS to provide improved in-flight estimates of all navigation quantities. The EAR/GEANS system is to begin flight tests in the Fall of 1978 in a B-52 test aircraft. A major technical issue in such tests is measuring how well the integrated system performed and then determining how each subsystem affected the measured performance.

In order to obtain an independent assessment of the navigation performance of the EAR/GEANS system, AFAL has established an in-house project to develop a computer program capable of post-processing in-flight recorded data. This program, known as an Error Isolation Filter (EIF), is a high-order Kalman filter/smoother designed to yield refined trajectory estimates and to detect off-nominal performance in various subsystems (radar, INS, baro-altimeter).

1.2 Objectives

For the GPS GDM system, the AFAL requires additional simulation and software support to properly address analysis problems in both the GDM system

and the IGI Simulation program. This additional support will reduce the technical, schedule, and cost risks associated with the GDM System and at the same time aid the AFAL in development of GPS technology in general.

For the EAR/GEANS system, the AFAL requires additional analysis and software support to develop appropriate error models and to code and test the EIF computer program.

The principal objective of the GPS-related effort has been to provide software and engineering services support for the Collins GDM program. That support has included adding capabilities to the AFAL IGI Simulation program and conducting analyses of GPS/inertial navigation system performance which pertain to the GDM. A secondary objective of the GPS-related effort has been to conduct simulation studies with the IGI program to benefit other present and future GPS navigation systems.

The principal objectives of the EAR/GEANS-related effort have been to provide analysis of AFAL-provided system error models, synthesis of the EIF state vector, and design, code, and preliminary test of the EIF software.

1.3 Scope of Effort

The objectives of this effort have been pursued under six defined tasks. These tasks are summarized in the following paragraphs.

The first task encompasses broad engineering support on the GDM software development throughout the period of performance on this contract. This task includes assisting AFAL in technical review of Collins software specifications, simulation test programs, and navigation processor support software, and providing an independent verification and assessment of software deliverables on the GDM. In addition, this task includes analysis of reduced INS control gains for GPS receiver aiding.

The second task is to develop an understanding of the AFAL IGI Simulation and conduct an altimeter modeling design study with that simulation. This effort involves a review of those difficulties, development of an alternate altimeter model, and demonstration of satisfactory GPS navigation system performance.

The third task is to implement in the IGI Simulation more detailed and realistic receiver error models for the GPS range and delta-range measurements. These models will be consistent with the fidelity of the existing inertial, altimeter, and clock error models in the IGI Simulation.

The fourth task is to implement in the AFAL IGI Simulator an error model of a low-accuracy strapdown system. The AFAL IGI Simulation currently employs a model only of a high-accuracy local-level wander-azimuth inertial system.

The fifth task is to explore the performance obtainable with an integrated GPS/strapdown navigation system involving low-accuracy strapdown inertial sensors.

The sixth task is to provide engineering support to the EAR/GEANS EIF development effort. This support includes review of EAR/GEANS system error models, synthesis of the EIF state vector, and EIF software design, code, and initial test.

1.4 Overview of Report

Chapter 2 presents results of the effort performed on Task 1, GDM Software Support.

Chapter 3 presents results of the effort performed on Task 2, Vertical Channel Analysis and Simulation.

Chapter 4 presents results of the effort performed on Task 3, Improved GPS Measurement Models.

Chapter 5 presents results of the effort performed on Task 4, Strapdown Inertial Simulation, and on Task 5, Integrated GPS/Strapdown Performance.

Chapter 6 presents results of the effort performed on Task 6, EAR/GEANS Error Isolation Filter Support.

1.5 Summary of Results

Conclusions and recommendations for each task area are presented in the corresponding chapter of this report, as outlined in the previous section. These results are briefly summarized by area in the following two subsections.

1.5.1 GPS Software Support Results

In the first GPS area, GDM software support, Intermetrics has analyzed several GDM technical problems and offered related recommendations to Collins. We have recommended that the GDM software be modified to incorporate a three-coefficient compensation equation for the g-sensitivity of onboard clock frequency; the least sensitive axis of the crystal clock should be aligned with the aircraft yaw axis. We have recommended that the GDM navigation software be modified to compensate the azimuth gyro g-sensitivity; if such a compensation scheme is not utilized, the Kalman filter process noise matrix should include an azimuth gyro g-sensitivity term. We have recommended several possible techniques for stabilizing rate aiding of the non-coherent mode of the GPS receiver by the navigation processor. These

techniques include a filter feedback limiter, reduced INS control gains, and measured code loop error compensation. The stability of several alternate rate-aiding designs was explored. The baseline design (suboptimal Kalman filter without stabilization compensation) is unstable when the Kalman cut-off frequency approaches the code loop noise bandwidth, as previously reported by Collins. The GDM stabilization technique improved stability, provided the compensation model is tuned to match the lowest-gain tracking loop dynamics. The recommended alternative is to reduce the rate at which the estimated INS errors are controlled by the Kalman filter; the system can thus be stabilized for Kalman cut-off frequencies more than ten times faster than for the baseline design. The associated rate-aiding software appears simpler than that for stabilization compensation. The stability improvement of the reduced-control-gain technique is less sensitive to the variable noise bandwidth of the code tracking loop.

In the second area, vertical channel analysis and simulation, Intermetrics has identified and corrected problems causing poor vertical-channel performance in the original Integrated GPS/Inertial (IGI) Simulator, demonstrated proper performance for a low-dynamic C5 mission, and compared simulated performance of three vertical-channel filter designs for a high-dynamic F4 mission. The two most significant vertical-channel changes to the IGI Simulator were changing the Kalman filter altimeter bias state from a random constant to a random walk, and correcting an error in the simulated GPS pseudo-range-rate measurement model. Simulation results for the C5 mission demonstrate GPS/inertial navigation errors consistent both with filter-computed uncertainties, and with Intermetrics' prior experience of GPS/inertial accuracy achievable. Simulator results for the F4 mission compared three vertical-channel filter models: a) altimeter bias plus scale-factor error states, b) bias error state, and c) scale factor error state. All three designs provide virtually identical navigation performance when GPS measurements are available. However, when GPS signals are not available (e.g., during severe jamming), and the aircraft is simultaneously performing climbing or diving maneuvers, filter a) performs better than b), and b) better than c); vertical- channel errors were approximately in the ratio of 2:3:4 for the F4 tactical mission simulated.

In the third area, improved IGI Simulator models, Intermetrics produced and documented an upgraded Simulator program. Emphasis was placed on high-fidelity barometric altimeter models, high-fidelity GPS pseudo-range and delta-pseudo-range error models, and on program structural changes. Simulated baro-altimeter errors include the effects of pressure-altitude error, scale factor error, due to non-standard temperature, static pressure defect, and altimeter lag. Simulated pseudo-range errors include the effects of GPS satellite clock phase drift and ephemeris error, atmospheric delays, user clock phase drift, and receiver phase noise. Simulated delta-pseudo-range errors include the effects of time rates-of-change of the pseudo-range errors, e.g., user clock frequency drift. This version of the Simulator

also implements the original high-fidelity error model for the Litton CAINS LN-15 baro-inertial navigation system (INS), structured in generalized form.

In the fourth and fifth task areas, integrated GPS/strapdown performance, Intermetrics added a strapdown inertial navigation system error model to the IGI Simulator, and obtained simulation results typifying strapdown performance for a high-dynamic F4 trajectory. The strapdown INS error model implemented is that for the Honeywell SIGN-III baro-inertial navigator, structured in a generalized form. Simulated performance results were obtained for a typical strapdown baro-inertial navigator under the high-dynamic F4 flight environment. These results demonstrate significant degradation in INS attitude errors as a result of sustained maneuvering. During circling flight, strapdown attitude errors were large compared with those of a typical local-level (gimballed) inertial system in the same environment. The resulting horizontal velocity and position errors of the strapdown system were also comparatively large. The dominant strapdown instrument error sources were gyro torquer scale factor errors and misalignments, and gyro g-sensitive drift rates.

1.5.2 EAR/GEANS Software Support Results

In the sixth area, EAR/GEANS Error Isolation Filter (EIF) support, Intermetrics has analyzed several aspects of the EIF computer program development, flight data recording requirements, EAR/GEANS error models, and optimal filter/smoother mechanization equations.

The EIF development plan describes five principal steps in computer program development and qualification: i) analysis, ii) top-level design and interface definition, iii) detailed design and coding, iv) testing, and v) maintenance. Sequencing, scheduling, and man-loading requirements have also been addressed.

EAR/GEANS flight data recording requirements developed by AFAL were reviewed and found adequate. High data-rate specific force need not be recorded, but can be computed with sufficient accuracy for EIF error propagation by back-differencing of inertial velocity data (with gravity compensation).

Intermetrics has reviewed AFAL-developed error models for the EAR/GEANS vertical channel, fundamental dynamics of the GEANS baro-damped space-stable inertial navigator, and EAR radar measurements and measurement matrices. We have noted that, for a second-order damping loop in the vertical channel, measurements of aircraft altitude alone do not provide observability of vertical velocity error, or separation of vertical acceleration and barometric altitude bias errors. Observability and separability require either difference measurements of inertial minus barometric altitude, or direct vertical velocity measurements. We have concurred with the fundamental error

dynamics model for the baro-damped space-stable navigator, with the exception of certain approximations to geodetic/geocentric coordinate transformations. Also, in the gyro drift model, two z-gyro drift states are inseparable and should be estimated as a single combined error source. We have also concurred with the EAR measurement models and measurement matrices developed by AFAL, insofar as geometric relationships between measurements and system error sources are concerned. There remain some questions regarding measurement error statistical characteristics, e.g., time-correlation of errors, and cross-coupling between measurements.

Intermetrics has reviewed the current literature on gravity perturbation modeling. Four representative space-domain gravity perturbation models have been examined, and their transfer to the time domain under various vehicle maneuvers analyzed. None of the models adequately represent the physical process during aircraft turns, or during repeated passes over the same ground track. Hence differences in theoretical completeness and frequency content of these gravity models are somewhat academic. For purposes of EAR/GEANS EIF development, the simulated environment model for gravity perturbations should be of higher faithfulness to the real world than the EIF estimator model. A deterministic space-domain gravity model is recommended for the environment simulator, *including local high-frequency perturbation* content. The EIF gravity model should account for the following factors: i) local gravity perturbation biases due to low-frequency global harmonics; ii) weak separability of gravity perturbation components from accelerometer biases; iii) cross-correlations between gravity perturbation components; and iv) non-uniform transformation from space to time domain during turns.

Intermetrics has recommended the EAR/GEANS EIF filter formulation, including the definitions of the filter state vector, process noise covariance matrix, state transition matrix, initial state vector estimate, and initial state error covariance matrix. The recommended filter state vector consists of 44 components*: three position errors, three velocity errors, three platform tilts, three accelerometer biases, three accelerometer scale-factor errors, three accelerometer misalignments (remaining three are zero by definition of ideal platform frame), three gyro biases (z term includes inseparable torquing error), six gyro g-sensitive drift coefficients, three baro-altimeter error sources, three antenna misalignments relative to case, three gimbal angle biases (fourth is inseparable from z-component of antenna/case misalignment), three radar range/range-rate errors, two monopulse angle-cosine errors, and three gravity perturbation components. The process noise covariance matrix represents random or unmodeled state driving noises; the latter are modeled by trajectory-dependent noise power density. The state transition matrix is represented by a first-order expansion in the

*Current version of EIF state vector.

integral of the fundamental dynamics matrix. The initial state vector estimate is zero, and the initial state error covariance matrix is computed in terms of rms Schuler position, velocity and tilt errors plus rms instrument errors.

The EAR/GEANS onboard navigation filter estimates 13 states pertaining to the INS, altimeter, and antenna subsystems. In the feedback mode, all thirteen filter states are utilized to correct data outputs from those subsystems. During post-flight analysis, certain EIF error states must be adjusted to compensate for feedback-correction jumps in the EAR/GEANS outputs. Adjustments are required in ten of the corresponding thirteen EIF states: three position errors, three velocity errors, three platform tilts, and one altimeter bias; the three antenna misalignments require no adjustment, since the EIF does not use onboard antenna attitude as its nominal value.

The forward pass of the EAR/GEANS EIF implements a forward-recursive optimal filter; the backward pass implements a backward-recursive optimal filter plus optimal smoother. Intermetrics recommends that the optimal filters be implemented as Kalman filters in triangular square root form, and the optimal smoother, as a Fraser two-filter smoother in triangular square root form. These algorithms are recommended since among existing formulations, they are the most stable numerically, and nearly the most efficient computationally. A modest increase in filter efficiency is possible using the U,D factored form of the triangular square root equations; however, the improvement is not sufficient to warrant recoding and retesting of available triangular square root subroutines.

SECTION II
GDM SOFTWARE SUPPORT

2.1 Chapter Summary

Intermetrics has reviewed various aspects of the Collins GDM navigation and receiver-aiding software design. Specific technical issues that have been analyzed in greater depth are the following:

i) Clock frequency g-sensitivity modeling and compensation;

ii) Azimuth gyro g-sensitivity calibration and compensation;

iii) Continuity of Kalman filter feedback to receiver aiding;

iv) Stability of receiver aiding in non-coherent mode;

v) Stability of alternate designs for rate aiding of non-coherent mode of a GPS receiver.

These topics are discussed in the following five sections, 2.2 to 2.6.

2.2 Clock Frequency G-Sensitivity Modeling and Compensation

This section comprises Intermetrics AFAL/GPS Analysis Memo #03-77. bu William S. Widnall, dated 31 August 1977 [17].

This technical memo documents recommendations that have previously been made to Collins personnel concerning compensation of the clock frequency G-sensitivity in the AFAL/Collins GPS/GDM.

2.2.1 Technical Discussion

Crystal clocks are sensitive to the applied specific force. It is thought that a simple linear model adequately describes the shift in frequency due to applied specific force. See for example Ref. [1]. The contribution to pseudo-range-rate measurement error $\delta\dot{r}$ is

$$\delta\dot{r} = \delta\dot{r}_o + \underline{c} \cdot \underline{f} \qquad (2.2\text{-}1)$$

where $\underline{c}$ is the clock frequency g-sensitivity vector, $\underline{f}$ is the specific force vector in aircraft coordinates, and $\delta\dot{r}_o$ denotes the error in measured pseudo range rate due to other effects.

The g-sensitivity effect can be quite significant. This author has not seen test data for the GDM clock (HP 10544A). However typical values for crystal clocks are of the order of 0.1 meter/sec/g for the least sensitive axis to 1.0 meter/sec/g for the most sensitive axis. If not calibrated and compensated, this effect may limit the achievable narrow-tracking-loop bandwidths and therefore the achievable anti-jamming performance. The Collins design did not include such compensation.

2.2.2 Recommendations

We have recommended that the GDM software be modified to incorporate a compensation equation for the g-sensitivity of the clock frequency. Three coefficients would be stored,

which would be used to multiply the three components of specific force to obtain the expected frequency shift. The three coefficients would be obtained from laboratory testing or from flight data analysis using the Error Isolation Filter.

The least sensitive axis of the crystal clock should be mounted in the aircraft lift-vector direction. The most sensitive axis should be mounted in the aircraft lateral direction.

Residual errors after compensation should be modeled in the Kalman filter with appropriate maneuver-dependent state driving noise and measurement error variance.

2.2.3 Status

The recommendation that compensation for clock-frequency g-sensitivity be included in the GDM software was made verbally to Collins personnel at a technical interchange meeting at Cedar Rapids, on 14-16 February 1977. At a later meeting on 26 April, Dick Carroll indicated that Collins has implemented three calibration coefficients in the software. He also indicated that maneuver-dependent clock phase error state driving noise has been added in the filter.

2.3 Azimuth Gyro G-Sensitivity Calibration and Compensation

This section comprises Intermetrics AFAL/GPS Analysis Memo #05-77, by William S. Widnall, dated 31 August 1977 [18].

This technical memo documents recommendations that have previously been made to Collins personnel concerning the calibration and compensation of the azimuth gyro g-sensitivity in the IMU of the AFAL/Collins GPS/GDM.

2.3.1 Technical Discussion

The KT-70 inertial measurement unit azimuth gyro has an uncompensated sensitivity to vertical specific force of about 4°/hr/g (data from Collins personnel). The steady gyro drift rate of about 4°/hr in the one-g environment due to this effect is compensated for in the navigation software by proper choice of the calibration value for azimuth gyro drift rate. However changes in gyro drift rate due to changes in the vertical specific force are not compensated. The short-duration variations in vertical specific force due to pull-ups or push-downs are not of great significance. More important is the long-duration change in vertical specific force associated with flying at a different altitude.

Gravity strength decreases with altitude approximately as

$$g(h) \approx g_o(1 - 2h/r_e) \qquad (2.3\text{-}1)$$

where g_o is the sea-level strength of gravity, r_e is earth radius, and h is the altitude above sea level. The vertical specific force, neglecting maneuver acceleration and Coriollis acceleration, is equal to gravity

$$f_z = g(h) \qquad (2.3\text{-}2)$$

The azimuth gyro drift rate due to this specific force is

$$\delta\omega_z = DZ_z\, g_o(1 - 2h/r_e) \qquad (2.3\text{-}3)$$

where DZ_z denotes the g-sensitivity. The change in this drift rate between sea-level and an altitude h is

$$\Delta \delta\omega_z = -DZ_z \, g_o \, 2h/r_e \qquad (2.3\text{-}4)$$

At 30,000 ft altitude and assuming $DZ_z = 4°/hr/g$ (and using $r_e = 20{,}900{,}000$ ft), the change in gyro drift rate is

$$\Delta \delta\omega_z = -0.012°/hr \qquad (2.3\text{-}5)$$

This is a significant change in gyro drift rate. However without some simulation results, this author cannot say if such a change will have a significant impact on navigation and receiver aiding accuracy.

2.3.2 Recommendations

We have recommended that the GDM navigation software be modified to compensate the azimuth gyro g-sensitivity. The compensation coefficient can be measured from IMU laboratory test data and/or from flight recorded data (using the Error Isolation Filter).

If such compensation is not adopted, the effect of the changes in gyro-drift rate perhaps can be minimized by providing adequate state driving noise variance in the Kalman filter model for azimuth gyro drift rate.

2.3.3 Status

The recommendation that Collins consider compensating the z gyro g-sensitivity was made verbally to Collins personnel at a technical interchange meeting at Cedar Rapids on 14-16 February 1977. It is my understanding, based on my 2 August telephone conversation with Dick Carroll, that the compensation recommendation was not adopted.

2.4 Continuity of Kalman Filter Feedback to Receiver Aiding

This section comprises Intermetrics AFAL/GPS Analysis Memo #04-77, by William S. Widnall, dated 31 August 1977 [19].

This technical memo documents recommendations that have previously been made to Collins personnel concerning possible discontinuities in the receiver rate aiding due to Kalman filter feedback of error estimates in the AFAL/Collins GPS/GDM.

2.4.1 Technical Discussion

The rate-aided receiver tracking loops for one channel of the GDM are shown in Figure 1. Illustrated are the variables associated with tracking a single satellite. Similar diagrams apply to the simultaneous tracking of the other satellites. Functions shown include the receiver rate aiding, the carrier tracking, and the code tracking.

The receiver rate aiding variable VAID for each channel is obtained from the navigation computer. In the initial Collins design (see Ref. [2], p. 313, Eq. (3.2.3.3-6)) VAID was comprised of

$$VAID = \dot{R}_S - (\bar{V}_{DYN} + \delta\bar{V}_R) \cdot \bar{e}_T + \varepsilon V_F \qquad (2.4\text{-}1)$$

where

$\dot{R}_S$ = Computed range rate of the satellite assuming zero user antenna velocity with respect to earth.

$\bar{V}_{DYN}$ = Inertial navigation indicated velocity plus computed antenna velocity relative to the inertial measurement unit.

$\bar{e}_T$ = Unit vector to the satellite from the user.

εV_F = Estimated user clock velocity error from the Kalman filter

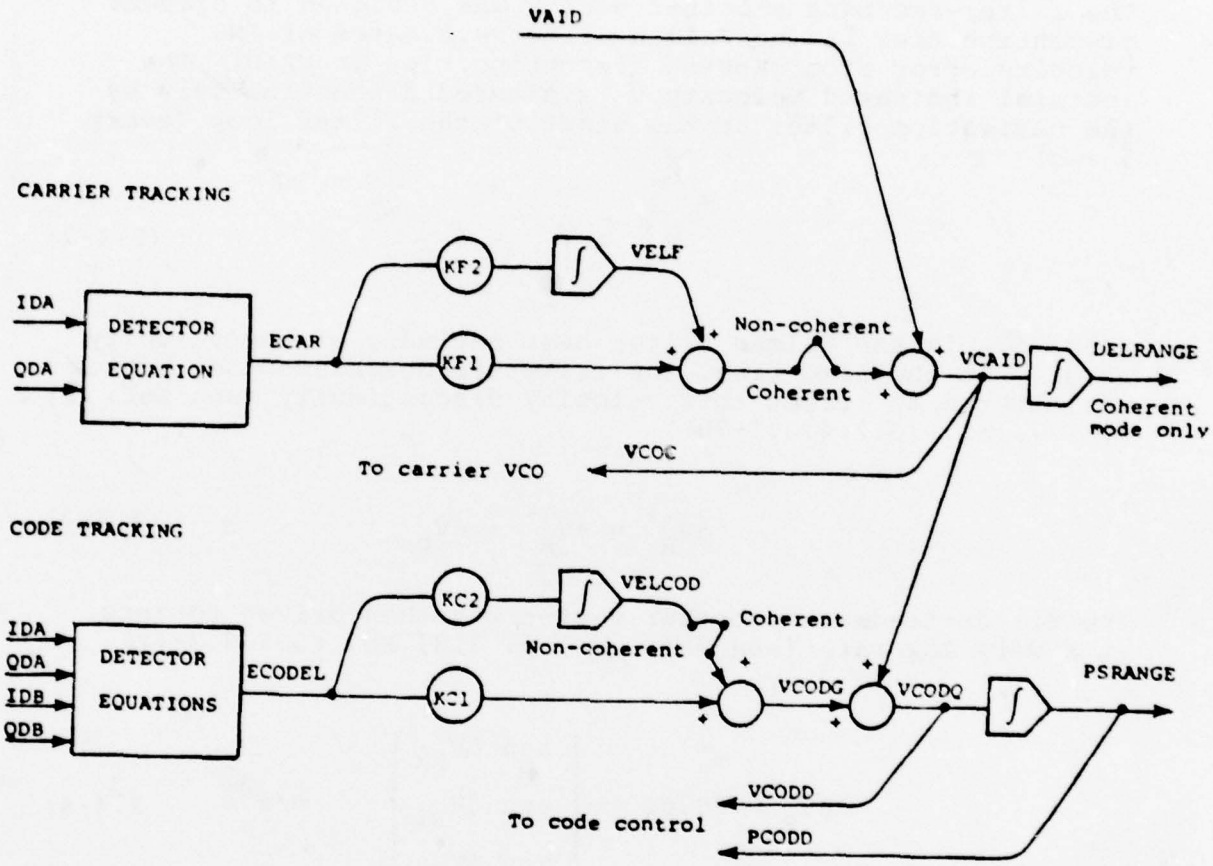

Figure 1: Rate-Aided Receiver Tracking Loops of the GDM

$\delta\bar{V}_R$ = Filter-feedback smoother vector

The filter-feedback smoother vector was designed to prevent discontinuities in the Kalman filter estimates of INS velocity error from causing discontinuities in VAID. The inertial indicated velocity $\bar{V}$ is altered discontinuously by the navigation filter at the start of the filter loop (every 5 sec)

$$\bar{V}^+ = \bar{V}^- - \delta\bar{V}_c \qquad (2.4\text{-}2)$$

where $\delta\bar{V}_c$ is the Kalman filter best estimate of the velocity error. At the same time, the filter-feedback smoother vector was altered to offset this velocity discontinuity (see Ref. (2), p. 227, Eq. (3.2.2.2.3-7b))

$$\delta\bar{V}_R{}^+ = \delta\bar{V}_R{}^- + \delta\bar{V}_c \qquad (2.4\text{-}3)$$

The filter-feedback smoother vector was then driven to zero at a very low rate (see Ref. (2), p. 313, Eq. (3.2.3.3-7))

$$\dot{\delta\bar{V}}_R = -0.02 \begin{bmatrix} \text{sgn } \delta V_{RX} \\ \text{sgn } \delta V_{RY} \\ \text{sgn } \delta V_{RZ} \end{bmatrix} \quad m/s^2 \qquad (2.4\text{-}4)$$

Preventing discontinuities in the VAID signal is necessary to prevent loss of carrier tracking. As seen in Figure 1, the rate aiding variable VAID feeds directly into the command to the carrier digital VCO. Carrier tracking error must be held to a few centimeters. The carrier tracking loop time constant is of the order of one sec. Hence discontinuities in the receiver aiding signal greater than about 0.02 m/sec per sec are likely to cause cycle slipping or loss of coherent tracking.

The initial Collins design was good as far as it went. However, we pointed out that the design did not suppress the effect of discontinuities in the Kalman filter estimates of clock frequency error.

2.4.2 Recommendations

We recommended that the GDM navigation computer software be modified to incorporate limiting of the Kalman filter feedback of the clock frequency estimates to the receiver aiding.

2.4.3 Status

The recommendation concerning the clock frequency estimates and receiver aiding was made verbally to Collins personnel at a technical interchange meeting at Cedar Rapids on 14-16 February 1977. At a later meeting on 26 April, Collins personnel indicated that they have redesigned the continuity logic in the following manner. The receiver rate aiding variable for each channel is now comprised of

$$VAID = \dot{R}_s - \bar{V}_{DYN} \cdot \bar{e}_T + \varepsilon V_F + \delta V_R \qquad (2.4\text{-}5)$$

where

δV_R = Filter feedback smoother variable for one channel only

and the other variables are as previously defined. The inertial indicated velocity $\bar{V}$ is altered discontinuously by the Kalman filter as before (Eq. (2)). The estimated clock frequency error is altered discontinuously by the Kalman filter as before

$$\varepsilon V_F^+ = \varepsilon V_F^- - \Delta V_{FC} \qquad (2.4\text{-}6)$$

where ΔV_{FC} is the Kalman filter computed change in clock frequency error estimate. At the same time, the filter-feedback smoother variable for each channel is altered to offset these discontinuities

$$\delta V_R^+ = \delta V_R^- - \delta \bar{V}_c \cdot \bar{e}_T + \Delta V_{FC} \qquad (2.4\text{-}7)$$

The filter-feedback smoother variables are driven to zero at the very low rate

$$\dot{\delta V}_R = -0.02 \text{ sgn } \delta V_R \quad m/s^2 \qquad (2.4\text{-}8)$$

This looks like a good implementation.

2.5 Stability of Receiver Aiding in Non-Coherent Mode

This section comprises Intermetrics AFAL/GPS Analysis Memo # 06-77, by William S. Widnall, dated 16 September 1977[20].

This technical memo discusses the known potential instability of the non-coherent mode of the AFAL/Collins GPS/GDM. Concerns are expressed as to the desirability and adequacy of the design changes that have been made to correct the stability problem. An alternate approach previously suggested to Collins personnel by the author is documented in this memo. Also presented here are two additional alternate approaches.

2.5.1 Technical Discussion

Collins designers have been aware that a potential stability problem exists in the GPS/GDM non-coherent mode. The problem is associated with the closed-loop Kalman filter and the very narrow code tracking loop bandwidths. It was discussed by Collins personnel at the Critical Design Review Meeting in December 1976, Ref. [3] . The essence of the problem is that the tracking loop bandwidths are made as slow as possible to reject wide-band noise due to jammers. This causes long-correlation-time errors in the pseudo-range measurements. The navigation Kalman filter that blends the GPS and INS data is sub-optimal and does not model the long-correlation time pseudo-range errors. The estimates of navigation errors from the Kalman filter are fed to the inertial navigation equations to provide closed-loop control of the inertial navigation errors. The corrected inertial navigation variables are in turn used to compute estimated range-rates to the GPS satellites to be used for receiver aiding. If a channel is in the non-coherent mode (carrier loop not tracking), the receiver aiding is applied directly to the code loop. It turns out that this rather complex system may be unstable.

An analysis of this problem and a discussion of the implemented design changes are presented by Will Mickelson of Collins in Ref. [4]. A very readable paper by Dick Carroll and Will Mickelson on the same subject was later presented at

the NAECON meeting, Ref. [5]. The design approach adopted includes the addition of compensation equations in the navigation computer that model approximately the responses of the code tracking loops to the Kalman filter feedback. These modeled responses are subtracted from the pseudo-range measurements obtained from the receiver computer. Figure 2 (from Ref. [5]) summarizes the information flow. (Where it says "INS Vertical Loop", read "INS Equations".) An additional change adopted is that the code tracking loop bandwidths have been increased. Linear stability analyses are presented in Refs. [4] and [5] that show the benefits of these changes.

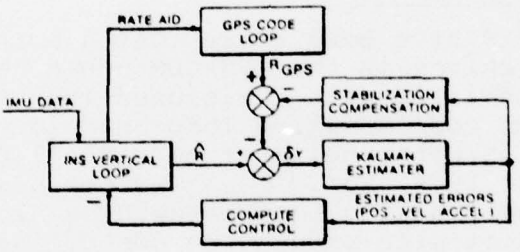

Figure 2: Generalized Information Flow Diagram

This author has pointed out a disadvantage of these changes. Wider code tracking loop bandwidths have been adopted. This gives up something in terms of anti-jamming performance. Generally one wants to have the bandwidths as narrow as possible, limited only by the physical considerations associated with the vehicle dynamics and the dynamic errors of the aiding signals and of the clock. It is not desirable to adopt wider bandwidths to help solve this stability problem.

This author has also expressed a fundamental concern that the modified system may still be unstable. The stability analysis presented in Ref.[4] and[5] is a classical frequency domain analysis employing a fundamental assumption that the Kalman filter gains remain at low steady state values. Stability is demonstrated for cases where the Kalman filter

response time is not significantly faster than the code-loop response time. However, it is a known and desirable characteristic of Kalman filters that they have time-varying gains. This permits them to make optimal use of the measurements as a function of changing measurement geometry and changing data availability. After a period of loss of signal, such as due to wing shadowing in a turn or due to jamming, the Kalman filter will have increased its gains so as to put greater weight on the GPS measurements (relative to the INS dead reckoning). How much these gains increase over their minimum values is a function of how long is the period of no GPS measurements. It is quite possible that at higher gain levels, at which the Kalman filter response time is significantly faster than the code-loop response time, the system may again be unstable.

2.5.2.1 Filter Feedback Limiter. A fundamental observation is that if the receiver-aiding was not a function of the Kalman filter error estimates, then there would be no stability problem. However, zero filter feedback is undesirable for two reasons: 1. The vertical channel would have to be stabilized in some other way (such as a conventional non-Kalman baro-inertial vertical channel). 2. the INS attitude errors, especially the azimuth error, would grow uncontrolled during a flight causing a larger maneuver-dependent error in the velocity aid.

The author has made the following suggestion to Collins personnel. Consider using the filter-feedback limiter concept of the coherent mode also in the non-coherent mode. The filter-feedback limiter concept active in the non-coherent mode ensures continuity of the receiver aiding signal by storing up the discontinuous Kalman filter velocity-error and clock-frequency-error estimates and metering out the related changes to the receiver aiding signals at a rate currently limited at 0.02 m/s^2. In the present design, the feedback limiter is not used in the non-coherent mode. If the limiter were retained in the non-coherent mode, it is possible that the limiter could suppress the stability problem. Assume that the system is unstable without the limiter. Further assume that the frequency of oscillation is about .03 rad/sec (the resonant frequency shown in Figure 8 of Ref. [5]). The period of oscillation is then about 200 sec. If the filter feedback limiter is set at 0.02 m/s^2 (current setting in non-coherent mode), then a possible system limit cycle would be as exhibited in Figure 3. The limit cycle amplitude might be 50 meters, which is unacceptable. If the feedback limiter were set at 0.001 m/s^2, the limit cycle amplitude might be 2.5 m, which is acceptable.

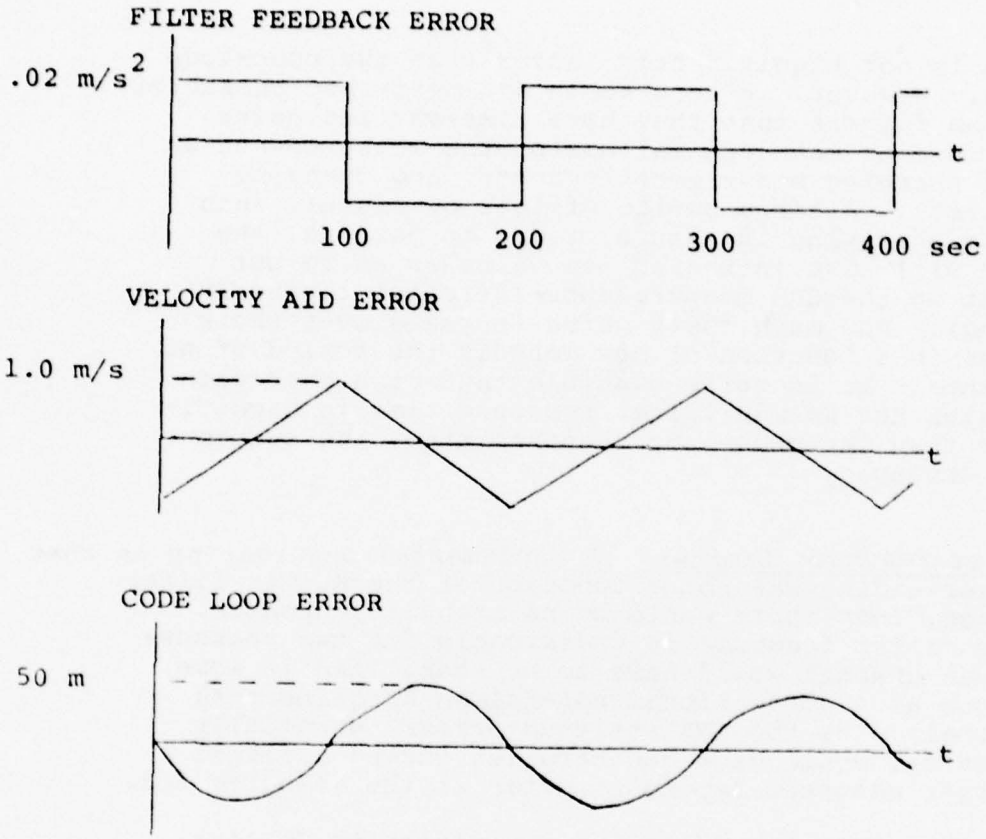

Figure 3: Possible Limit Cycle of Non-Coherent Mode with Filter Feedback Limiter

2.5.3 Reduced INS Control Gains. There may be other considerations which make it undesirable to reduce the filter feedback limiter to the order of 0.001 m/s^2. An alternate idea is to reduce the loop gain that is causing the instability by introducing reduced INS control gains. The present Collins GDM design applies the full value of the error estimates from the Kalman filter to the INS and clock variables. These full corrections are applied at the next filter cycle, 5 sec after the measurements. If instead say only 5% of the estimated errors were corrected each 5 sec, then the filter feedback gain has been reduced by a factor of 20. As long as the control action is properly modeled in the Kalman filter, there is no loss of estimation accuracy.

These new control gains cannot be made arbitrarily small, because the unaided vertical channel is unstable. In the example of 5% feedback each 5 sec, this has a feedback time constant of the order of 100 sec. It probably can be shown that this is adequate to stabilize the vertical channel. A time constant of 1000 sec on the other hand is probably too weak to stabilize the vertical channel.

The merit of this idea can be explored by a linear constant coefficient stability analysis employing similar assumptions to those employed in Refs. [4] and [5]. The inertial navigation errors plus the code tracking loop errors are modeled as being governed by

$$\dot{x}_t = F_t x_t + w + Au \qquad (2.5\text{-}1)$$

where x_t is true error state vector, F_t is its fundamental matrix, w is a vector of white noise disturbances, u is the error control vector, and A is a matrix allocating the error control vector to some of the states. A vertical channel analysis could have five states: three INS errors, and two code tracking loop errors, as in Refs. [4] and [5]. The Kalman filter processes a measurement vector z

$$z = Hx_t + v \qquad (2.5\text{-}2)$$

where H is the measurement gradient matrix and v is a vector of white noises. The vertical channel stability analysis can consider a single ranging measurement, ignoring the less accurate altimeter measurement, as in Refs. [4] and [5]. The Kalman filter can be modeled as being an analog filter governed by

$$\dot{x}_f = F_f x_f + u + K(z - Hx_f) \qquad (2.5\text{-}3)$$

where x_f is the filter state vector, F_f is its fundamental matrix, u is the same control vector as in Eq.(-1), and K is the Kalman gain matrix. The Kalman filter is sub-optimal, not modeling the code tracking loop error states. The vertical channel stability analysis considers the Kalman filter as having only three states, estimating the INS vertical channel errors.

In the present Collins design, the full value feedback control is essentially

$$u = -K(z - Hx_f) \qquad (2.5\text{-}4)$$

This clamps the filter estimates at zero, and provides true errors governed by

$$\dot{x}_t = (F_t - AKH)x_t + w - AKv \qquad (2.5\text{-}5)$$

The above equation is derived by using Eq.(-2) in Eq.(-4), by assuming x_f in Eq.(-4) is held at zero, and by using Eq.(-4) in Eq.(-1). The stability of the system can be explored by examining the roots of the characteristic equation

$$\det(s\,I - F_t + AKH) = 0 \qquad (2.5\text{-}6)$$

This would be a fifth order characteristic equation for three INS errors and two code loop errors (and without the stabilization compensation two states).

In the alternate design suggested here, the feedback is reduced by introducing a gain matrix C

$$u = -C\,x_f \qquad (2.5\text{-}7)$$

The filter estimates are no longer clamped at zero. The combined truth and filter states are governed by

$$\begin{bmatrix} \dot{x}_t \\ \dot{x}_f \end{bmatrix} = \begin{bmatrix} F_t & -AC \\ KH & F_f - KH - C \end{bmatrix} \begin{bmatrix} x_t \\ x_f \end{bmatrix} + \begin{bmatrix} w \\ Kv \end{bmatrix} \qquad (2.5\text{-}8)$$

The x_t row of Eq.(-8) is obtained by using Eq.(-7) in Eq.(-1). The x_f row of Eq.(-8) is obtained by using Eq.(-2) and Eq.(-7) in Eq.(-3). The stability of this alternate system can be explored by examining the roots of the characteristic equation

$$\det(s\,I - F) = 0 \qquad (2.5\text{-}9)$$

where F is the combined fundamental matrix of Eq.(-8). This would be an eighth order characteristic equation for three INS errors, two code loop errors, and three filter states.

Normally one would choose the C matrix to be diagonal (altitude error estimate controls INS altitude, etc.). The diagonal elements could all be chosen for simplicity as having equal values. Values of 0.01 in this analog analysis would correspond to the discrete 5% feedback every 5 sec.

The Kalman filter gains for this analysis should be set significantly higher than in the analysis of Refs.[4] and [5]. This is to explore the stability associated with higher gains after loss of measurements.

2.5.4 Measured Code Loop Error Compensation. A third Stabilization idea is presented here. Consider measuring the code loop error offset and compensate the pseudo-range measurements with this measured offset. The present Collins design models the response of each non-coherent code loop to the filter feedback in the rate aiding signal and subtracts the modeled response from the pseudo-range measurements as shown in Figure 2. Rather than model the code loop response, it is possible to measure the code loop response. The code tracking loop operates on a noisy error signal ECODEL. The average value of this noisy signal, say over a 5 sec interval, is a smoother measure of the tracking loop error. An assumption must be made about the tracking loop gain to convert this measurement to pseudo-range units. The loop-error measurement is then subtracted from the pseudo-range measurement that comes from the code offset command.

An advantage of this approach over the current Collins approach might be that direct measurements are more accurate than the math modeling approach. Furthermore, loop transients due to noise are directly observed and removed from the pseudo-range measurements.

Note a consequence of removing the long-correlation-time code tracking loop error from the pseudo range measurements will be to introduce a higher noise level into the individual measurements. However, it probably can be shown that the noise spectral density seen by the Kalman filter remains the same.

One implementation of this approach would involve introducing error accumulation equations for each channel in the receiver computer (analogous to the delta range accumulation equations). These integrals of the code loop error signals would be sampled by the navigation computer at the measurement times (every five sec). A back difference over the last 5 sec would yield the average error.

A more detailed discussion of measuring code loop error statistics is given in the Appendix of Ref. [6].

2.5.2 Recommendations and Status

The suggestion that the filter feedback limiter be used in the non-coherent mode was made to Dick Carroll of Collins by telephone on 2 August 1977. The additional suggestions concerning reduced INS-control gains and concerning measured-code-loop-error compensation were made to Dick Carroll by telephone today (16 September 1977). It is now quite late in the GDM software development schedule. Dick indicates it is unlikely that further changes can be made in the software unless the change requirement is quite urgent.

My current recommendations to the AFAL and Collins on this stability problem are:

1. Allow the limiter to run in the non-coherent mode. It will not hurt and it might help.

2. Continue linear stability analyses of the vertical and horizontal channels of the GDM. These should explore stability at higher quasi-static Kalman gains.

3. Examine the stability improvement with reduced INS control gains.

4. Implement now in the receiver-computer software an appropriate set of tracking loop statistics equations, with results delivered to the navigation computer interface, and to the flight recorded data.

With these analyses and immediate software changes, Collins can later implement in the navigation computer either the reduced INS-control gains idea or the measured-code-loop-error compensation idea or both, should the current design prove to be still unstable.

2.6 Stability of Alternate Designs for Rate Aiding of Non-Coherent Mode of GPS Receiver

The results of this study effort have been published in a separate document, "Stability of Alternate Designs for Rate Aiding of Non-Coherent Mode of a GPS Receiver", by William S. Widnall, dated 25 September 1978 [7]. This section comprises excerpts from Sections 1.1 and 7.0 of that report.

2.6.1 Anti-Jamming Characteristics of the GPS GDM

The anti-jamming characteristics of the GPS/GDM are summarized in Ref. [8]. A phased-array antenna is used to provide high gain in the directions of four GPS satellites and simultaneous low gain for jammer sources out of the main lobes. This provides 15 db of anti-jamming margin compared with the performance with a conventional low gain antenna. Inertial navigation system (INS) data is used to rate aid the GPS receiver. The aiding permits narrower bandwidth tracking loops in the GPS receiver. This provides an additional 10 to 12 db of anti-jamming margin compared with the performance of an unaided wide bandwidth receiver. In the absence of jamming, the normal tracking of each satellite signal includes a phase-locked loop (Costas loop) tracking of the carrier and non-coherent delay locked loop (NDLL) tracking of the pseudo-random code modulation. As jamming power increases, eventually a Costas loop loses lock. The GDM is designed to continue tracking after loss of carrier lock, using only the non-coherent code tracking. The non-coherent code loop tracking has about 8 db more jamming tolerance than the carrier loop.

2.6.2 Conclusions and Recommendations

The stability of alternate designs for rate aiding the non-coherent GDM GPS receiver has been explored.

A baseline design was defined to include the suboptimal Kalman filter (without the stabilization compensation) and the maximum rate error reset. Numerical computation of the poles of this system confirm the results previously reported by Collins personnel, namely the system is unstable when the Kalman cut-off frequency approaches the code tracking loop noise bandwidth. In the single axis vertical channel example and with the code loop noise bandwidth of 0.01 Hz, the system became unstable for Kalman filter cut-off frequency somewhere between .01 and .0316 rad/sec (.0016 and .005 Hz).

The GDM design, as documented and discussed in Refs. [4], [5], and [9], is similar to the baseline design but with the addition of stabilization compensation. The stabilization compensation does improve the stability of the system, provided the model in the compensation is tuned to match the tracking loop dynamics in its lowest-loop-gain condition. One defect in the present compensation design is that there exists the possibility of a static altitude error due to a non-zero steady state variable in the compensation. Fortunately this defect can be eliminated with a simple software change in the GDM data processor.

One alternate approach to improving the stability of the system is to significantly reduce the rate at which the estimated INS errors are controlled. In the vertical channel example it was demonstrated that with control gains of .005 sec^{-1} (200 sec control time constant) the system is stable for Kalman cut-off frequency more than a factor of ten faster than the tolerable filter frequency in the baseline design.

A different approach to improving the stability is to eliminate the code tracking error from the pseudorange measurements. If this can be done, the pseudorange measurements have uncorrelated random error, and the stability problem is eliminated. The poles of the system include tracking loop poles, regulated INS error poles, and Kalman filter error poles. Only the placement of the Kalman filter poles depends on the filter cut-off frequency. All poles of the system are stable, both for high-rate and low-rate control gains.

The principles involved in eliminating code tracking error from the pseudorange measurements were discussed. One key technical problem is the estimation of the detector gain, which is a function of the signal power. The Magnavox method of estimating detector gain was discussed. It appears that the Magnavox method cannot be used in the highest jamming environment because of the excessively long time required to estimate the signal strength. Perhaps an alternate method of calculating detector gain can be proposed that overcomes this problem. For example, the signal strength in the receiver preamplifier could be assumed known, based on assumed satellite power, path losses, antenna gain, and so forth. The modification of the signal in the receiver due to automatic gain control, and so forth, perhaps can be calculated as a function of available receiver variables.

We recommend the reduced-control-gain design for immediate implementation in the GDM. The required modifications to the GDM software appear easy to implement. The more extensive software associated with the stabilization compensation can be deleted. The reduced-control-gain design also has the fundamental advantage that the stability improvement provided is not dependent on the tracking loop bandwidth being some exact value.

To eliminate code tracking error from the pseudorange measurements, much more extensive software changes would be required in the GDM. Significant logic and calculations would have to be added to the software in the receiver controller computer. In spite of the lack of clear approach for the high jamming case plus the significant software changes required, we recommend that this approach be developed for advanced versions of the GDM. This approach with its decorrelated measurements and with its measured noise variance can lead to improved navigation accuracy, because the Kalman filter can accurately model the measurements and their time-varying statistics.

The numerical examples in this report have been carried out for a nominal code loop noise bandwidth of .01 Hz. The present GDM design employs a bandwidth of .03 Hz. The more stable alternate designs evaluated in this report remove stability from the design considerations that constrain the minimum bandwidth. Accordingly if the quality of the inertial system and of the receiver clock are sufficiently excellent, the noise bandwidth can be reduced. The anti-jamming characteristics will be improved.

SECTION III
VERTICAL CHANNEL ANALYSIS AND SIMULATION

3.1 Chapter Summary

Intermetrics has reviewed the AFAL Integrated GPS/Inertial (IGI) Simulator, designed and implemented alternate vertical channel models, and demonstrated satisfactory performance with the revised models. Specific technical issures that have been analyzed in depth are the following:

i) identification and elimination of problems causing poor vertical-channel performance in original simulator, and demonstration of proper performance for low-dynamic C5 mission;

ii) comparison of simulated performance of three vertical channel filter designs for high-dynamic F4 mission.

Results of these analyses are presented in Sections 3.2 and 3.3.

3.2 C5A GPS/Inertial Simulation Results

Under Task 2 of the AFAL GPS Software Support Contract, the AFAL IGI (Integrated GPS Inertial) Simulator has been modified to correct certain difficulties experienced by AFAL personnel with the simulated vertical channel performance. To obtain initial results, Myers and Butler found it necessary to zero an important source of altimeter error, the altimeter scale factor error. These difficulties and the initial results were reported in Ref. [10].

Intermetrics has made several revisions to the IGI simulator and has eliminated the problems causing poor vertical channel performance. The modified IGI simulator was delivered to the AFAL in May 1977. An analysis report comparing the performance of three alternate Kalman filter vertical channel designs will appear shortly. However, the results in this report are for a simulated high-dynamic F4 mission. Major Myers requested that we also run one low-dynamic C5 case, similar to the case of Ref.[10], to demonstrate conclusively that we have eliminated the difficulties. We have run such a case. This memo presents the results.

This case is similar to that of Ref. [10] in that it has the same C5 trajectory and has a Kalman filter whose only model for altimeter error is a single scale factor error state. The case differs in many details, including truth state error models, truth state initial conditions, and Kalman filter noise covariance modeling. It is beyond the scope of this memo to list all of these differences. Complete model descriptions are included in the Task 2 report. The two changes which are perhaps of the greatest significance in obtaining the good vertical channel performance are: 1) changing the Kalman filter scale factor error state from a random constant to a random walk, and using the spectral density of the noise of this random walk to model the varying effect of the altimeter zero-setting error when the altitude is changing; 2) correcting an error in the simulated GPS pseudo-range rate measurements associated with the clock frequency error model.

Simulation results for the C5 case are shown in the enclosed figures. The position and velocity errors of the baro-inertial navigator (unaided by GPS measurements) are shown in Figures 4 and 5. The errors in the best estimates of position, velocity, attitude, user clock phase, and frequency are shown in Figures 6 through 9. The error in the estimate of the effective altimeter scale factor is shown in Figure 10. These plots of estimation error also include the Kalman filter computed uncertainty in the estimate (which is the square root of the appropriate element of the covariance matrix).

One conclusion from these results is that the vertical channel performance is satisfactory. The errors in the estimates of altitude, vertical velocity, and altimeter scale factor error are generally within the filter computed one-sigma uncertainties. The level of the errors in altitude and vertical velocity are consistent with the authors' experience of the accuracy achievable with GPS-inertial systems.

The large peaking of errors and computed uncertainties at 230 min has been traced to an error in the IGI simulator. The error has been found in the satellite selection algorithm coding (subroutine OPTSEL). The coding causes an erroneous comparison of the GDOP's of various satellite groups which are in view at a given satellite selection time with the GDOP of the most favorable satellite group at a previous satellite selection time. If the GDOPs of all combinations (of four) of the in-view satellite set at the given satellite selection time is greater than that of the satellite group at the previous satellite selection time, then the old satellite group is retained. This error causes the possible use by the measurement updating sequence of satellites that are actually not in view at the measurement time. The consequence of which is degraded GPS navigation accuracy.

Figure 6 shows the position errors for the C5-A mission. After about 85 min of flight, a group of satellites is selected which at that time has a very low value for GDOP. However, this set of satellites was maintained for the remainder of the mission even though one or more of these satellites were no longer in view, and the GDOP of this satellite group is probably no longer optimum shortly after 85 min. The disposition of this satellite group appears to pass through some sort of singular configuration at around 230 min. Even though some of these satellites are not visible, the IGI simulator incorporated measurements from them as though they were visible.

Intermetrics has designed a change to the satellite selection algorithm, and this change will be incorporated and tested during our Task 3 work.

A comparison of the enclosed figures with the results presented in Ref. [10] exposes the effect of some of the changes we have made to the IGI simulator. Eliminating the driving noise on the longitude and latitude error states has eliminated the large growth in position error covariance between measurements. Significantly reducing the driving noises during unaccelerated flight on the velocity error states and the attitude error states has reduced significantly the growth in velocity and attitude error covariance between measurements. Note the order-of-magnitude lower azimuth error covariance.

Evidence of the satellite selection error is not obvious in the Ref. [10] results, although the divergence in the last hour of the Ref. [10] results may be related to this error.

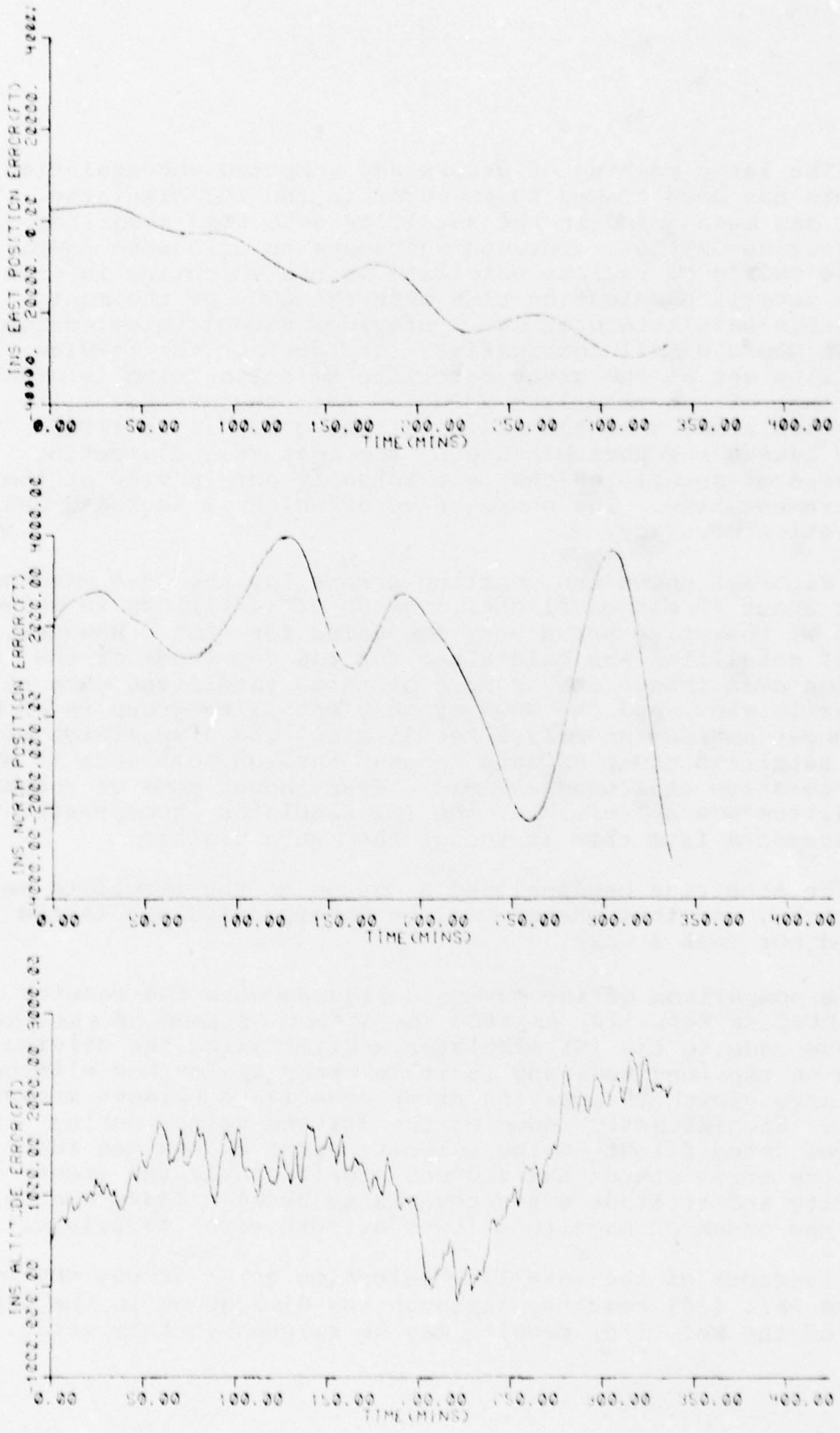

Figure 4: Unaided INS Position Errors

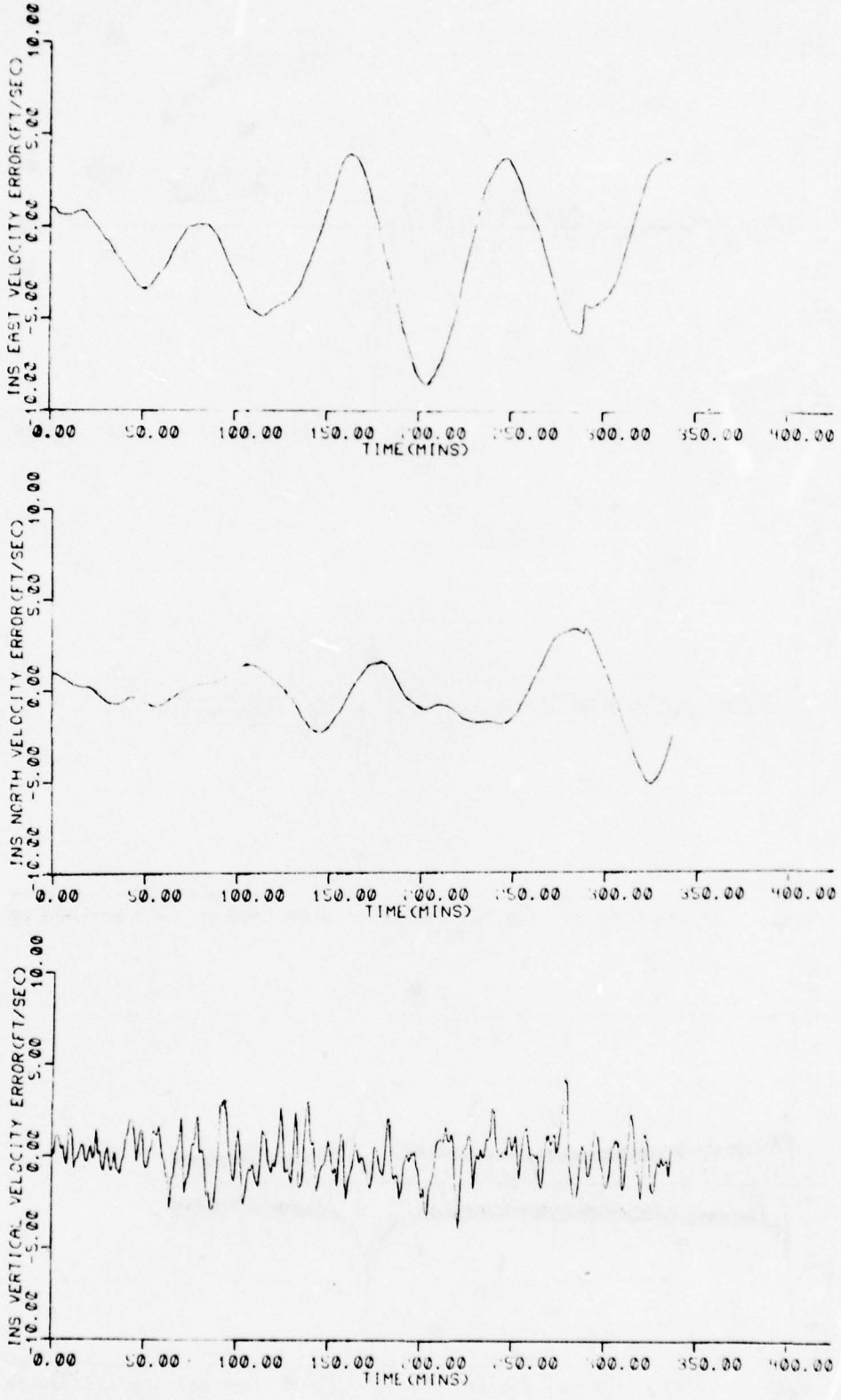

Figure 5: Unaided INS Velocity Errors

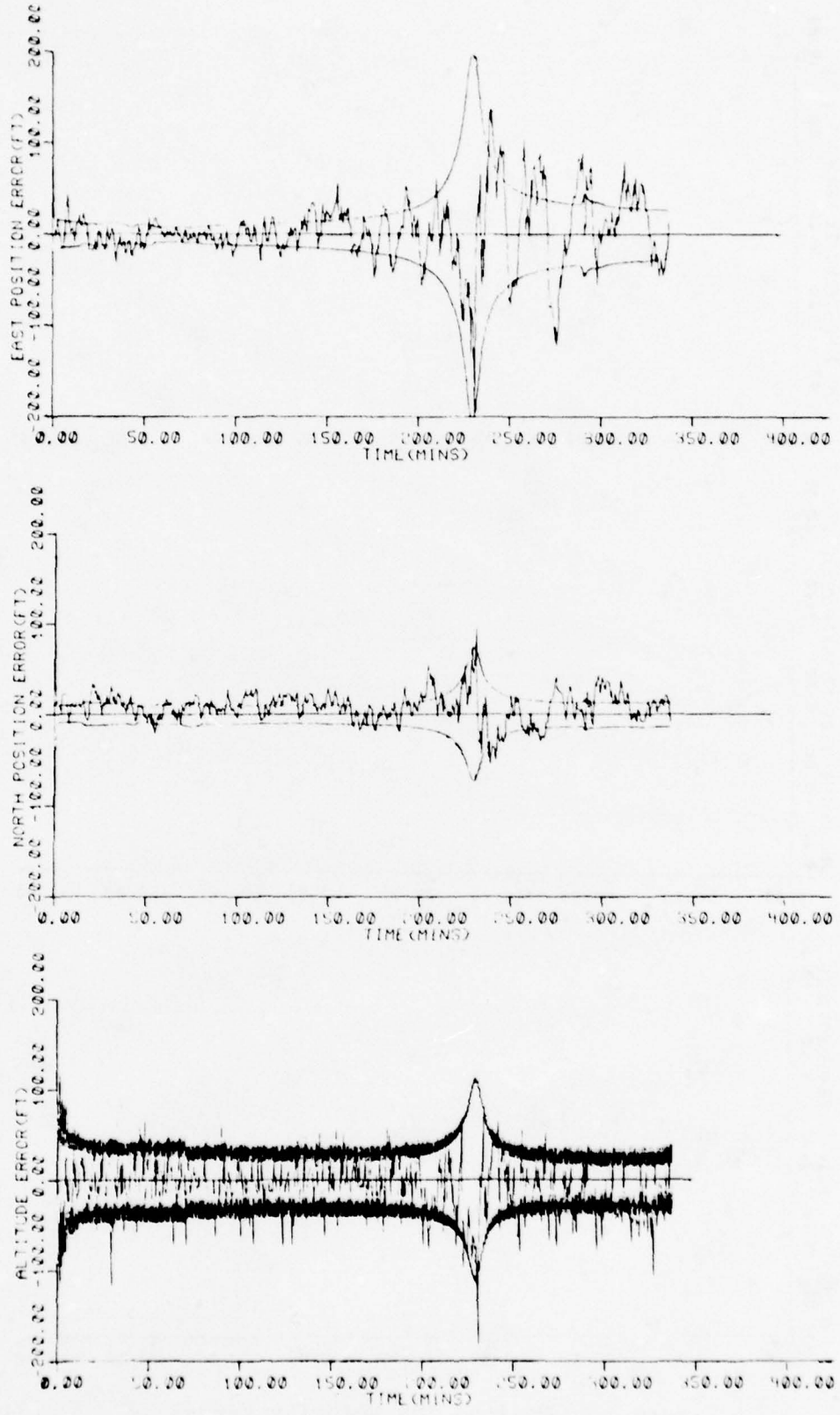

Figure 6: Position Estimation Errors

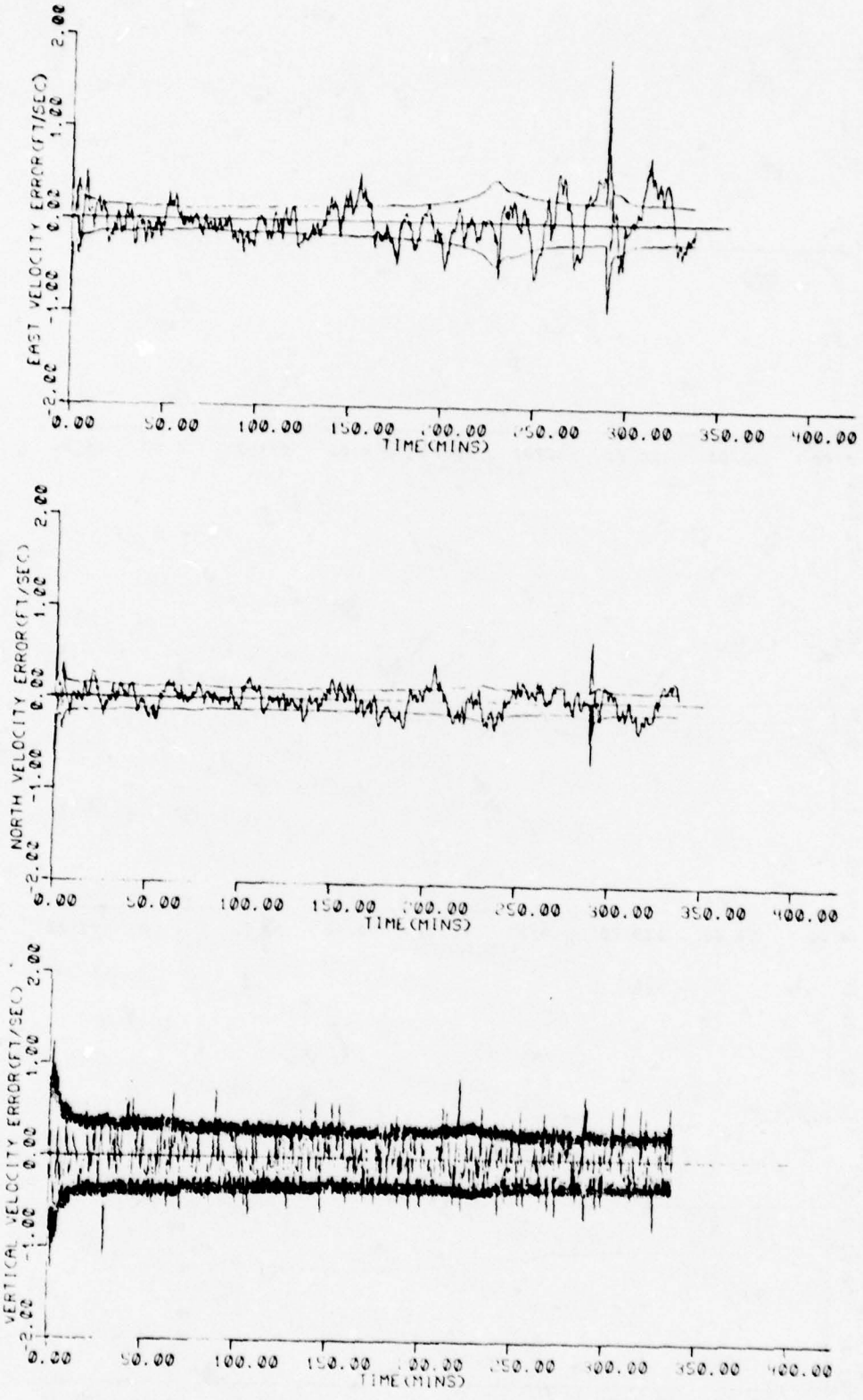

Figure 7: Velocity Estimation Errors

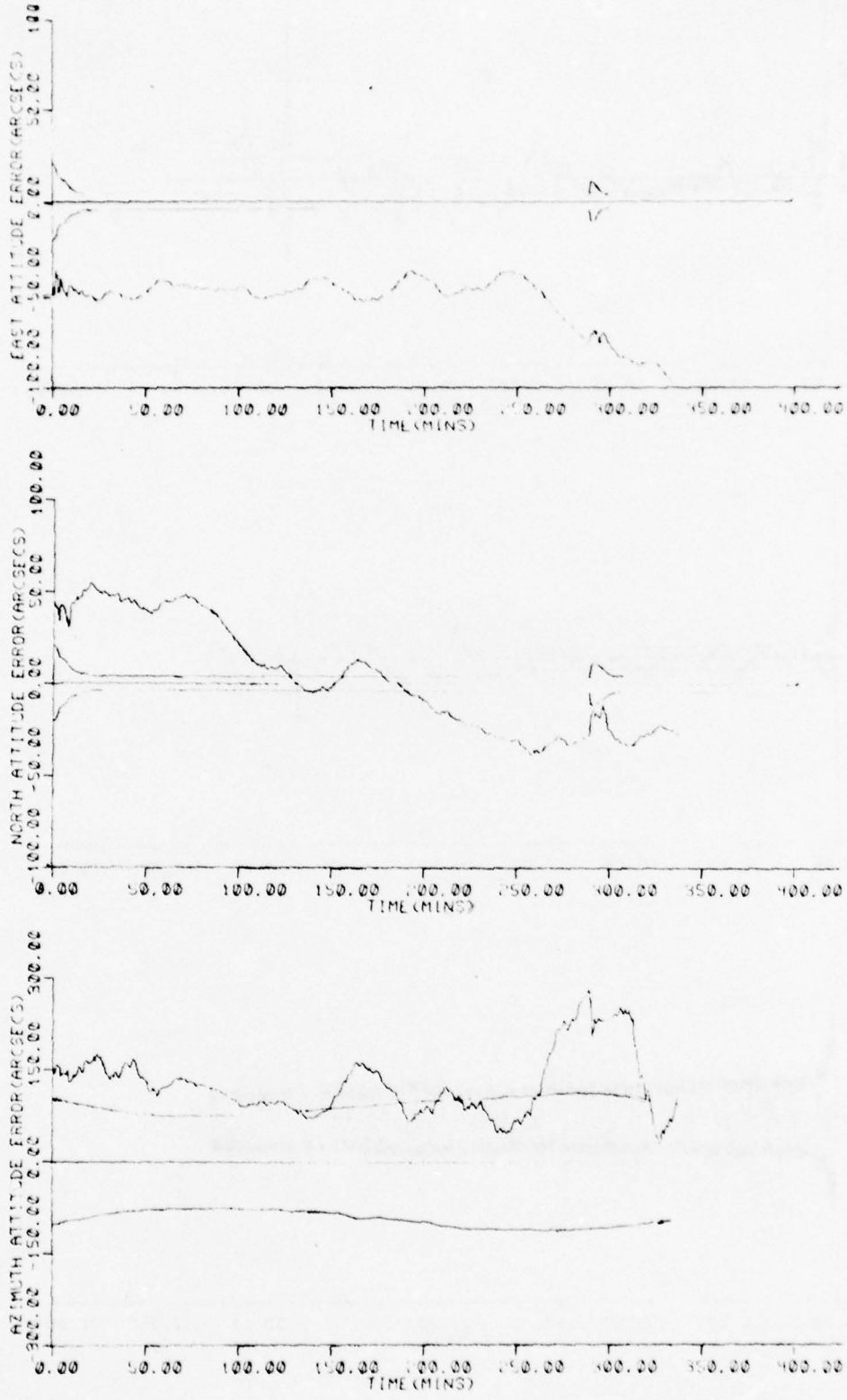

Figure 8: Attitude Estimation Errors

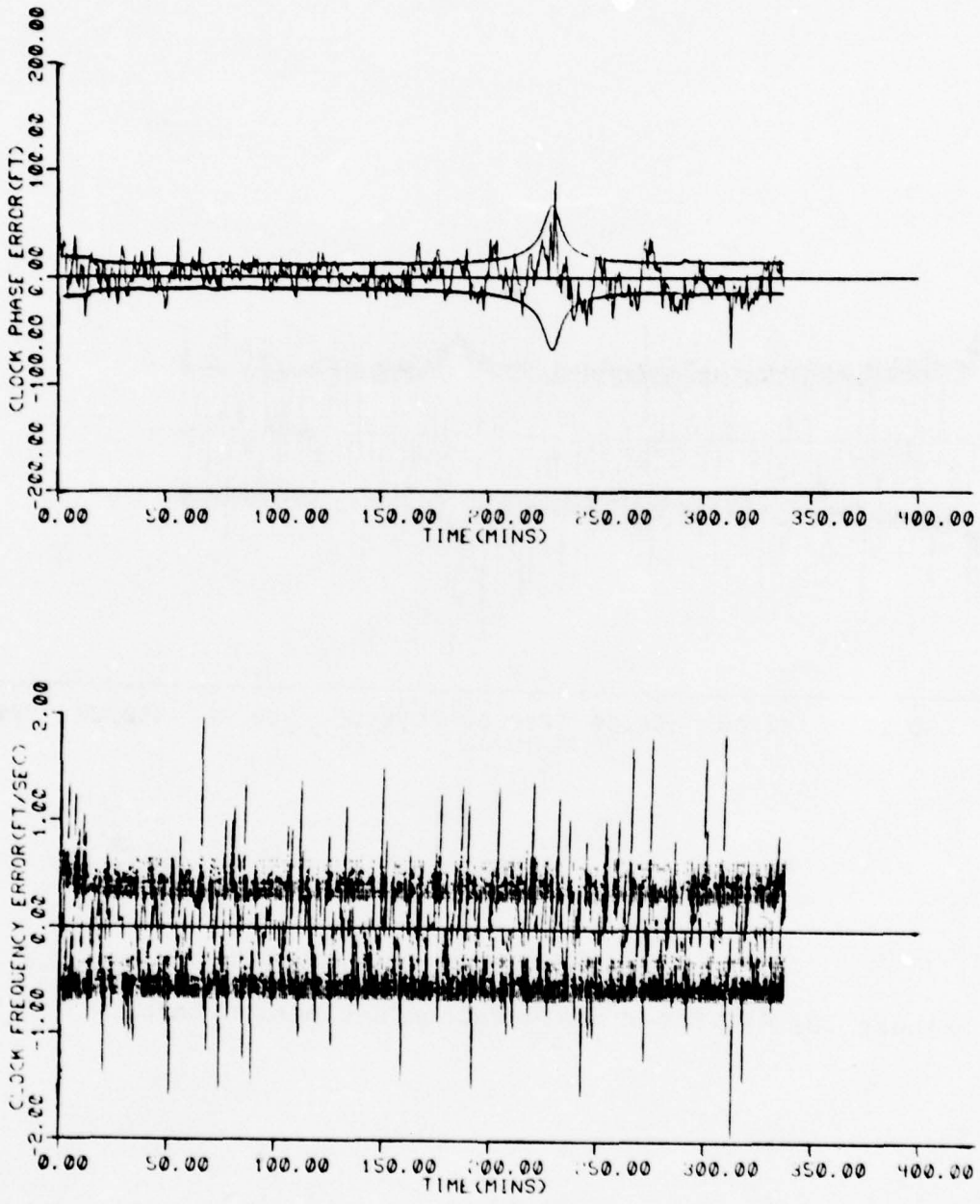

Figure 9: Clock Phase and Frequency Estimation Errors

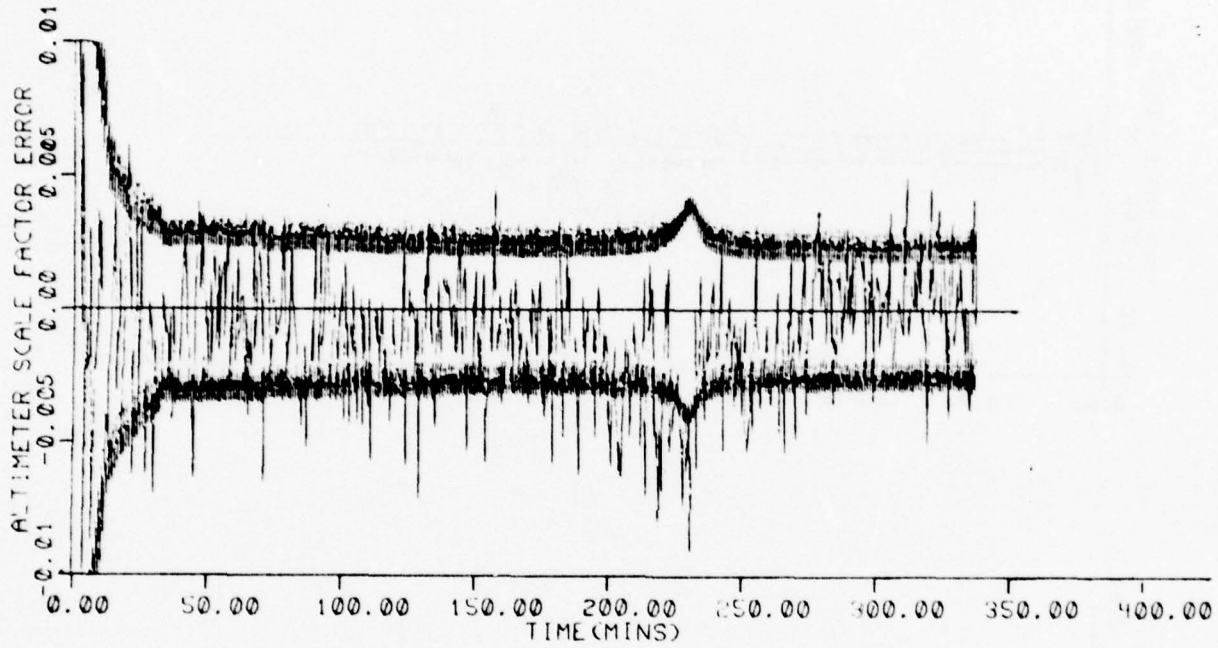

Figure 10: Altimeter Scale Factor Estimation Error

3.3 Comparison of Three Vertical Channel Filter Designs

The results of this Intermetrics study have been published in a separate report, "Comparison of Three Vertical Channel Designs for Integrated GPS/Inertial Navigation Systems", by William S. Widnall and Prasun K. Sinha, dated 27 July 1977 [13]. This section comprises excerpts from Sections 1.3 and 5 of that report.

The IGI Simulator is used to evaluate alternate Kalman filter vertical channel designs. Section 2 summarizes the truth model provided by the simulator. The error models of the baro-inertial navigator and of the GPS measurements are presented. A F4 aircraft trajectory has been selected to drive the error models. This trajectory is also described in Section 2. The baro-inertial navigation errors produced by the assumed sources of error and by the assumed trajectory are plotted and presented.

Section 3 presents a basic recursive (Kalman) filter for blending the inertial navigation and GPS measurement data. Then three alternate vertical channel filter designs are presented:

1. Filter A has two states representing the altimeter sources of error, an altimeter bias state and an altimeter scale factor error state;

2. Filter B has a single altimeter error state, an altimeter bias state;

3. Filter C has a single altimeter error state, a scale factor error state.

Appropriate expressions are developed for the spectral densities of the assumed noises driving these states. These noises model the important sources of error that have not been included as states.

Section 4 presents the results of running each of these three filter designs in the IGI simulator with the same truth model for the errors and with the same F4 trajectory. The comparative performance is discussed.

Conclusions are presented in Section 5.

The Integrated GPS/Inertial (IGI)Simulator has been utilized to explore several design issues associated with the vertical channel of a GPS/baro/inertial navigation system. The primary issues explored were associated with the modeling of barometric altimeter error in the Kalman filter. Should two-state variables be used in the filter to model altimeter error, or is one sufficient? If only one state is used, should it be a bias-like error model or should it be a scale-factor error model? How can an assumed white noise driving a single error state be used to model the effect of other sources of error?

The assumed navigation system is comprised of: a local-level wander azimuth inertial navigation system with associated barometric altimeter for stabilizing the vertical channel, a GPS pseudo range and range-rate receiver, and a navigation computer hosting a Kalman filter to integrate the baro/inertial and GPS data.

The error model in the simulator has fifty-four states representing the inertial navigation position, velocity, and attitude errors, the gyro sources of error, the accelerometer sources of error, the gravity deflections and anomaly, the barometric altimeter sources of error, and the GPS receiver clock phase and frequency errors. Significant sources of barometric altimeter error included are the zero-setting error, the scale factor error, the static pressure measurement error, and the altimeter lag.

The simulated flight path is representative of a F-4 aircraft tactical mission profile. There are periods of straight and level flight, dives and climbs, and high-g evasive maneuvering. There is a seven minute period during which jamming prevents the use of GPS measurements. During this period, the aircraft dives 15,000 feet to a hypothetical target area, then climbs back to altitude.

Three Kalman filter vertical channel designs were evaluated. Filter A has seventeen states and filters B and C have sixteen states. The first fifteen states are common to all three filters. These are the states modeling INS position, velocity, and attitude errors (9); receiver clock phase and frequency errors (2); gyro drift rates (3); and vertical acceleration error (1). The modeling of these fifteen states is similar

to that in the Kalman filter in the original IGI simulator, except that maneuver-dependent variances of the driving noises have been introduced to model the effects of accelerometer scale factor errors and input axis misalignments and to model the effects of gyro g-sensitive drift rates.

Filter A has two states representing the altimeter sources of error: one state a bias error and the other state a scale factor error. Filter B has only one altimeter error state, and it is a random walk bias model. Filter C also has only one altimeter error state, but it is a random walk scale factor error model. The single-state error models have variances for their driving noises that are functions of the altitude changes.

Analysis of the alternate designs, including the comparative simulation results has led to several observations and conclusions. The three filter designs provide essentially identical navigation performance when GPS measurements are available. The differences in performance arise during loss of signal.

Filter A with its two-state altimeter error model provides the best vertical channel performance during loss of signal. After processing external (GPS) measurements during descents and climbs, the filter is able to calibrate both the zero-setting error and the scale factor error. This leads to improved vertical channel performance during the subsequent dive and climb in the period of no external measurements (jamming). In the jamming period, peak altitude error was 400 feet and the largest vertical velocity error was about two feet per second.

Filter B with its single-state altimeter bias model converges to a correct estimate of the combined altimeter error while processing external measurements. During the jamming period, the bias estimate holds constant. In the dives and climbs during the jamming period, the true altimeter scale factor error causes shifts in the altimeter error, which cannot be compensated by filter B. The simulation results exhibited altitude errors from -340 to 680 feet and a peak vertical velocity error of about 3 feet/sec.

Filter C with its single-state altimeter scale factor model has the worst vertical channel performance. The estimate of the effective scale factor

error converges to a correct value while processing external measurements. This effective scale factor error estimate when multiplied by the current altitude gives a value for baro altitude error that matches the total baro altitude error from the several sources of error. During the jamming period, the effective scale factor error estimate holds constant. The accuracy of the baro altitude error estimate, during dives and climbs in this jamming period, depends on the difference between the estimated effective scale factor error and the true scale factor error. In the simulation case, the estimated scale factor error was 0.08 and the true scale factor error was 0.03. The difference of 0.05 provided a strong excitation to the errors in the filter estimates of vertical velocity and altitude. Altitude errors ranged from 770 feet to -885 feet and the peak vertical velocity error was larger than 4 feet/sec. The vertical velocity estimation errors of the filter were actually larger than the vertical velocity errors of the no-filter baro-inertial system. If the period of jamming had started at a higher altitude or had the zero setting error been smaller, then the difference between the effective scale factor error and the true scale factor error would have been smaller and the subsequent vertical channel errors during the dives and climbs would have been smaller.

A filter similar to filter C was evaluated by Myers and Butler. It also had a single-state altimeter error model, which was a scale factor error. However, this state was modeled as a random constant rather than a random walk. In the simulation results, while processing GPS measurements (no jamming) the filter diverged from correct estimates of vertical velocity, altitude, and even latitude and longitude. While we have not attempted to re-run this exact design, we believe the design diverged because of the random constant model. With such a model, the filter will converge to a fixed estimate of the effective scale factor error and the computed uncertainty will go to zero. With complete confidence in its calibrated baro altimeter data, and because of the closed baro-inertial loop, the filter computed uncertainty in the estimate of altitude also goes to zero. The filter then ignores current external (GPS) measurements as far as altitude updating is concerned. If there is actually a large altitude estimation error, the GPS measurement residuals must be put somewhere, and this leads to forced

errors in the estimates of latitude, longitude, and clock phase. The filter C evaluated in this report avoids these performance difficulties by using a random walk error model. The variance assigned to the driving noise is sufficient to prevent the filter from becoming over confident.

The other estimations errors of the three Kalman filter designs were also analyzed. The horizontal position and velocity errors, the attitude errors, and the clock phase and frequency errors for the three cases were essentially identical including during the period of jamming. The differences in the vertical channel designs produced no significant differences in these other errors.

The three filters exhibited good self consistency. The filter computed uncertainties were generally in agreement with the estimation errors. An exception was the north position error, which had a bias value exceeding the computed uncertainty. Changes to the measurement processing are proposed which should eliminate the bias. The horizontal components of attitude error also have values exceeding the computed uncertainties. These biases are the unobservable tips due to various sources of horizontal acceleration measurement error. The maneuver dependent driving noises for the velocity error states, the attitude error states, and the baro altitude error state help provide the desired consistent performance.

SECTION IV
IMPROVED IGI SIMULATOR MODELS

4.1 Chapter Summary

Intermetrics has upgraded the AFAL Integrated GPS/Inertial (IGI) Simulation Program. The new version of the IGI Simulator implements GPS pseudorange and delta-pseudorange plus barometric altimeter error models whose fidelity is comparable to that of the existing inertial navigation system (INS) error models. Emphasis has been placed on the following technical areas:

i) Upgraded barometric altimeter error models;

ii) Upgraded GPS pseudorange and delta-pseudorange error models;

iii) Program structural changes.

These areas are discussed further in subsection 4.2.

4.2 Revised IGI Simulator Computer Program

Results of Intermetrics' effort on upgrading the IGI Simulator have been published in a separate document, "Integrated GPS/Inertial Simulator Computer Program," by Prasun K. Sinha, dated 26 August 1977 [11]. The following paragraphs and figure are excerpted from Sections 1 and 2.1 of that document.

The Air Force Avionics Laboratory (AFAL) is engaged in developing a Generalized Development Model (GDM) of the Global Positioning System (GPS) user equipment. To supplement the GDM and GPS evaluator developments, a computer program has been developed for simulating Integrated GPS/Inertial (IGI) aircraft navigation systems. The IGI Simulator is an analytical tool which can be used to perform system analyses, equipment evaluation studies and to aid in the establishment of specifications for IGI navigation systems. This report documents the August 1977 version of the IGI Simulator and is intended as a user's guide.

The IGI Simulator is described in Section 2 of this report. Section 2 presents the basic equations for propagation of the states of the simulation and filter models. Specific models for simulating the Litton CAINS LN-15 Inertial/GPS and a Kalman filter mechanization are also presented. Section 2 concludes with a brief discussion of the nature of the GPS measurements and a presentation of the GPS measurement processing equations. Section 3 describes the inputs to the Simulator and presents a sample input file. Section 4 describes the outputs from the Simulator and presents a sample of the printout generated using the sample input file of Section 3. While not directly part of the IGI Simulator outputs, Section 4 presents samples of plots generated by the data output by the simulator to a plot file. A complete listing of the August 1977 version of the IGI Simulator is included in Appendix A. Appendix B of this report contains a derivation of the GPS measurement gradient vectors used in the IGI Simulator.

The August 1977 version of the IGI simulator uses a direct linear simulation approach [10] in which the differential equations representing the Inertial Navigation System (INS) indications of position, and velocity as well as the INS attitude errors are linearized about a precomputed reference flight trajectory [12]. The INS indicated data computed in this manner is then processed together with GPS pseudo-range and delta range measurements in a linearized Kalman filter to obtain estimates of errors in the INS indicated position, velocity and other sources of error mechanized in the filter. The user's navigation parameters are then updated using these error estimates. Figure 11 shows a functional diagram of the basic structure of the IGI simulator.

The main monitor program IGISIM, sequences the IGI simulator through the various phases shown in Figure 11. All program initialization that is independent of the simulation and filter error models is carried out in subroutine GPSINIT. The simulation model equations and the filter error model equations are integrated in subroutine STATEUD. The GPS pseudo-range and delta range measurements are incorporated in subroutine MEASUD. Simulation outputs occur in two forms: (i) printed output via subroutine PRINTS, and (ii) output for plotting purposes which is transferred to a plot file via subroutine PLDATA. The true reference trajectory data which drives the INS error model is precomputed by a separate program PROFGEN [12]. Besides driving the error model, the true reference trajectory data is also used to construct simulated true pseudo-range and delta range measurements.

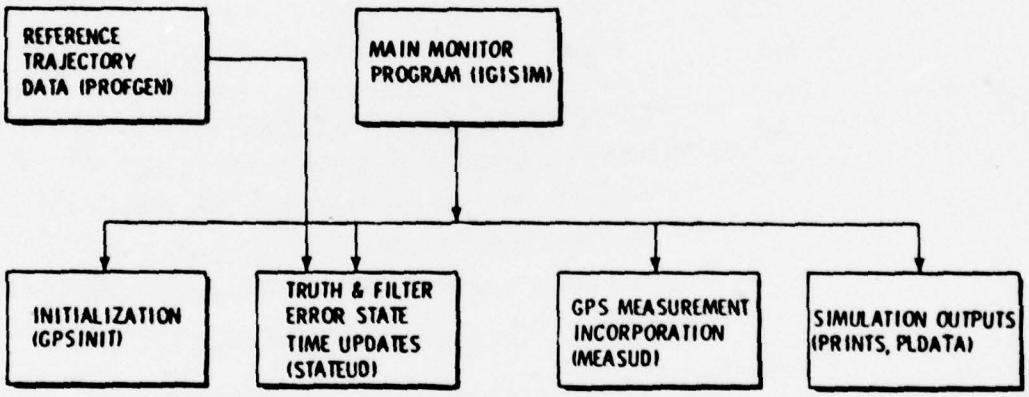

Figure 11: Basic Structure of IGI Simulator

SECTION V
INTEGRATED GPS/STRAPDOWN PERFORMANCE

5.1 Chapter Summary

Intermetrics has added a strapdown inertial simulation capability to the IGI simulator. The error model implemented is that of the Honeywell SIGN-III baro-inertial navigator. This error model was also derived and documented in Ref. [14]. The structure of the error model is quite general, so users of this strapdown version of the IGI simulator can simulate many other strapdown systems simply by altering the values assumed for the individual sources of error.

In the process of checking out the strapdown error model in the IGI simulator, a "stress-test" was conducted using a high-dynamic F4 aircraft trajectory. Analysis indicated that the simulation indeed was giving correct answers, and the large navigation errors observed were explainable by a few key sources of angular velocity error.

Strapdown inertial system characteristics are described in Section 5.2. The integrated GPS/ Strapdown Inertial Simulator and the simulated performance results are described further in Sections 5.3 and 5.4, respectively.

5.2 Strapdown Inertial Navigation Systems

This section is excerpted from Section 1.2 of Ref. [15] by Prasun K. Sinha and William S. Widnall.

Strapdown Inertial Navigation Systems are characterized by having all inertial instruments mounted directly on to the vehicle for which the navigation function is to be provided. The task of physical instrumentation of reference frames by a series of gimbals is thus replaced by on-board computation of the vehicle orientation with respect to a reference frame, based on information from the vehicle-mounted gyros. Strapdown systems therefore requrie a more extensive computer, but may have advantages over gimballed systems in terms of power requirements, packaging flexibility, ease of maintenance, and perhaps cost. A major disadvantage of strapdown systems vis-a-vis the gimballed systems is that they are less accurate.

The primary cause of the strapdown system's inaccuracy is the fact that the inertial angular velocity of the Inertial Measurement Unit (IMU) frame is equal to the inertial angular velocity of the vehicle. The vehicle mounted instruments can thus be subjected to a relatively harsh dynamic environment since there is no gimballed structure to isolate the sensors from the angular motion of the vehicle. Because of these environmental considerations, the instruments are required to have a high dynamic range which usually results in a compromise in accuracy.

5.3 Integrated GPS/Strapdown Inertial Simulator

Intermetrics has produced a second upgraded version of the AFAL IGI Simulator that models a strapdown inertial navigation system, its error sources, and a representative GPS/strapdown navigation filter. This second version of the revised simulator is described in a separate document, "Integrated GPS/Strapdown Inertial Simulator Computer Program," by Prasun K. Sinha, dated December 1977 [16]. The following paragraphs are excerpted from Sections 1 and 2.1 of that document, and pertain to the December 1977 version of the simulator.

The IGI Simulator is described in Section 2 of this report. Section 2 presents the basic equations for propagation of the states of the simulation and filter models. Specific models for simulating the Honeywell SIGN-III Inertial/GPS and a Kalman filter mechanization are also presented. Section 2 concludes with a brief discussion of the nature of the GPS measurements and a presentation of the GPS measurement processing equations. Section 3 describes the inputs to the Simulator and presents a sample input file. Section 4 describes the outputs from the Simulator and presents a sample of the printout generated using the sample input file of Section 3. While not directly part of the IGI Simulator outputs, Section 4 presents samples of plots generated by the data output by the simulator to a plot file. A complete listing of the December 1977 version of the IGI Simulator is included in Appendix A. Appendix B of this report contains a derivation of the GPS measurement gradient vectors used in the IGI Simulator.

The fundamental difference between this December 1977 version of the IGI simulator and the August 1977 version of the IGI simulator (which is documented in Intermetrics Report 236, dated 26 August 1977) is that this simulator includes a strapdown INS error model whereas the earlier simulator includes a local-level INS error model.

The December 1977 version of the IGI Simulator uses a direct linear simulation approach [10] in which the differential equations representing the Inertial Navigation System (INS) indications of position, and velocity as well as the INS alignment variables are linearized about a precomputed reference flight trajectory [12]. The INS indicated data computed in this manner is then processed together with GPS pseudo-range and delta pseudo-range measurements in a linearized Kalman filter to obtain estimates of errors in the INS indicated position, velocity and other sources of error mechanized in the filter. The user's navigation parameters are then updated using these error estimates.

The main monitor program IGISIM, sequences the IGI simulator through the various phases shown in Figure 11. All program initialization that is independent of the simulation and filter error models is carried out in subroutine GPSINIT. The simulation model equations and the filter error model equations are integrated in subroutine STATEUD. The GPS pseudo-range and delta pseudo-range measurements are incorporated in subroutine MEASUD. Simulation outputs occur in two forms: (i) printed output via subroutine PRINTS, and (ii) output for plotting purposes which is transferred to a plot file via subroutine PLDATA. The true reference trajectory data which drives the INS error model is precomputed by a separate program PROFGEN [12]. Besides driving the error model, the true reference trajectory data is also used to construct simulated true pseudo-range and delta pseudo-range measurements.

5.4 Strapdown Inertial Navigation System Performance

The results of Intermetric's simulations of integrated GPS/strapdown inertial system performance have been published in a separate document, "Some Efforts of High Dynamic Trajectories on Strapdown Inertial Navigation System Performance", by Prasun K. Sinha and William S. Widnall, dated 6 January 1978 [15]. This document presents the results obtained from simulation of a typical strapdown inertial navigator mounted in an aircraft such as an F-4 which flies a trajectory representative of a

tactical mission profile. The error model for the strapdown baro-inertial navigator and the flight trajectory which drives the error model are presented in Section II. The results of the simulation are presented and discussed in Section III. Conclusions are presented in Section IV. The conclusions are repeated here as the remainder of this section.

The performance of a typical strapdown inertial navigation system in a high dynamic aircraft flight environment has been simulated. The results demonstrate significant degradations in the three components of INS attitude error as a result of the sustained maneuvering. The large horizontal attitude errors then propagate into large horizontal velocity errors.

The aircraft trajectory included two 360^{o} circles, one turning to the right followed by one turning to the left. Because angular velocity error in a steady turn describes a coning motion in east-north-up coordinates with the axis of symmetry vertical, the resulting sinusoidal east and north components of angular velocity error have no net integral at the end of each complete circle. Hence the horizontal components of attitude error are not significantly changed by a circle.

The azimuth error in circling flight is changed. The sources of error that gave the largest contribution to azimuth error in each circle, for the steeply banked turns simulated, were:

1) the torquer scale factor error of the right-wing axis gyro
2) the misalignments of the belly-axis and right-wing axis gyros about the forward axis
3) the g-sensitivity of the belly-axis gyro to specific force along that axis. The change in azimuth due to the first effect has a sign which depends on whether the aircraft is turning left or right, so its net effect may be small if an aircraft trajectory circles both ways a comparable amount. The second and third effects contribute azimuth error rates whose signs do not depend on whether the aircraft is turning left or right, so their effects rectify. If the circling turns were not steeply banked turns, then one would expect the torquer scale factor error of the belly-axis gyro to also be a significant source of error. And if there is no torquer scale factor asymmetry, this effect will rectify.

The aircraft trajectory also included several segments of coordinated zig-zag maneuvering. Very large attitude error about the forward axis developed during this maneuvering. The sources of error making the largest contribution to forward attitude error were: 1) the assumed gyro torquer scale factor asymmetry of the forward-axis gyro, and 2) the misalignment of the forward-axis gyro about the belly axis.

The first source of error has a large effect because the assumed zig-zag maneuvering involves repeated left and right roll rates along a roughly constant heading. The amplitude of these roll angle changes times the difference between the torquer scale factor error for positive and negative torquing is the net attitude error in the forward direction introduced by each roll-left--roll-right cycle.

The second source of error is signficiant because of an interesting property of coordinated turns in aircraft. Regardless of whether the aircraft is turning to the left or turning to the right, the angular velocity component along the right-wing is positive. Hence the forward-axis gyro, if misaligned about the belly-axis, always contributes a forward-axis angular velocity error in a turn whose sign is independent of the turn direction.

The sources of error that gave the largest contribution to up (or azimuth) attitude error, for zig-zag portions of the trajectory, were 1) the misalignment of the belly-axis and right wing axis gyros about the forward axis, 2) the g-sensitivity of the belly-axis gyro to specific force along that axis, and 3) the belly-axis gyro torquer scale factor asymmetry. The torquer scale factor error of the right-wing axis gyro was not one of the largest contributors to azimuth error in the zig-zag maneuvering because its contribution in a right turn is the negative of its contribution in a left turn (equal bank angles assumed.)

The attitude errors of this strapdown system in this highly maneuvering environment are large compared with the attitude errors of a typical local level inertial system subjected to the same environment. The resulting horizontal velocity and position errors are large compared with the errors of a local level system in the same environment. The reader who wishes to make such a comparison may refer to Reference[13], in which the error model of a local level LN-15 is exercised using the same high-dynamic aircraft trajectory.

SECTION VI
EAR/GEANS ERROR ISOLATION FILTER SUPPORT

6.1 Chapter Summary

The Air Force Avionics Laboratory (AFAL) is sponsoring the integration of the Westinghouse-developed Electronically Agile Radar (EAR) with the Honeywell Gimballed Electrostatic Gyro Aircraft Navigation System (GEANS) to provide accurate inflight estimates of position and velocity as a function of time. In addition, AFAL is supporting the EAR/GEANS program by developing flight data analysis software to obtain a performance assessment after each flight.

The flight data analysis software is to take the form of an Error Isolation Filter (EIF) computer program. The EIF is a high-order Kalman filter/smoother designed to yield refined trajectory estimates and to detect off-nominal performance in various subsystems (EAR radar, INS, altimeter, etc.).

Intermetrics has provided analytic support to AFAL in several areas related to the EAR/GEANS EIF development. Specific issues that have been analyzed in depth are the following:

i) EAR/GEANS EIF development plan;

ii) Vertical channel error model for the EAR/GEANS;

iii) Fundamental error dynamics for a space stable navigator;

iv) Error model for the baro-damped GEANS inertial navigator;

v) Radar measurements and measurement matrices for EAR;

vi) Geodetic error models for simulating and estimating INS error behavior;

vii) EAR flight test data recording requirements;

viii) Filter synthesis for the EAR/GEANS Error Isolation Filter;

ix) Feedback correction equations for EAR/GEANS EIF;

x) Filter/Smoother Mechanization Equations for EAR/GEANS EIF.

Results of these analyses are presented in Sections 6.2 to 6.11.

6.2 EAR/GEANS EIF Development Plan

Results of Intermetrics' effort on this subtask have been published in a separate document, "Error Isolation Filter for EAR/GEANS Development Plan," by Peter A. Grundy, dated 30 September 1977 [22].

This document outlines a proposed development plan for the EIF for the EAR/GEANS system. It addresses five broad areas which constitute the principal steps in the computer program development and qualification, to wit:

i) Analysis;

ii) Top-level design and interface definition;

iii) Detailed design and coding;

iv) Testing;

v) Maintenance.

In addition, the report addresses the interleaving and sequencing of these tasks and outlines a preliminary schedule and manloading plan.

6.3 Vertical Channel Error Model for EAR/GEANS

This section comprises Intermetrics AFAL/GPS Analysis Memo #07-77, "Review of AFAL Technical Memorandum 'A Vertical Channel Error Model for EAR/GEANS'", by Peter A. Grundy, dated 22 September 1977 [23]. The subject AFAL technical memorandum is Reference [24].

I have reviewed the above referenced memo as requested in our EAR/GEANS EIF support effort task statement. The following comments seem to be appropriate.

6.3.1 Observability in Second-Order Damping Loop

We are in agreement as to the appropriate models (Eqs. (9) and (11) in the above memo) for third and second order damping loops. I would, however, like to point out an additional characteristic of the second order loop performance, which may impact the EIF design.

Consider the four state model for the second order vertical channel

$$\begin{bmatrix} \dot{\delta h} \\ \dot{\delta v_z} \\ \dot{\delta a_z} \\ \dot{\delta h_b} \end{bmatrix} = \begin{bmatrix} -c_1 & 1+c_1c_4 & 0 & c_1 \\ -c_2+2w_s^2 & c_2c_4 & 0 & c_2 \\ 0 & 0 & 0 & 0 \\ 0 & 0 & 0 & 0 \end{bmatrix} \begin{bmatrix} \delta h \\ \delta v_z \\ \delta a_z \\ \delta h_b \end{bmatrix} + \underline{w}$$

$$\dot{\underline{x}} = F \underline{x} + \underline{w} \qquad (6.3\text{-}1)$$

The corresponding frequency domain equations can be readily derived as

$$(s^2+(c_1-c_2c_4)s + c_2-2w_s^2[1+c_1c_4])\delta h = (1+c_1c_4)\delta a_z + (c_1s+c_2)\delta h_b$$

$$(s^2+(c_1-c_2c_4)s + c_2-2w_s^2[1+c_1c_4])\delta v_z = (s+c_1)\delta a_z + (c_2s+2w_s^2c_1)\delta h_b$$

(6.3-2)

Using the final value theorem, it can be seen that, for step inputs of vertical acceleration error δa_z and barometric altitude error δh_b, the steady-state altitude and velocity errors are given by

$$\delta h_{ss} = \frac{1+c_1c_4}{c_2-2w_s^2(1+c_1c_4)}\,\delta A_z + \frac{c_2}{c_2-2w_s^2(1+c_1c_4)}\,\delta H_b$$

$$\delta v_{z_{ss}} = \frac{c_1}{c_2-2w_s^2(1+c_1c_4)}\,\delta A_z + \frac{2w_s^2c_1}{c_2-2w_s^2(1+c_1c_4)}\,\delta H_b \qquad (6.3\text{-}3)$$

where δA_z, δH_b are the magnitudes of the forcing function steps. Note that if the vertical acceleration error step magnitude (e.g., vertical accelerometer bias) and the barometric altitude error satisfy the relation

$$\delta A_z = -\frac{c_2}{1+c_1c_4}\,\delta H_b \qquad (6.3\text{-}4)$$

the steady state altitude error is zero but a vertical velocity bias of

$$\delta v_z = \frac{c_1}{c_2}\,\delta A_z \qquad (6.3\text{-}5)$$

persists. Measurements of aircraft altitude alone do not provide observation of the vertical velocity error or separation of vertical acceleration and barometric altitude error biases.

Stated in another fashion, substitution of the state

$$\begin{bmatrix} \delta h \\ \delta v_z \\ \delta a_z \\ \delta h_b \end{bmatrix} = \begin{bmatrix} 0 \\ c_1/c_2 \\ 1 \\ -(1+c_1c_4)/c_2 \end{bmatrix} \delta A_z \qquad (6.3\text{-}6)$$

into Equation (1) yield a zero state time-derivative vector. This state therefore represents a possible constant system mode with zero altitude error. Note that a 100 μg vertical acceleration error results in a substantial .36 m/sec vertical velocity error bias.

Recurr now to the standard definition of observability. For an n-dimensional state vector $\underline{x}$, we observe the rank of the observability matrix

$$Z = \begin{bmatrix} H \\ H\ F \\ \vdots \\ H\ F^{n-1} \end{bmatrix} \qquad (6.3\text{-}7)$$

where H is the measurement gradient matrix. For the error state considered, H, for an altitude measurement, is given by

$$H = [1\ 0\ 0\ 0] \qquad (6.3\text{-}8)$$

The observability matrix is, therefore

$$Z = \begin{bmatrix} 1 & 0 & 0 & 0 \\ -c_1 & 1+c_1c_4 & 0 & c_1 \\ c_1a+d & -(1+c_1c_4)a & 1+c_1c_4 & -c_1a+c_2 \\ -(c_1a+d)a - c_1d & (1+c_1c_4)(a^2+d) & -(1+c_1c_4)a & (c_1a-c_2)a + c_1d \end{bmatrix} \tag{6.3-9}$$

where

$$a = c_1 - c_2c_4$$

$$d = 2w_s{}^2(1+c_1c_4) - c_2$$

The fourth row is readily seen to be a linear combination of the second and third rows

$$\text{row}_4 = d\,\text{row}_2 - a\,\text{row}_3 \tag{6.3-10}$$

The rank of Z is then three and the system has one unobservable mode.

Error state observability can be obtained through additional measurements:

i) inertial altitude difference measurement - i.e., the difference between INS and barometric indicated altitude. For this measurement, the gradient matrix is

$$H = [1\ 0\ 0\ -1] \tag{6.3-11}$$

The observability matrix for three altitude measurements plus one altitude-difference measurement can be shown to be of the full rank.

Practical observability with this measurement, however, is another matter. For the gains given in the memo

$$c_1 = .01 \text{ sec}^{-1}$$

$$c_2 = 2.81 \times 10^{-5} \text{ sec}^{-2} \qquad (6.3\text{-}12)$$

$$c_4 = 1 \text{ sec}$$

for each 10 meters of short-correlation baro-altitude error, a corresponding vertical acceleration estimation uncertainty of

$$\sigma_{\delta a_z} = 28 \text{ } \mu g\text{'s} \qquad (6.3\text{-}13)$$

will result. Furthermore, the filter designer must also consider that the noise in the altitude difference measurement is correlated with the error state driving noise, so further deweighting of the altitude difference measurement would result.

ii) Direct velocity measurement - i.e., the difference between the INS indicated and an external measure of vertical velocity. For this measurement, the gradient matrix is

$$H = [0 \ 1 \ 0 \ 0] \qquad (6.3\text{-}14)$$

and the observability matrix resulting from a combination of altitude and vertical velocity measurements can be shown to be of full rank. I understand this to be the main operating mode of the system, where the EAR radar is obtaining both position and velocity measurements, so the above comments are not directly relevant. However, should the radar fail in flight, and the analyst desire to evaluate GEANS by comparison to CIRIS data, the above observations become directly relevant.

6.4 Fundamental Error Dynamics for a Space Stable Navigator

This section comprises Intermetrics AFAL/GPS Analysis Memo #08-77, "Review of AFAL Technical Memorandum 'Fundamental Error Dynamics for a Space Stable Navigator'," by Peter A. Grundy, dated 22 September 1977 [25]. The subject AFAL Technical Memorandum is Ref. [26].

We are in agreement as to the developed fundamental error model. We suggest, however, the slightly different and simpler derivation of the platform attitude error expressions.

The inertial system misalignment or attitude error is contained in the error in the coordinate transformation matrix $\hat{C}^i_p$. For small angles, we can define this error to be a vector $\underline{\beta}$.

The computed transformation matrix is related to the true by the expression (Ref.[27], pp. 21-22, 25)

$$\hat{C}^i_p = (I - B^i)C^i_p \tag{6.4-1}$$

where B^i is the skew-symmetric-matrix form of the vector β. Taking the time derivative of the above equation

$$\dot{\hat{C}}^i_p = -\dot{B}^i C^i_p + (I - B^i)\dot{C}^i_p \tag{6.4-2}$$

The time derivative of the direction cosine matrices is given by (Ref. [27] pp. 16-17)

$$\begin{aligned} \dot{\hat{C}}^i_p &= \hat{C}^i_p \hat{\Omega}^p_{ip} \\ \dot{C}^i_p &= C^i_p \Omega^p_{ip} \end{aligned} \tag{6.4-3}$$

where $\hat{\Omega}^p_{ip}$, Ω^p_{ip} are the skew-symmetric-matrix form of the

angular velocity vectors $\hat{\underline{w}}^p_{ip}$, $\underline{w}^p_{ip}$.

Hence, we obtain

$$\hat{C}^i_p \, \hat{\Omega}^p_{ip} = -\dot{B}^i \, C^i_p + (I - B^i) C^i_p \, \Omega^p_{ip} \qquad (6.4\text{-}4)$$

We define the angular velocity error of the platform with respect to inertial space as

$$\delta \underline{w}^p_{ip} = \hat{\underline{w}}^p_{ip} - \underline{w}^p_{ip} \qquad (6.4\text{-}5)$$

Substituting Equations (1) and (5) (in skew-symmetric-matrix form) into Equation (4), and neglecting second order terms, yields

$$\dot{B}^i = -C^i_p \, \delta\Omega^p_{ip} \, C^p_i \qquad (6.4\text{-}6)$$

which in column vector form, is written as

$$\dot{\underline{\beta}}_i = -C^i_p \, \delta \underline{w}^p_{ip} \qquad (6.4\text{-}7)$$

6.5 Error Model for the Baro-Damped GEANS Inertial Navigator

This section comprises Intermetrics' AFAL/GPS Analysis Memo #09-77, "Review of AFAL Technical Memorandum 'An Error Model for the Baro-Damped GEANS Inertial Navigator'," by Peter A. Grundy, dated 18 October 1977[28]. The subject AFAL Technical Memorandum is Ref. [29].

Comments on the above memo contents are directs to three general areas.

6.5.1 Formulation of Vertical Channel Aiding Error Model

This area exhibits the normal awkwardness associated with describing effects associated with the geographic frame in another coordinate system. While the formulation hangs together, numerous approximations are required to obtain a reasonably simple set of error differential equations. Error differential equations for terrestrial navigators are more naturally expressed in the frame they are attempting to navigate, i.e., that defined by geographic longitude, latitude and altitude.

A couple of particular observations in relation to the analytical development in this area are submitted for your consideration. In relation to equation (3-9) in the memo, the approximation

$$r_o \cos D_o \approx r_o \qquad (6.5\text{-}1)$$

is not by itself a good approximation. The deviation of the vertical D_o, at Dayton latitudes, approaches its maximum value of ~3 mrads. The error in the approximation of equation (1) is therefore

$$\frac{1}{2} r_o D_o^2 \sim 90 \text{ ft} \qquad (6.5\text{-}2)$$

If this approximation error persisted through the formulation, it would be interpreted by the estimator as a reference (baro) altitude error. Note, furthermore, that the error magnitude is comparable to the assumed steady-state standard deviation for the "error in Blanchard-computed altitude" state e_{BA} and hence is not readily negligible.

The above approximation is partially compensated, however, by the additional approximation

$$(C_n^i \underline{u}_h^n)^T \underline{r}^i \approx |r| \qquad (6.5\text{-}3)$$

so that the total computation error for Δh is less than 1 ft. and clearly negligible.

The above considerations are brought up because it is not explicitly stated in the memo what the GEANS algorithms for computation of the aiding variable Δh is. The onboard scheme should be carefully analyzed to ascertain the absence of deterministic error forcing functions such as that described by equation (6.5-1).

6.5.2 Computation of Geographic Coordinates

It is not clear to this reader what the intended use of the formulas presented in Sections 3.4 and 4.7 for computation of geographic coordinates are. It should, however, be pointed out that the stated expressions contain significant errors.

Consider, in particular, the expression for computation of geographic latitude L (equation (3-19) in the memo). Referring to the elliptical cross-section depicted in Fig. 12 it can be shown that the geographic latitude L is related to the geocentric latitude L_{CO} of a point on the surface of the ellipsoid by the expression

$$\tan L_{CO} = (1-e^2) \tan L \qquad (6.5\text{-}4)$$

where e is the eccentricity of the reference ellipsoid. For the WGS-72 earth model, e = .08181881066; hence

$$L = \arctan(1.00673966 \tan L_{CO}) \qquad (6.5\text{-}5)$$

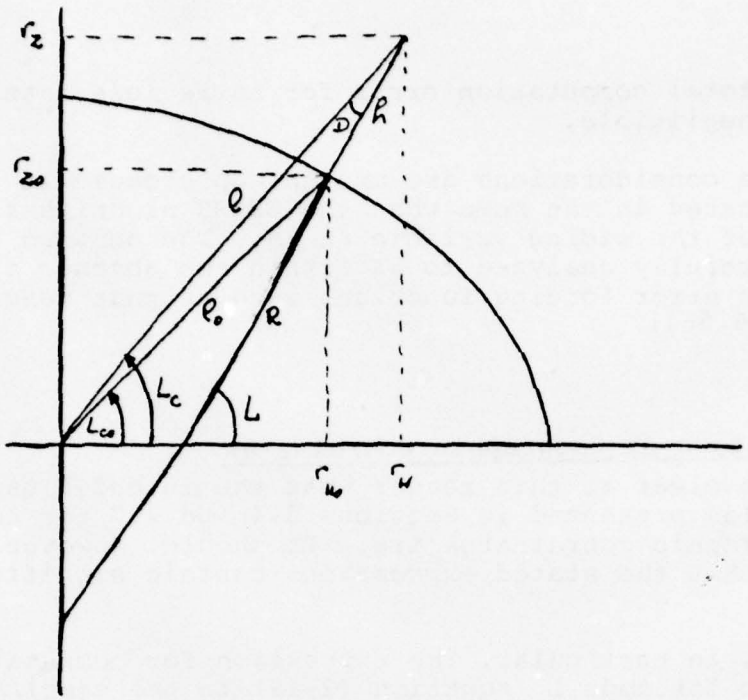

Figure 12: Elliptical Cross-Section

Note, however, that the aircraft at altitude h, has not changed geographic latitude. The geocentric latitude, as determined from

$$L_c = \arctan \frac{r_z}{r_H} \qquad (6.5\text{-}6)$$

has certainly changed from its surface value of L_{CO}. Alternatively, aircraft motion along the geocentric radius ρ causes geographic latitude to change while geocentric latitude remains constant. Equation(-5) (or equation (3-19) in the memo) do not reflect this effect.

An alternative algorithm obtains L_C as in equation(-6). The geographic latitude differs from this value by the deviation of the vertical D

$$L = L_C + D \qquad (6.5\text{-}7)$$

The deviation of the vertical is given by

$$D = f \sin 2L_C (1-h/a) + \frac{1}{2} f^2 \sin 2L_C (2 \cos 2L_C + 1) + O(f^3) \qquad (6.5\text{-}8)$$

to an accuracy of .5 ft, where f is the earth's flattening

$$(1-f)^2 = 1-e^2 \qquad (6.5\text{-}9)$$

and a is the earth's equatorial radius.

Note that, at 45° latitude, neglecting the altitude effect, causes a geographic north position error of ~3 ft per 1000 ft of aircraft altitude. This computation error is clearly unacceptable for such purposes as comparison of GEANS solution to CIRIS solution.

From similar considerations as above, computation of latitude and longitude errors from north and east position errors should rely on the north and east radii of curvature

$$\rho_N = a(1-e^2)/(1-e^2 \sin^2 L)^{3/2}$$
$$\rho_E = a \cos L/(1-e^2 \sin^2 L) \qquad (6.5\text{-}10)$$

rather than the equatorial radius as in equations (4-17) and (4-18). The involved errors are of the order of 3 ft per 1000 ft of position error at 45° latitude.

6.5.3 Gyro Error Model

As formulated in the model, the RATS drift error is inseparable from the Z gyro g-insensitive drift state. This fact is apparent from the following two considerations:

i) Both states are modeled as random constants

ii) Both states contribute identically to the observables. That is, both states directly drive the platform attitude errors through the coefficient vector

$$\underline{c} = \begin{bmatrix} \frac{1}{\sqrt{2}} (a_{11} - a_{12}) \\ \frac{1}{\sqrt{2}} (a_{21} - a_{22}) \\ \frac{1}{\sqrt{2}} (a_{31} - a_{32}) \end{bmatrix} \qquad (6.5\text{-}11)$$

6.6 Radar Measurements and Measurement Matrices for EAR

This section comprises Intermetrics AFAL/GPS Analysis Memo #10-77, "Review of AFAL Technical Memorandum 'Radar Measurements and Measurement Matrices for EAR'," by Peter A. Grundy, dated 18 October 1977 [30]. The subject AFAL Technical Memorandum is Ref. [31].

The developed measurement sensitivity matrices properly represent the geometrical relation between measurement residuals and system errors. However, I do not understand the EAR measurement process sufficiently well to comment on the measurement error model itself.

In particular, items of concern include

- The model assumes the sensor measurement error to be purely random. Is this an adequate representation?
- Is there significant cross-coupling between the various EAR measurements? For example, is the checkpoint position error significant relative to the truly random measurement noise so that the additive errors in the position measurement quadruple should be considered highly correlated?
- How is the position ambiguity resulting from the range/range-rate fix resolved? Does this resolution affect azimuth/elevation measurement errors in poorly conditioned geometries?

The above issues, if relevant, may affect the EIF filter synthesis process.

6.7 EAR Flight Test Data Recording Requirements

This section comprises Intermetrics' AFAL/GPS Analysis Memo #78-01, "Review of AFAL Technical Memorandum 'EAR Flight Test Data to be Recorded on the CIRIS Recorder for Error Isolation Filter Postprocessing'," by Lawrence F. Wiederholt, dated 26 January 1978 [32]. The subject AFAL Technical Memorandum is Ref. [33].

In general, the data recording requirements are sufficient to operate the EIF. Two areas commented on here are the specific force determination and the unit vectors associated with the measurements.

No accelerometer data is directly recorded because of the high data rates involved. Instead, specific forces will be computed by back-differencing $\underline{r}$ and solving Eq. (3-12b) of Ref. [29] for f^P. This method of determining specific forces is acceptable because a high accuracy is not required for the transition matrix which is the only use made of specific force. This approach was used on the CIRIS program.

Unit vectors associated with the velocity and position measurements (Block 2 and 3) are recorded. These unit vectors are required for the H matrix evaluation and probably for the EIF residual computation also. This depends on the exact form used to compute the EIF residuals which has not been completely defined yet. The concern is whether flight recorded values from the onboard system or computed values from the EIF computation should be used. In forming the residuals EIF computed values should be used because they are more accurate than the flight recorded values. Because of the sensitivity of the state vector update to errors in the residual, the most accurate values available should be used.

The state vector update is less sensitive to the H matrix evaulation, so use of flight recorded values here may be acceptable although an analysis should be performed to justify this usage. Using flight recorded values eliminates the need to compute the unit vectors in the EIF, yet if they are computed for the residual they should be used for the H matrix also. One may still want to record the unit vectors to provide measurement direction information useful to the analyst. Also the computations required to define the unit vectors in the EIF should be examined to insure having all the required data.

6.8 Geodetic Error Models for Simulating and Estimating INS Error Behavior

This section comprises Intermetrics AFAL/GPS Analysis Memo #78-02, "Review of AFAL Memorandum ' Geodetic Error Models for Simulating and Estimating INS Error Behavior', AFAL-TM-77-44," by Peter A. Grundy, dated 6 March 1978 [34]. The subject AFAL technical memorandum is Ref. [35].

6.8.1 Introduction

This memo contains comments and recommendations resulting from a review of the above referenced document. Section-2 of this memo defines the geodetic error quantities and discusses their significance for the EAR/GEANS error source recovery problem. Section-3reviews relevant papers quoted in your memorandum in terms of their implications for this process, and Section-4 summarizes conclusions and suggestions reached in this analysis.

6.8.2 Basic Concepts

Geodetic errors represent a source of acceleration disturbance for an inertial navigator attempting to track a vehicle's position relative to the reference ellipsoid. In particular, for a high accuracy system such as GEANS, they represent one of the limiting effects on navigation performance.

The gravity disturbance vector $\delta\underline{g}$ is defined as the difference between the actual and modeled gravity vectors when evaluated at the same point

$$\delta\underline{g} \equiv \underline{g}_{actual}\Big|_p - \underline{g}_{model}\Big|_p \qquad (6.8\text{-}1)$$

The gravity disturbance vector $\delta\underline{g}$ is expressed in geodetic coordinates (north-east-down) as

$$\delta\underline{g}^n = \begin{bmatrix} g_o\,\zeta \\ -g_o\,\eta \\ \Delta g \end{bmatrix} \qquad (6.8\text{-}2)$$

where

ζ = gravity deflection about east

η = gravity deflection about north

Δg = gravity anomaly

g_o = gravity magnitude

In addition, the undulation N is defined as the altitude difference between the actual surface of constant gravity potential (the "geoid") and the modeled surface (the "reference ellipsoid").

Gravity disturbances enter the inertial solution because accelerometers measure specific force $\underline{f}_m$. In order to generate acceleration for integration of the inertial navigation equations, a modeled value of gravity must be added to it

$$\hat{\underline{a}} = \underline{f}_m + \underline{g}_{model} \qquad (6.8\text{-}3)$$

An inertial navigator's vertical channel is inherently unstable, and must be stabilized through some external altitude reference. Such external references (e.g., baro-altimeter) provide altitude with respect to the geoid, and hence, cause an error in the INS indication of altitude over the reference ellipsoid.

In general, geodetic errors are partitioned into global and local components, depending on the area of interest. Global errors, for the restricted area flights envisioned for EAR/GEANS, appear as acceleration error biases to the INS. For local-level navigators, such global errors are indistinguishable from accelerometer biases due to the quasi-constant orientation of the instruments to the gravity error components. In strapdown systems, such correlation does not develop, because the instruments can be rapidly rotated. Space-stable systems represent an in-between case, where the separability depends on the level of stability that can be assumed for the instrument error sources.

To illustrate, for an at-rest system, the platform rotates, with respect to local geodetic axes, at earth rate (15°/hr). Assuming that the instruments are initially aligned with these axes, after three hours they have rotated 45° relative to the gravity disturbance components. If the instrument errors are sufficiently stable, some of the error sources are clearly separable.

Although local gravity disturbances are actually deterministic, they are usually treated at zero-mean, two-dimensional spatial random processes because of their wide frequency spectrums. This type of modeling is specially suited to optimal (Kalman) estimation applications. This is the case for the EAR/GEANS problem, where it is proposed to apply a Kalman estimator to recover the system sources of error in the presence of external disturbances, of which gravity errors are a prime example.

Two properties usually associated with local gravity error models are that 1) they are homogeneous; that is, the spatial autocorrelation (acf) function at any point is only a function of the distance shifts

$$\phi(x, y, x+\Delta x, y+\Delta y) = \phi(\Delta x, \Delta y) \qquad (6.8\text{-}4)$$

and 2) they are isotropic; that is, that acfs are independent of direction of shift

$$\phi(\Delta x, \Delta y) = \phi(r)$$

$$r = \sqrt{\Delta x^2 + \Delta y^2} \qquad (6.8\text{-}5)$$

6.8.3 Literature Review

This section considers some of the documents referenced in your memorandum, from the point of view of their application to the EAR/GEANS error analysis problem. The discussion is divided into three subsections: 1) modeling, with review of papers by Shaw et al [36], Kasper [37], Jordan [38,39]. Nash [40], and Bernstein and Hess[41]; 2) estimation, containing a discussion of the Rose and Nash[42]paper; and 3) compensation, with consideration of documents by Chatfield et al [43]and Junkins[44].

6.8.3.1 Quality Error Modeling

6.8.3.1.1 Space-Domain Models

Two standard papers (Shaw, Paul and Henrikson[36], and Jordan[38]) establish the theoretical basis for gravity error model development. Shaw et al demonstrate that local vertical deflection components can be treated as the outputs of a linear two-dimensional system driven by a random input (gravity anomalies), with the frequency response function of the linear system derived from the flat earth approximation to the Vening Meinesz formulas [46] They show that for any homogeneous, isotropic model for the gravity anomaly, the correlation functions for the vertical deflection components are given by

$$\phi_{\zeta\zeta}(\rho_1,\rho_2) = \sigma_\delta^2[\phi_{gg}(r)/\sigma_g^2 - f(r)\cos 2\Theta]$$

$$\phi_{\eta\eta}(\rho_1,\rho_2) = \sigma_\delta^2[\phi_{gg}(r)/\sigma_g^2 + f(r)\cos 2\Theta] \qquad (6.8\text{-}6)$$

$$\phi_{\zeta\eta}(\rho_1,\rho_2) = \phi_{\eta\zeta}(\rho_1,\rho_2) = -\sigma_\delta^2 f(r)\sin 2\Theta$$

where

σ_δ^2 = deflection variance

ϕ_{gg} = anomaly autocorrelation function

σ_g^2 = anomaly variance

r = shift distance = $\sqrt{\rho_1^2 + \rho_2^2}$

Θ = shift angle from north = $\tan^{-1}(\rho_1/\rho_2)$

f = anomaly model dependent function

Shaw et al point out that the deflection variance σ, independently of the selected anomaly model, is given by

$$\sigma_\delta^2 = \sigma_g^2 / 2g_o^2 \qquad (6.8\text{-}7)$$

as long as the anomaly is isotropic and homogeneous; and that, even though the anomaly process is isotropic, the deflection statistics are direction dependent. The deflections can only be considered isotropic in an ensemble sense, i.e., when averaged over a uniformly distributed shift angle Θ.

In addition, Jordan[38] derives theoretical constraints between deflections and anomaly and the undulation of the geoid, thus allowing formulation of consistent statistics for all four geodetic quantities. The undulation and anomaly autocorrelation functions are related through the two-dimensional Poisson equation

$$\left(\frac{\partial^2}{\partial\rho_1^2} + \frac{\partial^2}{\partial\rho_2^2}\right)\phi_{NN}(\rho_1,\rho_2) = -\frac{1}{g_o^2}\,\phi_{gg}(\rho_1,\rho_2) \qquad (6.8\text{-}8)$$

while the deflections satisfy

$$\phi_{\zeta\zeta}(\rho_1,\rho_2) = -\frac{\partial^2\phi_{NN}}{\partial\rho_2^2}(\rho_1,\rho_2)$$

$$\phi_{\eta\eta}(\rho_1,\rho_2) = -\frac{\partial^2\phi_{NN}}{\partial\rho_1^2}(\rho_1,\rho_2) \qquad (6.8\text{-}9)$$

where ϕ_{NN} is the undulation autocorrelation function.

A variety of gravity error models have been suggested which satisfy all or some of the above constraints. Jordan[39] provides a comparative evaluation of a representative set of four of these models.

- a model proposed by Shaw et al, where the anomaly autocorrelation function is assumed to be exponential, and vertical deflection statistics are obtained through the Vening Meinesz formulas - E model
- a model proposed by Kasper [37], where the anomaly is assumed to be a second-order Markov process, and the vertical deflection statistics are obtained through the Vening Meinesz formulas - K-2 model
- two models proposed by Jordan, where the undulation is assumed to be a second-order and a third-order Markov process, and the anomaly and deflection statistics are derived through equations (6.8-8 and 9) - J-2, J-3 models.

E-Model

$$\phi_{gg}(r) = \sigma_g^2 \, e^{-r/d}$$

K-2 Model

$$\phi_{gg}(r) = \sigma_g^2[1 + (r/d)]e^{-r/d} \qquad (6.8\text{-}10)$$

J-2 Model

$$\phi_{NN}(r) = \sigma_N^2[1 + (r/d)]e^{-r/d}$$

$$\phi_{gg}(r) = \sigma_g^2[1 - (r/2d)]e^{-r/d}$$

J-3 Model

$$\phi_{NN}(r) = \sigma_N^2[1 + (r/d) + (r^2/3d^2)]e^{-r/d}$$

$$\phi_{gg}(r) = \sigma_g^2[1 + (r/d) - (r^2/2d^2)]e^{-r/d}$$

The characteristic distances of the various models are related to the convenient and measurable anomaly correlation distance c_g according to

$$\begin{aligned} c_g &= d && \text{E-model} \\ c_g &= 2.146d && \text{K-2 model} \\ c_g &= 0.6252d && \text{J-2 model} \\ c_g &= 1.361d && \text{J-3 model} \end{aligned} \qquad (6.8\text{-}11)$$

The vertical deflection correlation functions which result from application of the Vening Meinesz formulas to these generating functions are given Table 1.

The statistics derived above are valid at a constant geodetic altitude (usually the surface of the earth). Bernstein and Hess [6] have investigated the gravity error sensitivity to altitude, and report changes of the order of 25% at 20,000 ft and 50% at 40,000 ft for the anomaly variance for some simple models (E and K-2 above). However, they also report that, at larger shifts from the origin, the acf is basically unchanged. Thus, the effect of increasing altitude is to suppress high frequency (short wavelength) components. This conclusion is supported by gravity field spherical harmonic analysis, where the magnitude of the nth degree harmonic component is found to be proportional to $(r_e/r)^{2n}$, with $r = r_e + h$. Hence, with increasing altitude, the higher degree (higher frequency) harmonics experience larger suppression.

6.8.3.1.2 Translation to Time Domain

The previous section presented space-domain statistics for various random gravity error models. However, for INS linear error analysis or for Kalman estimation, the time-domain statistics are the desired parameters.

Space and time domains are related by the vehicle motion

$$\begin{aligned} \underline{r}(t_1,t_2) &= \int_{t_1}^{t_2} \underline{v}(t)dt \\ r &= |\underline{r}| \\ \theta &= \tan^{-1}(r_x/r_y) \end{aligned} \qquad (6.8\text{-}12)$$

where $\underline{v}$ is the vehicle velocity vector.

Table 1
Vertical Deflection Space-Domain Correlation Functions

	$\Phi_{\zeta\zeta}(\rho_1,\rho_2)$	$\Phi_{\eta\eta}(\rho_1,\rho_2)$	$f(r)$	$\Phi_{\zeta\eta}(\rho_1,\rho_2)$
E	$\sigma_\delta^2[e^{-r/d}-f(r)\cos 2\theta]$	$\sigma_\delta^2[e^{-r/d}+f(r)\cos 2\theta]$	$\frac{2d^2}{r^2}-(1+\frac{2d}{r}+\frac{2d^2}{r^2})e^{-r/d}$	$-\sigma_\delta^2 f(r)\sin 2\theta$
K-2	$\sigma_\delta^2[(1+\frac{r}{d})e^{-r/d}-f(r)\cos 2\theta]$	$\sigma_\delta^2[(1+\frac{r}{d})e^{-r/d}+f(r)\cos 2\theta]$	$\frac{6d^2}{r^2}-(\frac{r}{d}+3+\frac{6d}{r}+\frac{6d^2}{r^2})e^{-r/d}$	$-\sigma_\delta^2 f(r)\sin 2\theta$
J-2	$\sigma_\delta^2[(1-\frac{r}{2d})e^{-r/d}-f(r)\cos 2\theta]$	$\sigma_\delta^2[(1-\frac{r}{2d})e^{-r/d}+f(r)\cos 2\theta]$	$\frac{r}{2d}e^{-r/d}$	$-\sigma_\delta^2 f(r)\sin 2\theta$
J-3	$\sigma_\delta^2[(1+\frac{r}{d}-\frac{r^2}{2d^2})e^{-r/d}-f(r)\cos 2\theta]$	$\sigma_\delta^2[(1+\frac{r}{d}-\frac{r^2}{2d^2})e^{-r/d}+f(r)\cos 2\theta]$	$\frac{r^2}{2d^2}e^{-r/d}$	$-\sigma_\delta^2 f(r)\cos 2$

For the vertical deflections to constitute stationary random processes, requires that r and Θ be functions only of the time step $\Delta t = t_2 - t_1$. This situation only prevails if 1) the velocity vector is constant, or 2) the deflections are considered in an ensemble sense and the velocity is a stationary random process.

For the EAR/GEANS modeling/estimation problem, however, we are concerned with single-case, maneuvering flight performance. Therefore, in principle, any selected gravity error model should exhibit non-stationary statistics. This model characteristic is consistent with the Kalman estimation structure.

Unfortunately, for any but the simplest maneuver models, the mathematics of the problem become intractable, and simplifications, usually in the form of taking ensemble averages, must be enforced to obtain analytical, closed-form expressions which will provide insight into the nature of the process statistics.

A particularly simple maneuver to analyze is the so-called random heading maneuver, where the vehicle is assumed to move at constant speed on a constant, random heading which is uniformly distributed over 360°. Taking ensemble averages over the distributed heading (thereby eliminating the non-isotropic character of deflection processes), and substituting $r = v|t|$, where v is the aircraft speed, yields the gravity error time-domain acfs of Table 2 for the four models whose space domain acfs where given in Table 1.

It can be expected that EAR/GEANS flight test trajectories will consist of constant speed, constant heading segments joined by short, constant bank angle turns. These two maneuver models therefore also merit analysis.

For the constant heading segments, it is convenient to transform east and north vertical deflection components to along- and cross-track components

$$\begin{bmatrix} \lambda \\ \mu \end{bmatrix} = \begin{bmatrix} \cos\Theta & -\sin\Theta \\ \sin\Theta & \cos\Theta \end{bmatrix} \begin{bmatrix} \zeta \\ \eta \end{bmatrix} \qquad (6.8\text{-}13)$$

Substituting $r = v|t|$, and transforming to track coordinates, yields the time-domain acfs presented in Table 3 for the four considered models.

The turn maneuver model is particularly difficult to analyze due to the non-isotropicity of the deflection statistics and the non-linear relationship between space and time domains. For a simplistic evaluation, consider an isotropic deflection process (or ensemble statistics over uniformly distributed polar angles, for a non-isotropic one), for example, the exponential acf

$$\phi_{\zeta\zeta}(r) = \sigma_\delta^2 \, e^{-r/d} \qquad (6.8\text{-}14)$$

Table 2
Time-Domain Correlation Functions for
Random Heading Maneuvers

	$\phi_{gg}(t)$	$\phi_{\zeta\zeta}(t) = \phi_{\eta\eta}(t)$
E	$\sigma_g^2 e^{-\beta\|t\|}$	$\sigma_\delta^2 e^{-\beta\|t\|}$
K-2	$\sigma_g^2(1+\beta\|t\|)e^{-\beta\|t\|}$	$\sigma_\delta^2(1+\beta\|t\|)e^{-\beta\|t\|}$
J-2	$\sigma_g^2(1-\frac{\beta\|t\|}{2})e^{-\beta\|t\|}$	$\sigma_\delta^2(1-\frac{\beta\|t\|}{2})e^{-\beta\|t\|}$
J-3	$\sigma_g^2(1+\beta\|t\|-\frac{\beta^2t^2}{2})e^{-\beta\|t\|}$	$\sigma_\delta^2(1+\beta\|t\|-\frac{\beta^2t^2}{2})e^{-\beta\|t\|}$

$\beta = v/d$ $\qquad \phi_{\zeta\zeta}(t) = \phi_{\eta\zeta}(t) = 0$

. . .

Table 3
Time-Domain Correlation Functions for Constant Heading Maneuver

	$\phi_{gg}(t)$	$\phi_{\mu\mu}(t)$	$\phi_{\lambda\lambda}(t)$
E	$\sigma_g^2 e^{-\beta\|t\|}$	$\sigma_\delta^2[\frac{2}{\beta^2t^2} - 2(\frac{1}{\beta\|t\|} + \frac{1}{\beta^2t^2})e^{-\beta\|t\|}]$	$\sigma_\delta^2[-\frac{2}{\beta^2t^2} + 2(1 + \frac{1}{\beta\|t\|} + \frac{1}{\beta^2t^2})e^{-\beta\|t\|}]$
K-2	$\sigma_g^2(1 + \beta\|t\|)e^{-\beta\|t\|}$	$\sigma_\delta^2[\frac{6}{\beta^2t^2} - (2 + \frac{6}{\beta\|t\|} + \frac{6}{\beta^2t^2})e^{-\beta\|t\|}]$	$\sigma_\delta^2[-\frac{6}{\beta^2t^2} + (2\beta\|t\|+4+\frac{6}{\beta\|t\|} + \frac{6}{\beta^2t^2})e^{-\beta\|t\|}]$
J-2	$\sigma_g^2(1 - \frac{\beta\|t\|}{2})e^{-\beta\|t\|}$	$\sigma_\delta^2 e^{-\beta\|t\|}$	$\sigma_\delta^2(1 - \beta\|t\|)e^{-\beta\|t\|}$
J-3	$\sigma_g^2(1 + \beta\|t\| - \frac{\beta^2t^2}{2})e^{-\beta\|t\|}$	$\sigma_\delta^2(1 + \beta\|t\|)e^{-\beta\|t\|}$	$\sigma_\delta^2(1 + \beta\|t\|) - \beta^2t^2)e^{-\beta\|t\|}$

$\beta = v/d$ $\quad \phi_{\mu\lambda} = \phi_{\lambda\mu} = 0$

and an aircraft flying a circle at constant speed and constant bank angle (resulting in constant radial acceleration a). The distance shift between any two points on the circle at two times t_1, t_2, $t_2-t_1 = \tau$, is

$$\Delta r = (2v^2/a)\sin(a\tau/2v) = 2R\sin(\pi\tau/T) \qquad (6.8\text{-}15)$$

where R is the circle radius and T is the period.

The corresponding time-domain exponential acf is then

$$\phi_{\zeta\zeta}(\tau) = \sigma_\delta^2 \, e^{-(2R/d)\sin(\pi\tau/T)} \qquad (6.8\text{-}16)$$

For small R/d (an aircraft at 300 knots with a 45° bank angle turns with a radius of approximately 1.5 n.mi., versus a gravity correlation distance of about 20 n.mi.) we can rewrite Equations (11) and (9) (transformed using $r = v\tau$) as

$$\phi_{\zeta\zeta}(\tau) = \sigma_\delta^2[1 - (2R/d)\sin(\pi\tau/T)]$$
$$\phi_{\zeta\zeta}(\tau) = \sigma_\delta^2[1 - (2R/d)(\pi\tau/T)] \qquad \tau \leq T \qquad (6.8\text{-}17)$$

The encountered process statistics will thus be significantly different to the constant heading equivalent when $\pi\tau/T << 1$ does not hold. The above model (with $\tau \leq T/2$) could be considered to represent the ensemble statistics within the maneuver for a 180° turn when the vehicle heading entering the turn is viewed as a uniformly distributed random variable.

The above simplistic discussion was presented to illustrate the fact that maneuvering statistics are significantly different than those in straight flight. A treatment of this subject has not been found in the literature, and considerable more modeling effort may be required in this area.

Finally, the EAR/GEANS flight trajectories may include repeated tracings of a standard ground track, i.e., a tracking maneuver. In this case, gravity errors across a track period will be perfectly correlated, and the acfs will be modulated by the tracking frequency, as discussed by Nash[40]. He considers a vehicle moving back and forth along a fixed heading line, with period T, and shows that the time-domain acf is given by

$$\phi(\tau) = \begin{cases} \int_0^{v\tau} \phi(r)[(1 - (2\tau/T))\delta(r-v\tau) + (2/vT)]dr & 0 < \tau < T/2 \\ \phi(-\tau) & \text{all } \tau \\ \phi(\tau+T) & \text{all } \tau \end{cases}$$

(6.8-18)

6.8.3.1.3 Model Evaluation

Four representative space-domain gravity error models have been presented, and their transfer to the time-domain under various vehicle maneuvers discussed. None of these adequately represents the underlying processes during turns, but the difficulty lies with the nature of the maneuver rather than distinguishing features between one model or another. Similarly, the effect of tracking maneuvers is basically independent of the assumed local statistics. Any model comparison must therefore rely on behavior under the other maneuver models considered.

Two relevant criteria on which to base a comparison of the suggested models for EAR/GEANS purposes, are

1) Is the Jordan model's completeness (in terms of representing the four gravity error variables in a theoretically consistent manner) material?

2) Are the differences in model frequency content observable to the estimation process?

The first consideration translates into i) is estimation of the undulation of the geoid of interest?, and ii) is the undulation observable? As stated in Section 6.8.2, the governing assumption is that gravity errors are not to be estimated per se, but rather are of interest only to the extent that they disturb the recovery of desired EAR/GEANS error sources. Furthermore, the undulation, which corrupts the baro-altimeter indication of altitude above the reference ellipsoid, will not be separable from other slowly-varying sources of baro-altitude error. Hence, the undulation is neither of interest nor observable, and model completeness a la Jordan is immaterial to the EAR/GEANS problem. Had the undulation been observable (or of interest), information about the anomaly and deflection processes could have been obtained from it through the appropriate cross-correlation functions (or vice versa).

The considerations for the anomaly are not directly analogous to those for the undulation. The GEANS mechanization incorporates vertical channel baro-stabilization through a critically-damped second-order loop with natural frequency $\omega_n \sim .005$ rad/sec[24]. The response time of this loop is only slightly faster than the anomaly correlation time for an aircraft speed of 300 knots and an anomaly correlation distance of 20 n.mi., so that steady-state analysis is not directly applicable. However, to provide some insight, let us assume that the loop response is significantly faster. Then, the steady-state altitude and vertical velocity errors are given by [23],

$$\delta h_{ss} = \frac{1+k_1k_4}{k_2-2\omega_s^2(1+k_1k_4)}\,\delta A_z + \frac{k_2}{k_2-2\omega_s^2(1+k_1k_4)}\,\delta h_b$$

$$\delta v_{z_{ss}} = \frac{k_1}{k_2-2\omega_2^2(1+k_1k_4)}\,\delta A_z + \frac{2\omega_s^2 k_1}{k_2-2\omega_s^2(1+k_1k_4)}\,\delta h_b \qquad (6.8\text{-}19)$$

where k_1, k_2 are the stabilization loop gains, k_4 is the altimeter lag compensation coefficient, δA_z is the vertical acceleration error, and δh_b is the baro-altitude error.

Given EAR-based observations of altitude and vertical velocity, δA_z can be isolated from equations (6.8-19) In turn, δA_z is the linear combination of accelerometer bias, accelerometer scale factor, and gravity anomaly effects. The frequency content of accelerometer bias induced errors (modulated by earth, transport rates) and accelerometer scale factors (modulated by aircraft vertical maneuvers) is clearly different from that of anomaly induced errors, and should therefore allow error source separation.

The critical parameter for anomaly observability is the rms vertical velocity (and altitude) observation error resulting from smoothing the set of measurements obtained over the anomaly correlation distance. If this parameter is smaller than the anomaly-induced error in equations (-14), then the anomaly is, in practical terms, an observable process, and, if not accounted for in the filter state model, will lead to corrupted estimation solutions.

The gravity errors of interest are, therefore, the vertical deflections and possibly the anomaly. All four of the models considered in Section 6.8.3.1 provide theoretically consistent statistics for these three error states and thus constitute potentially acceptable models for the estimation process. As all four seem to provide comparable quality fits to available data (gravity anomalies), it is valid to wonder whether differences between them are of any significance for the EAR/GEANS problem.

Jordan [39] provides a comparative evaluation of the four proposed gravity deflection models in terms of the induced steady-state rms position and velocity errors of an externally-damped inertial navigator. He concludes that, for the speed regimes of interest to EAR/GEANS ($\tau_g = c_g/v < .1$ hr), there is no appreciable difference between the various model-induced performances. The differences appear at process correlation times which are of the order of, or larger than, the Schuler period. This differentiation would appear to be related to the model's "roundedness at the origin", i.e., whether the acf derivative at zero shift is non-zero. The frequency components which contribute to a non-zero derivative at the origin would appear high frequency (relative to Schuler) at high vehicle speeds and would tend to be filtered out by the INS, while they would be passed at low vehicle speeds. The roundedness at the origin consideration, compatible with intuitive physical understanding of gravity error processes as resulting from the local mass distribution of the earth, would tend to favor the K-2 and J-3 models over the E and J-2 models.

For the EAR/GEANS estimation problem, however, we are not only concerned with the steady-state INS response, but also with short-term transient responses observable through EAR measurements. The cutoff frequency for model differentiation is, therefore, not the Schuler, but rather that frequency at which, given the EAR measurement rate and accuracy, faster induced variations in the observable variables appear white to the estimator.

Figure 13 plots the power spectral densities (PSDs) for the four involved gravity deflection models obtained by translating the space domain acfs to the time-domain through the random heading maneuver model of Section 6.8.3.1.2. The plots present normalized PSDs ($G(\omega)/\sigma\delta^2\,\tau g$) versus normalized frequency ($\omega_N = \omega\,\tau g$).

$$
\begin{aligned}
G^N_E &= 2\alpha/(\alpha^2+\omega_N^2) && \text{E-model}\\
G^N_{K-2} &= 4\alpha^3/(\alpha^2+\omega_N^2)^2 && \text{K-2 model}\\
G^N_{J-2} &= \alpha(\alpha^2+3\omega_N^2)/(\alpha^2+\omega_N^2)^2 && \text{J-2 model}\\
G^N_{J-3} &= 2\alpha^3(\alpha^2+5\omega_N^2)/(\alpha^2+\omega_N^2)^3 && \text{J-3 model}
\end{aligned}
\qquad (6.8\text{-}20)
$$

where $\alpha = c_g/d$, d = model characteristic distance, and

$$
\alpha = \begin{cases} 1 & \text{E-model}\\ 2.146 & \text{K-2 model}\\ 0.6252 & \text{J-2 model}\\ 1.361 & \text{J-3 model} \end{cases}
\qquad (6.8\text{-}21)
$$

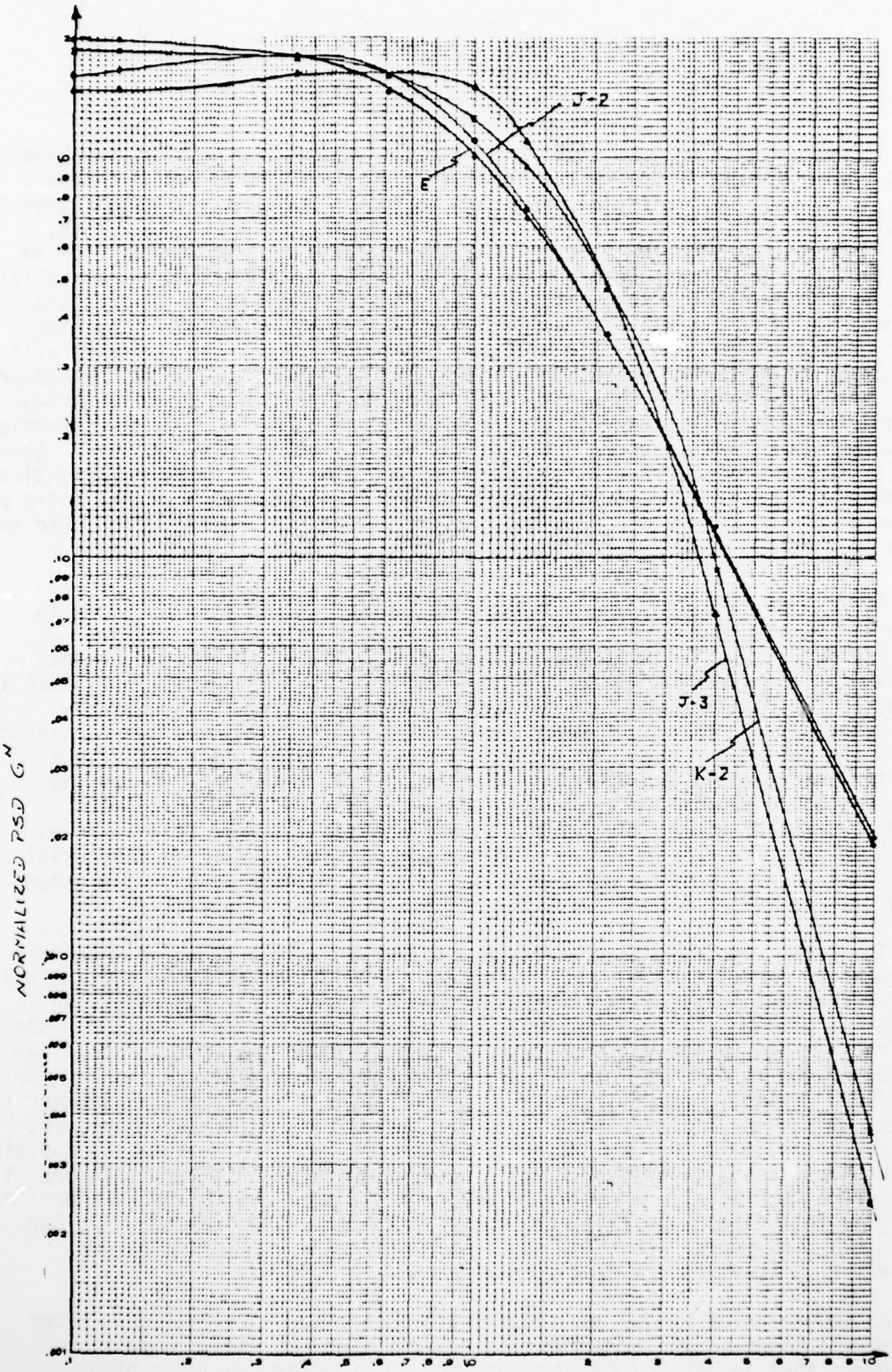

Figure 13: Normalized Frequency f_N

It can readily be seen that the major differentiation between the models lies in their high frequency content ($\omega_N >> 1$) where the E- and J-2 models fall as $1/\omega_N^2$, while the K-2 and J-3 models fall as $1/\omega_N^4$. Consider then the spectra as a series of individual frequency components, and recall that, according to the sampling theorem, two observations per cycle are required to identify the signal component (assuming perfect measurements). The ability of the Kalman filter to recover any frequency component above $\omega_N \sim 4$ (and thereby to differentiate between the gravity models) depends on obtaining perfect measurements at a rate of $8/\tau_g$. Additionally, as measurements will be corrupted by random noise, smoothing will be required to bring the measurement effective random error to a level comparable to the observable navigation error induced by the frequency components in question. As the effective measurement rms random error drops as the square root of the number of measurements smoothed (i.e., $1/\sqrt{n}$), the observation rate required for differentiation of proposed gravity models is of the order of $8k^2/\tau_g$, where k is the ratio of measurement rms random error to the gravity induced navigation error over the time of interval $\tau_g/8$.

These considerations are similar to the discussion presented above in relation to observability of the gravity anomaly, except that in the deflection case we are concerned with observability of the high frequency portion of the spectrum rather than the whole of it. The measurement rate and accuracy (in position and velocity spaces) expected from EAR should be evaluated both to establish the anomaly observability and to provide guidance as to the deflection model selection. Based on my previous experience with doppler radars (Teledyne/Ryan APN-200 type), it is quite likely that the combination of required measurement rate and accuracy to allow filter differentiation between the various gravity models will not be available, in which case, selection of one of these models over another is immaterial from this point of view. Observability of gravity anomalies, on the other hand, may be quite possible with current standard technology.

The above comparison was based on acf transformation to the time-domain through the random heading maneuver model. Application of this same analysis to the constant, deterministic heading maneuver model is hampered by the inability to find closed-form analytical expressions for the resultant PSDs for the K-2 and E-models. The argument has been made that the similarities noted for the random heading maneuver for the E- and J-2 models and for the K-2 and J-3 models would carry over to this maneuver. However, inspection of the acfs (see Table 3) shows that, for the J-2 and J-3 models, the acfs decay exponentially (as dominant mode) while the E and K-2 model acfs contain terms proportional to $d^2/v^2 t^2$, which decay significantly slower than any of the exponential terms. I would therefore expect that the E- and J-2 model PSDs would exhibit larger low frequency content than the corresponding PSDs for the other two models. What the physical significance of this apparent behavior is, is an interesting question.

A comparison of along- and cross-track deflection PSDs for the J-2 and J-3 models shows a similar pattern as observed for the random heading maneuver; that is, at low frequencies they are similar, while at high frequencies, the J-2 PSDs fall as $1/\omega_N^2$ while the J-3 PSDs fall as $1/\omega_N^4$. In

addition, in both cases, the along-track component PSD significantly differs from the cross-track component PSD due to the ratio of 1:2 in their respective correlation distances.

The turning maneuver represents an environment which is not easily represented by any of the postulated models. The situation is of concern because it may (again depending on the observability afforded by EAR measurements) corrupt estimation of GEANS error sources. Consider the following heuristic arguments: a turn is a situation where the actual spatial shift between any two points on the vehicle track is smaller than would be inferred from the standard $r = v\,t$ transformation (length of the cord versus length of the arc). Therefore, the true correlation between deflections at the two points will be stronger than modeled, and the induced acceleration error will be more "bias-like" than that represented by the filter. Part of this effect will therefore, if observed, be assigned to modeled states that exhibit more correlated behavior in a turn, i.e., probably to accelerometer scale factors. The extent to which these heuristic considerations represent a meaningful concern bears further analysis and/or simulation.

The final item to be considered relates to the tracking maneuver discussed in Sect. 6.8.3.1.2 and in particular, the generation of an harmonic component in the gravity error spectrum at the tracking frequency. This effect will only be of concern if the induced harmonic is an integral fraction of one of the INS oscillation mode frequencies (i.e., Schuler, 24 hr), in which case it may lead to miss-assignment of this gravity induced error to one of the corresponding GEANS error sources. This consideration is most readily laid to rest by appropriate flight path design.

6.8.3.2 Gravity Error Estimation

The recovery of gravity errors through optimal estimation has been a singularly unsuccessful field. Chatfield et al[43] describe one such attempt and report a total lack of success in estimating gravity deflections from simulated aircraft flight data; yet, their measurement rate was obviously too slow relative to the estimator model correlation times to expect much. Rose and Nash[42]conducted a more thorough investigation of the limiting effects on gravity recovery accuracy and the sensitivity of the results to the presence of modeling errors in the estimator formulation; yet, their results raise as many questions as they answer. . .

Rose and Nash's configuration consists of a high-quality military inertial navigator, position and velocity reference systems, and a Kalman filter/smoother that optimally combines these two data streams and attempts to recover the values of the encountered gravity deflections. The carrier vehicle is a ship straight-steaming at 10 knots, and the gravity deflections are modeled as second-order Markov processes.

Rose and Nash identify as the first deflection recovery limitation the so-called "bias problem", i.e., the similar frequency content of low frequency deflection components (i.e., "global" terms) and position reference bias error

or IMU bias-like instrument error sources. Note, however, that a 100 ft position error causes the "platform" to be tipped by only 1 sec ($\sim\delta p/R_e$), and thus allows observation of vertical deflections exceeding this value. Smaller position reference bias errors will result in correspondingly smaller platform tips, so this effect is not expected to be significant for EAR/GEANS. If correlation with IMU error sources is now considered, it should be noted that, as discussed in Sect. 6.8.2, their error signatures are modulated by earth rate (and aircraft transport rate) and thus will exhibit different frequency content than gravity "bias" errors. For the highly stable instrument error models assumed for GEANS, high correlation between these states should not develop. The conclusion reached in this paper is thus directly resultant from the large (.06 nmi ~ 3.6 sec) position reference bias and the fixed orientation between IMU instruments and gravity deflections imposed by the INS mechanization.

Rose and Nash present the results of steady-state covariance analysis of recovery accuracy sensitivity to system parameters. They indicate that the primary disturbances are the position reference noise and the vertical deflections themselves. This conclusion seems plausible enough, at least for a given stability of IMU instrument error sources. However, the shape of the sensitivity curves (in particular, the sensitivity to the deflections (see Figures 14 and 15)) and the limiting values reached when the primary disturbances tend to zero would seem to be dependent on the particular model assumed for the rest of the system (i.e., INS). The paper states that part of the accelerometer bias error is modeled as a Markov process, although the variance and correlation time are not specified. If this correlation time is similar to that of the deflections, both error source models would exhibit similar frequency content, and separation of their effects would be difficult. In this case, reducing the rms measurement noise improves the estimate of the linear combination of error sources, but not particularly of the error sources themselves. Also, if one of the error sources in the linear combination is dominant (i.e., much larger noise power) then estimation of the linear combination is approximately equivalent to estimation of the dominant member; as the dominance disappears (decreasing noise power of dominant), the recovery accuracy of the once-dominant term decreases on a relative basis and is eventually limited by the separability problem. This consideration may explain the shape of the "sensitivity to rms value of deflection process" curve presented in the paper.

The authors go on to state that increasing the measurement rate beyond the assumed two per gravity deflection correlation distance does not materially improve the deflection estimates. I assume that they mean this statement to apply at their standard rms position measurement noise value of .08 nmi (i.e., close to the limiting value for deflection recovery accuracy), since taking 2n measurements of rms value σ over the gravity deflection time is, in steady-state, equivalent to taking two measurements with rms value $\sigma/\sqrt{n}$, and the deflection recovery accuracy is clearly sensitive to the rms value of measurement noise, as shown in Figure 15. The observed insensitivity to measurement rate is probably a result of the presence of a "bias-limited" process, i.e., one which is not diminished by averaging. We do not believe that the modeled position reference bias represents such an effect, since, based on frequency content, it is clearly separable from the

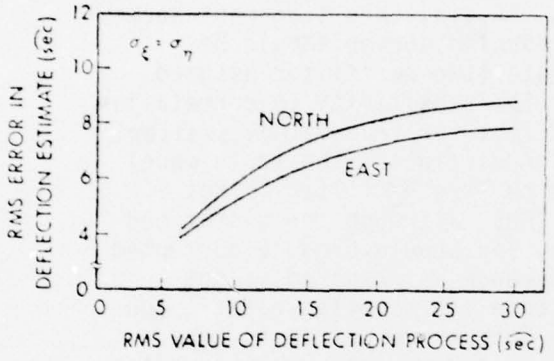

RMS deflection recovery error versus rms value of deflection process.

Figure 14

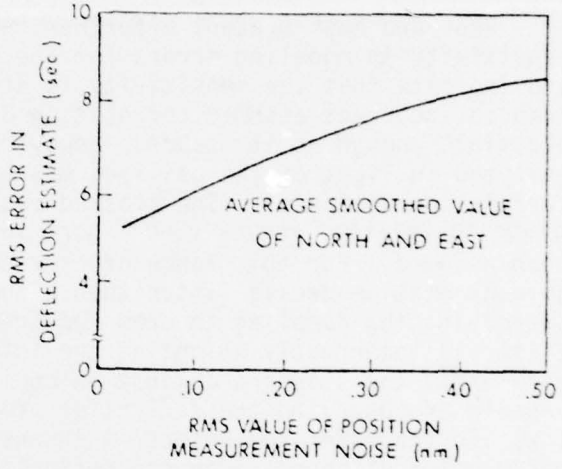

Sensitivity of deflection estimate errors to the rms value of the position measurement noise.

Figure 15

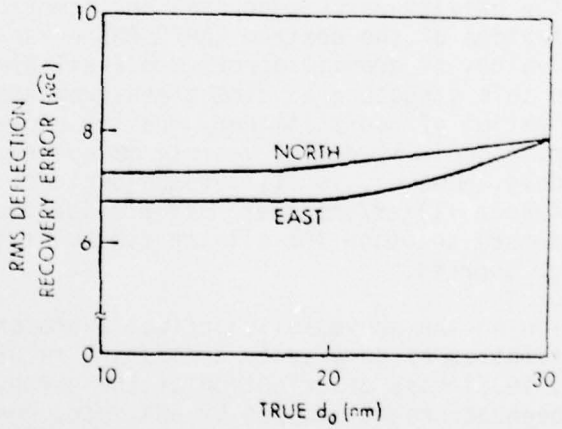

Sensitivity of rms deflection recovery error to an incorrectly modeled correlation distance for the deflection process (filter assumes $d_0 = 20$ nm).

Figure 16

AD-A078 607 INTERMETRICS INC CAMBRIDGE MASS F/G 17/7
GPS AND EAR/GEANS SOFTWARE SUPPORT.(U)
AUG 79 N A CARLSON , W S WIDNALL , P K SINHA F33615-77-C-1044
UNCLASSIFIED IR-397 AFAL-TR-79-1127 NL

2 OF 2
AD A078607

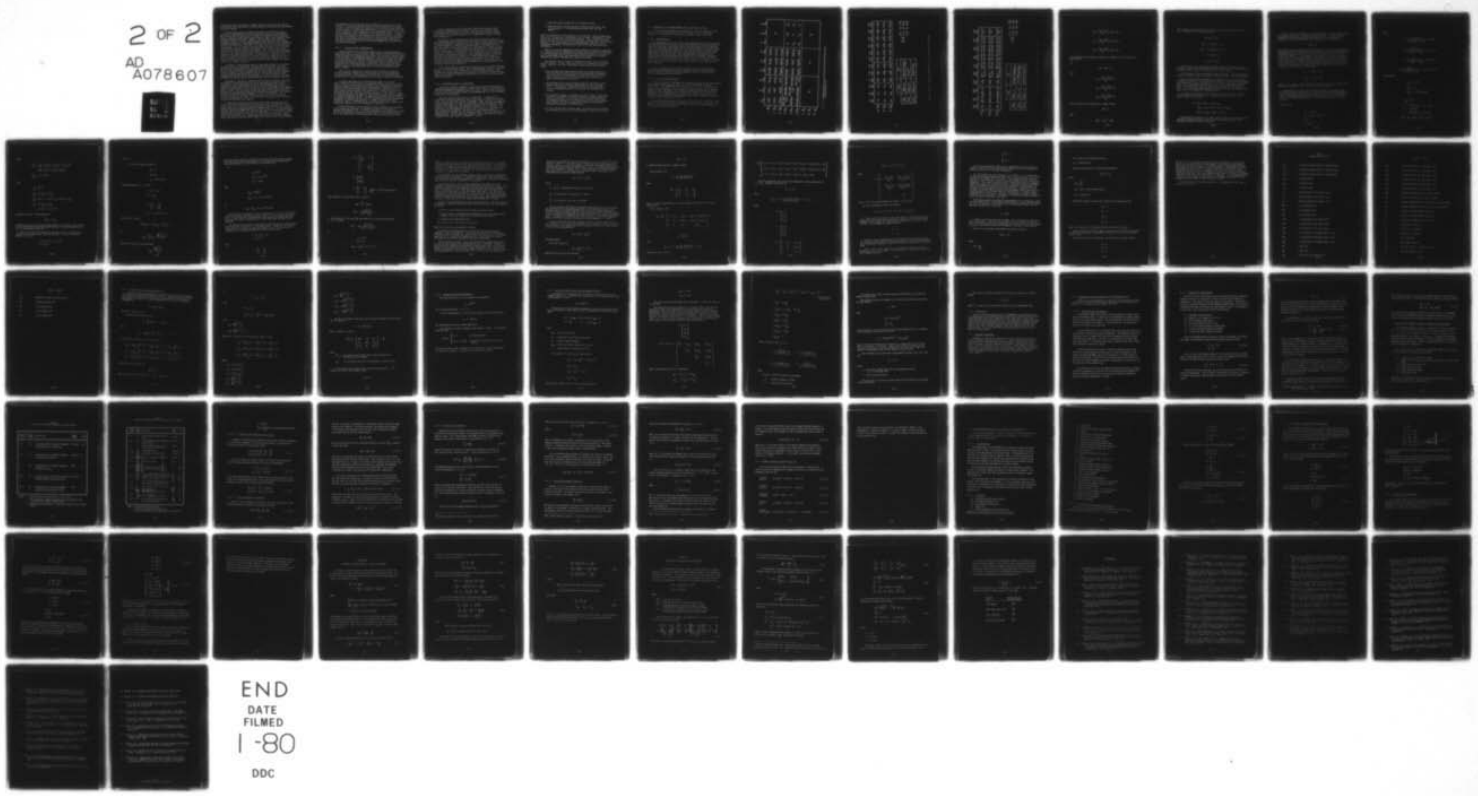

END
DATE FILMED
1-80
DDC

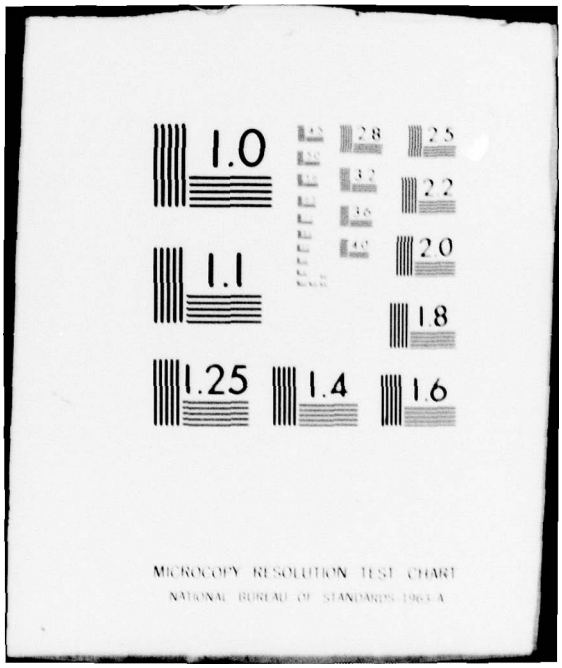
1.0
1.1
1.25
1.4
1.6
2.8
3.2
3.6
4.0
2.5
2.2
2.0
1.8
MICROCOPY RESOLUTION TEST CHART
NATIONAL BUREAU OF STANDARDS-1963-A

time-varying deflection process. Another example of "bias-limited" effects is the error source correlation discussed above for deflection and accelerometer bias error sources.

Rose and Nash present a further investigation of recovery accuracy sensitivity to modeling errors for the deflection process in the estimator, and indicate that the sensitivity is higher to mismodeled process variance than to incorrect assumed correlation distances. Again, this statement seems plausible enough as it stands. However, the presented curves should be analyzed in light of the utilized measurement rate (two per filter assumed correlation distance). The plotted results for the sensitivity to correlation distance modeling errors (See Figure 16) appear flat for true values smaller than assumed. For this range of time correlation distances, the truth model autocorrelation decays faster than assumed and the "truth" filter is not satisfying the sampling theorem requirements. Thus, although the mismatched filter is incorrectly weighting the information, and should produce corrupted estimates, the standard against which its performance is compared is not capable of observing the deflection process because its sampling rate it too low. Furthermore, the effect is insensitive to further reduction in true correlation distance since the deflection process already appears like white noise to the "truth" estimator.

In summary, it would appear that the conclusions reached in this paper are restricted by the particular assumed system configuration, and that extreme care should be exercised in attempting to extrapolate these results to a different environment. In addition, the paper does not cover certain areas of interest for the EAR/GEANS problem, such as modeling and estimation of gravity deflections during vehicle turns. On the other hand, it does indicate that the deflections are recoverable, to some level which, for the EAR/GEANS application, may be quite better than the 5 to 8 sec achieved here.

Conceptually, therefore, standard Kalman filtering represents a possible technique for recovering the gravity error processes and removing them as disturbances from the estimation of the desired EAR/GEANS error sources. If externally derived sample values of gravity errors are available, they can readily be incorporated in this structure as direct measurements of the modeled gravity states. The utilization of non-stationary gravity processes may be necessary in the estimator, especially during vehicle maneuvers; the structure of such non-stationary models, however, is still to be derived. But, if properly formulated, the Kalman filter/smoother will provide the optimal (in the minimum variance sense) solution for all the system states, including the desired EAR/GEANS error sources.

A simplifying variation on the above fully optimal approach may be of value. The largest uncertainties as to gravity errors are related to short term effects (i.e., turns, local mass distribution of the earth, etc.), while longer term effects have been accurately mapped by DMA, etc. On the other hand, the high stability of GEANS error sources implies that a leisurely observation rate may well be sufficient for their recovery [47]. We can therefore consider updating the estimator at a rate which is slow relative to the local gravity error correlation time (say, a measurement update every 10 minutes), thereby making the uncertain gravity effects appear like "white noise" to the estimator

and automatically resolving the issue of modeling the gravity field time structure. Of course, attendant recovery accuracy penalties will be paid in that 1) short correlation time processes will not be estimated (EAR error sources?), and 2) a proportional degradation in rms recovery accuracy of $\sqrt{n}$ (less if process is "bias-limited") will be encountered, where n is the ratio of the measurement rates implemented in the compared processes. If these penalties are acceptable, this approach may obviate the concern of modeling the local fine-structure gravity processes. Note that this approach does not require interference with the rate at which measurements are taken inflight, but only with the rate at which measurements are utilized in the post-flight environment.

6.8.3.3 Gravity Error Compensation

Given the difficulty of modeling gravity errors as random processes, and the availability of gravity data at DMA, we may consider deterministically compensating gravity induced errors by addition of a suitable "control" term to the estimator error propagation equations. Even if some residual compensation error remains, the magnitude should be significantly smaller than that of the whole value error, and the estimator sensitivity to modeling errors should be proportionately reduced. Furthermore, some of the bothersome characteristics of the whole value error (such as non-isotropicity) may be largely removed by the compensation process, making the residual errors easier to model.

Traditionally, deterministic gravity models followed the spherical harmonic expansion approach, with coefficients derived from observations of satellite orbits. Such models are generally too coarse for adequate representation of gravity disturbances in the areas of interest to EAR/GEANS.

Of greater applicability are deterministic models fit to local data. Chatfield et al[43] describe an approach where a replica of the local gravity field is constructed as a combination of a reduced set of ellipsoid spherical harmonics and a potentially large number of subterranean point masses (acting through Newton's mass-attraction law), which best fit, in a least-squares sense, observed local gravity data. A highly accurate fit is obtained through this technique (residual rms errors of the order of .3 μgs are reported); however, the number of required point masses (10722) represents an extreme computational burden. The computational penalty could presumably be reduced by loosening the quality-of-fit requirement (an order of magnitude degradation in residual rms fit error is probably acceptable) without significant impact on EAR/GEANS error source recovery accuracy; however, the computation cost will, in all likelihood, still be high.

Junkins [44] proposes the utilization of local approximating polynomials, fit by regression techniques, to represent the gravity errors over a prespecified geographic cell. The clear advantage of this method lies in that the local approximating functions are much simpler than global expressions, due to the significantly reduced geographic area over which they are valid.

Junkins proposes the use of nth order Chebyshev polynomials, with coefficients determined by least-squares fitting of local gravity data, as the model basis functions, since he finds that they provide a uniform distribution of errors over the cell (i.e., homogeneous isotropic residual error processes?).

Of concern in this approach would seem to be selection of the cell size and maximum order of the Chebyshev polynomials, as representing a trade-off between computation and model accuracy. Junkins [45] presents an evaluation of the model as a function of these parameters, by comparison to a point-mass gravity error model (model 310), and shows rms fit error of less than 1 μg for 1° x 1° cells and polynomial maximum order 3 (implies approximately nine polynomial coefficients). The fidelity of the cited model 310 to the fine structure of the gravity field is not known to me, so that the relevance of these quoted accuracies to the EAR/GEANS problem is uncertain. Note that the utilized cell dimension is significantly larger than the correlation distances utilized for statistical gravity error models; it is not clear to me how the higher frequency components of the gravity error processes (which may be important for EAR/GEANS) can be approximated to that accuracy with that few coefficients.

Still, there does not seem to be any reason why, with suitable selection of cell size and polynomial order, this technique cannot represent a feasible approach for gravity error compensation in the EAR/GEANS problems. The computational burden imposed by the requirement to adequately represent those gravity error frequency components observable to the filter may bear further evaluation, however.

6.8.4 Recommendations for EAR/GEANS

The previous section presented a discussion of possible modeling and compensation approaches to attempt to remove gravity errors as a disturbance from the estimation of EAR/GEANS sources of errors. Based on that discussion, we now present some guiding concepts and recommendations as to the techniques to be used in this problem.

The model selection decision is to be two-fold: i) what model is suitable for simulation purposes, and ii) what model is suitable for estimation? These two decisions are not independent. Apart from the fact that the simulator model should at least be as faithful to the real-world environment as the filter model, it is also important that any lack of fidelity of the simulation not compensate a corresponding inadequacy in the estimator. In particular, you have suggested the use of the J-3 model for simulation and the J-2 model for estimation. On the positive side, both models are computationally tractable, and the simulation model is more involved than the estimator model. On the other hand, however, we must note that both models incorporate the same incorrect assumptions, in that

1) they both assume isotropicity of the anomaly process,

2) they both yield incorrect statistics during aircraft turns, due to the assumed r = vt transformation between space and time domains.

Given the importance of gravity errors in this problem, I would strongly urge that, if at all possible, a deterministic gravity model, generated by fitting actual data, be utilized for simulation purposes. The utilization of such data in at least one test case will provide some confidence that the formulated estimator is not simply tuned to the simulation model, and that it will successfully accomplish the transition to the real flight data processing environment.

When utilizing the deterministic gravity model for simulation, consideration should be given to representation of model residual errors, if significant. It is believed that these would be of high frequency content, arising out of gravity measurement errors and intersample gravity variations, and would therefore be suitably represented by a white noise model.

The estimator should include the deterministic model also, if computationally feasible. If not, states shall have to be allocated to this error source. Design of the filter state model should consider the following points.

- For the GEANS space-stable mechanization and assumed stability of IMU error sources, global gravity errors are probably observable. Such errors should be compensated, or additional states shall have to be included for them, as the formulated local gravity error models do not support a bias level.

- The observability of gravity anomaly should be determined for the expected EAR vertical velocity measurement rate and rms random error. If observable, it should be included in the state model to avoid corrupting estimation of "vertical" accelerometer error sources.

- If the gravity anomaly is included in the error state, it should be of benefit to represent the cross-correlations between anomaly and vertical deflections. In this case, the first-order Markov model you suggest as possible for the deflections would not be applicable. The J-2 model, for which an appropriate shaping filter has been formulated, would seem a suitable choice.

- For any selected gravity process model, the formulation of estimator non-stationary statistics for turning maneuvers should be considered.

6.9 Synthesis of the EAR/GEANS Error Isolation Filter

This section comprises Intermetrics AFAL/GPS Analysis Memo #03-78, "Filter Synthesis for the EAR/GEANS Error Isolation Filter," by Lawrence F. Wiederholt, dated 10 May 1978 [48].

6.9.1 Introduction

This memorandum defines the filter for the EAR/GEANS Error Isolation Filter. The focal point of this activity is the state vector selection which involves two major subsystems: the GEANS inertial navigation system and the EAR radar unit. Since the performance characteristics of the GEANS INS are better known than that of the EAR radar, emphasis in the state selection is placed on the radar unit rather than the INS. Also, since the error characteristics and performance of the INS are well known and understood, the related state elements and corresponding models are selected with considerable confidence. Recommendations for state elements and models are made for radar but their adequacy must be verified by test data either from bench measurements or flight data, since the error characteristics and performance of the radar are less well understood.

This memo includes and is organized according to the following topics: INS and radar measurement state vector selection, process noise covariance matrix definition, transition matrix evaluation, initial state vector and initial covariance matrix definitions.

6.9.2 State Vector Selection

The INS state vector is defined first, followed by that for the radar measurement. The INS state selection starts with the "truth" model defined by J. Burns[29] The fundamental matrix derived by J. Burns is included here in Figure 17 for convenience. This is an error state formulation in the inertial reference frame. The object is to develop a suboptimal model with a reduced state vector by eliminating states from the truth model which are either not observable or not separable for the expected test flight trajectories. All instrument error parameters are estimated in the platform frame to facilitate physical interpretation of the results.

The position, velocity and tilt errors will of course be retained as filter states. Starting with the gyro instruments, some reductions are possible. In the terms driving the tilt angle error states, there is a linear combination which cannot be separated given by

		1 δr_{ix}	2 δr_{iy}	3 δr_{iz}	4 δv_{sx}	5 δv_{sy}	6 δv_{sz}	7 β_{ix}	8 β_{iy}	9 β_{iz}
1	$\dot{\delta r}_{ix}$	$-C_1C_x^2$	$-C_1C_xC_y$	$-C_1C_xC_z$	$1+C_1C_4C_x^2$	$C_1C_4C_xC_y$	$C_1C_4C_xC_z$			
2	$\dot{\delta r}_{iy}$	$-C_1C_xC_y$	$-C_1C_y^2$	$-C_1C_yC_z$	$C_1C_4C_xC_y$	$1+C_1C_4C_y^2$	$C_1C_4C_yC_z$		0	
3	$\dot{\delta r}_{iz}$	$-C_1C_xC_z$	$-C_1C_yC_z$	$-C_1C_z^2$	$C_1C_4C_xC_z$	$C_1C_4C_yC_z$	$1+C_1C_4C_z^2$			
4	$\dot{\delta v}_{sx}$	$(3C_x^2-1)\omega_s^2 - C_2C_x^2$	$(3\omega_s^2-C_2)C_xC_y$	$(3\omega_s^2-C_2)C_xC_z$	$C_2C_4C_x^2$	$C_2C_4C_xC_y$	$C_2C_4C_xC_z$	0	$-f_{iz}$	f_{iy}
5	$\dot{\delta v}_{sy}$	$(3\omega_s^2-C_2)C_xC_y$	$(3C_y^2-1)\omega_s^2 - C_2C_y^2$	$(3\omega_s^2-C_2)C_yC_z$	$C_2C_4C_xC_y$	$C_2C_4C_y^2$	$C_2C_4C_yC_z$	f_{iz}	0	$-f_{ix}$
6	$\dot{\delta v}_{sz}$	$(3\omega_s^2-C_2)C_xC_z$	$(3\omega_s^2-C_2)C_yC_z$	$(3C_z^2-1)\omega_s^2 - C_2C_z^2$	$C_2C_4C_xC_z$	$C_2C_4C_yC_z$	$C_2C_4C_z^2$	$-f_{iy}$	f_{ix}	0
7	$\dot{\beta}_{ix}$									
8	$\dot{\beta}_{iy}$		0			0			0	
9	$\dot{\beta}_{iz}$									

Figure 17: Fundamental Matrix for Second Order Altitude-Aided Space-Stable System-Component Form

		14 AB_x	15 AB_y	16 AB_z	17 ASF_x	18 ASF_y	19 ASF_z	20 AMX_y	21 AMX_z	22 AMY_x	23 AMY_z	24 AMZ_x	25 AMZ_y
4	$\dot{\delta V}_{sx}$	a_{11}	a_{12}	a_{13}	$a_{11}f_{px}$	$a_{12}f_{py}$	$a_{13}f_{pz}$	$-a_{11}f_{pz}$	$a_{11}f_{py}$	$a_{12}f_{pz}$	$-a_{12}f_{px}$	$-a_{13}f_{py}$	$a_{13}f_{px}$
5	$\dot{\delta V}_{sy}$	a_{21}	a_{22}	a_{23}	$a_{21}f_{px}$	$a_{22}f_{py}$	$a_{23}f_{pz}$	$-a_{21}f_{pz}$	$a_{21}f_{py}$	$a_{22}f_{pz}$	$-a_{22}f_{px}$	$-a_{23}f_{py}$	$a_{23}f_{px}$
6	$\dot{\delta V}_{sz}$	a_{31}	a_{32}	a_{33}	$a_{31}f_{px}$	$a_{32}f_{py}$	$a_{33}f_{pz}$	$-a_{31}f_{pz}$	$a_{31}f_{py}$	$a_{32}f_{pz}$	$-a_{32}f_{px}$	$-a_{33}f_{py}$	$a_{33}f_{px}$

	D.E.	1σ
AB_I	$\dot{AB}_I = 0$	4.9×10^{-4} m/sec^2
ASF_I	$\dot{ASF}_I = 0$	5×10^{-5}
AMI_J	$\dot{AMI}_J = 0$	5×10^{-5} rad.

$$C_p^i \triangleq \begin{pmatrix} a_{11} & a_{12} & a_{13} \\ a_{21} & a_{22} & a_{23} \\ a_{31} & a_{32} & a_{33} \end{pmatrix}$$

Figure 17: (Contd.) - Additional F-Matrix Entries for Accelerometer Error Model

		26 GB_x	27 GB_y	28 GB_z	29 GFX_x	30 GFX_z	31 GFY_y	32 GFY_z	33 GFZ_y	34 GFZ_z	35 GR_+
7	$\dot{\beta}_{ix}$	$-a_{13}$	$\frac{-1}{\sqrt{2}}(a_{11}+a_{12})$	$\frac{1}{\sqrt{2}}(a_{11}-a_{12})$	$-a_{13}f_{pz}$	$\frac{1}{\sqrt{2}}a_{13}\cdot(f_{px}-f_{py})$	$-\frac{1}{2}(a_{11}+a_{12})\cdot(f_{px}+f_{py})$	$\frac{1}{2}(a_{11}+a_{12})\cdot(f_{px}-f_{py})$	$\frac{1}{2}(a_{11}-a_{12})\cdot(f_{px}+f_{py})$	$-\frac{1}{2}(a_{11}-a_{12})\cdot(f_{px}-f_{py})$	$\frac{a_{11}-a_{12}}{\sqrt{2}}$
8	$\dot{\beta}_{iy}$	$-a_{23}$	$\frac{-1}{\sqrt{2}}(a_{21}+a_{22})$	$\frac{1}{\sqrt{2}}(a_{21}-a_{22})$	$-a_{23}f_{pz}$	$\frac{1}{\sqrt{2}}a_{23}\cdot(f_{px}-f_{py})$	$-\frac{1}{2}(a_{21}+a_{22})\cdot(f_{px}+f_{py})$	$\frac{1}{2}(a_{21}+a_{22})\cdot(f_{px}-f_{py})$	$\frac{1}{2}(a_{21}-a_{22})\cdot(f_{px}+f_{py})$	$-\frac{1}{2}(a_{21}-a_{22})\cdot(f_{px}-f_{py})$	$\frac{a_{21}-a_{22}}{\sqrt{2}}$
9	$\dot{\beta}_{iz}$	$-a_{33}$	$\frac{-1}{\sqrt{2}}(a_{31}+a_{32})$	$\frac{1}{\sqrt{2}}(a_{31}-a_{32})$	$-a_{33}f_{pz}$	$\frac{1}{\sqrt{2}}a_{33}\cdot(f_{px}-f_{py})$	$-\frac{1}{2}(a_{31}+a_{32})\cdot(f_{px}+f_{py})$	$\frac{1}{2}(a_{31}+a_{32})\cdot(f_{px}-f_{py})$	$\frac{1}{2}(a_{31}-a_{32})\cdot(f_{px}+f_{py})$	$-\frac{1}{2}(a_{31}-a_{32})\cdot(f_{px}-f_{py})$	$\frac{a_{31}-a_{32}}{\sqrt{2}}$

	D.E.	1σ
GB_I	$\dot{GB}_I = 0$	4.8×10^{-9} RAD/SEC
GFI_J	$\dot{GFI}_J = 0$	4.8×10^{-9} (RAD/SEC)/g
$GR_\pm$	$\dot{GR}_\pm = 0$	4.8×10^{-9} RAD/SEC

$$C_p^i \triangleq \begin{pmatrix} a_{11} & a_{12} & a_{13} \\ a_{21} & a_{22} & a_{23} \\ a_{31} & a_{32} & a_{33} \end{pmatrix}$$

Figure 17: (Contd.) - Additions to F- Matrix for Gyro Error Model

$$\dot{\beta}_{ix} \alpha \frac{(a_{11} - a_{12})}{\sqrt{2}} (GBZ + GR_{+})$$

$$\dot{\beta}_{iy} \alpha \frac{(a_{21} - a_{22})}{\sqrt{2}} (GBZ + GR_{+})$$

$$\dot{\beta}_{iz} \alpha \frac{(a_{31} - a_{32})}{\sqrt{2}} (GBZ + GR_{+})$$

The terms GBZ and GR_{+} cannot be separately estimated so their sum defines a new variable.

Let

$$GZR = GBZ + GR_{+}$$

then

$$\dot{\beta}_{ix} \alpha \frac{(a_{11} - a_{12})}{\sqrt{2}} GZR$$

$$\dot{\beta}_{iy} \alpha \frac{(a_{21} - a_{22})}{\sqrt{2}} GZR$$

$$\dot{\beta}_{iz} \alpha \frac{(a_{31} - a_{32})}{\sqrt{2}} GZR$$

This new state will be defined as a random constant

$$\dot{GZR} = 0$$

and

$$\sigma_{GZR}^{2} = \sigma_{GBZ}^{2} + \sigma_{GR_{+}}^{2}$$

The remaining gyro terms are the gyro biases GB_I and the g-sensitive terms GFI_J. Comparing their magnitudes, one has

$$\dot{\beta} \alpha (GB_I + GFI_J f)$$

$$GB_I = 10^{-3} \text{ deg/hr} \quad (1\sigma)$$

$$GFI_J = 10^{-3} (\text{deg/hr})/g \quad (1\sigma)$$

$$f = 1g \text{ (gravity)}$$

$$\dot{\beta} \alpha (10^{-3} + 10^{-3})$$

The two terms are of comparable magnitude, therefore both terms will be retained. Since for the space stable platform, gravity does not align with any one axis during a flight, all the GFI_J terms must be retained.

This concludes the gyro instrument parameter selection. The gyro biases and g-sensitive terms are the only gyro error sources included in the state vector.

Next, the accelerometer parameters are considered. All the accelerometer misalignment states will not be estimatable unless an accurate attitude reference is available which is not the case here. So, the y-axis and the x-y plane are chosen as an accelerometer reference, eliminating the states AMX_y, AMY_x, and AMY_z. This leaves AMX_z, AMZ_x, and AM_{zy} as the accelerometer misalignment states. This reference selection does redefine platform tips and gyro misalignments, which is of neglectible consequence here.

The remaining accelerometer error terms are significant enough to retain. The accelerometer error terms are of comparable magnitude which for a 2g specific force is illustrated

$$\dot{\delta V} \alpha (ABI + ASF_I f + AMI_J f) a_{k_i}$$

$$= (50 \mu g + 50 \times 10^{-6} \, 2g + 50 \times 10^{-6} \, 2g) a_{k_i}$$

$$= (50 \text{ g} + 100 \text{ g} + 100 \text{g}) \times 10^{-6} \, a_{k_i}$$

The comparable magnitudes of all terms plus the inability to make any other particular assumptions leads to retaining all the remaining terms. This concludes the state selection for the INS.

The next subsystem considered is the baro-altimeter. J. Burns in Ref. [29] has proposed four states to represent the baro-altimeter. Since a detailed knowledge of the performance of the baro-altimeter is not of interest, a reduction to a single state modeled as a random walk was considered, i.e.,

$$\dot{\delta h}_B = w_B$$

where w_B represents the combined effects of the error in the Blanchard-computed algorithms with perfect data, error due to dynamic lag, error due to temperature measurement and error due to static pressure measurement, all of which are separately modeled in J. Burn's model. The impact of this single state model is that the process noise covariance for w_B is large to include all the error effects and a correlated model for δh_B has been replaced with an uncorrelated model (white noise). The baro-altimeter model effects both the altitude error δh and vertical velocity error δV_z which are directly driven by the baro error state. This relationship is shown in the steady state expressions derived by P. Grundy [23], Eq. (6.3-3) of this report,

$$\delta h_{ss} = a\ \delta A_z + b\ \delta h_B$$

$$\delta V_{z_{ss}} = c\ \delta A_z + d\ \delta h_B$$

where a, b, c, d are constant coefficients based on the vertical channel gains and Schuler frequency, δA_z is the vertical acceleration error.

A degradation of δh and δV_z by δh_B effect the ability to estimate the vertical acceleration error term δA_z. This effect must be analyzed before the single state model can be used for the baro error state. For representative values, the δh_B terms dominate the δh_{ss} value whereas the $\delta V_{z_{ss}}$ value has significant contributions from both the δA_z and δh_B terms which is shown as follows.

From Ref.[24],

$$C_1 = 0.01/\text{sec}$$

$$C_2 = 2.81 \times 10^{-5}/\text{sec}^2$$

$$C_4 = 1$$

$$w_s^2 = g/R$$

then

$$a = \frac{c_2}{c_2 - 2w_s(1 + c_1 c_4)} = 4 \times 10^4$$

$$b = \frac{1 + c_1 c_4}{c_2 - 2w_s(1 + c_1 c_4)} = 1.13 \approx 1.0$$

$$c = \frac{c_1}{c_2 - 2w_s(1 + c_1 c_4)} = 401.6 \approx 400$$

$$d = \frac{2w_s^2 c_1}{c_2 - 2w_s(1 + c_1 c_4)} = 1.25 \times 10^{-3} \approx 10^{-3}$$

From Ref.[89]:

$$\sigma_{C_{DL}} = .2 \text{ sec}$$

$$\sigma_{C_{TP}} = .01$$

$$\sigma_{C_{SP}} = 5 \times 10^{-4} \text{m/(m/sec)}^2$$

$$\sigma_{e_{BA}} = 30 \text{ m}$$

V_h = 9000 ft/min = 45.72 m/sec

h = 10,000 m

V = 554 knots = 282.4 m/sec

$$\delta h_B = e_{BA} + C_{DL} V_h + C_{TP} h + C_{SP} |V|^2$$

Then

$$\sigma^2_{\delta h_B} = \sigma^2_{e_{BA}} + \sigma^2_{C_{DL}} V_h^2 + \sigma^2_{C_{TP}} h^2 + \sigma^2_{C_{SP}} |V|^4$$

$$= (900 + 83.61 + 10{,}000 + 1589)\text{m}^2$$

$$\sigma^2_{\delta h_B} = 1.3 \times 10^4 \text{ m}^2$$

Take

$$\sigma_{\delta_{AZ}} = 50 \text{ } \mu\text{g}$$

$$\sigma^2_{h_{ss}} = a^2 \sigma^2_{AZ} + b^2 \sigma^2_{hB}$$

$$\sigma^2_{h_{ss}} = 407 + 1.3 \times 10^4 \approx 1.3 \times 10^4 \approx b^2 \sigma^2_{hB}$$

$$\sigma^2_{Vz_s} = c^2 \sigma^2_{AZ} + d^2 \sigma^2_{hB}$$

$$= 4 \times 10^{-2} + 1.9 \times 10^{-2}$$

Therefore, the δh_{ss} is approximated by

$$\delta h_{ss} \approx b \, \delta h_B$$

Although δh_B and δA_z are coupled to measurements of δh and δV_z, δh_B is almost entirely determined from δh measurements and δA_z is determined principally from δV_z measurements given δh_B.

Given a large white noise model for δh_B, the ability to estimate δA_z is analyzed using a steady state covariance analysis. The error covariance equation is given by

$$\dot{P} = FP + PF^T + Q - KRK^T$$

$$K = P H^T R^{-1}$$

Set $\dot{P} = 0$

$F = 0$ since the models assumed are

$$\dot{\delta A}_z = 0$$

$$\dot{\delta h}_B = w_b$$

w_b = white noise

Assume measurements of V_z, then

$$H = [c \ , \ d]$$

$$R^{-1} = \frac{1}{\sigma_v^2}$$

$$Q = \begin{bmatrix} 0 & 0 \\ 0 & Q_b \end{bmatrix}$$

$$\dot{P} = 0 = Q - P H^T R^{-1} H P$$

Solving for P, one has

$$d^2 Q_B \sigma_v^2 = (d^2 P_{hB_\infty} - c^2 P_{AZ_\infty})^2$$

or

$$P_{AZ_\infty} = \frac{d^2}{c^2} P_{hB_\infty} \pm \frac{\sqrt{d^2 Q_B \sigma_v^2}}{c^2}$$

Similarly for P_{hB} from δh measurements

$$P_{hB_\infty} = \frac{\sqrt{\sigma_h^2 Q_B}}{b^2}$$

(Using the same value Q_B for both velocity and position measurements assumes that they occur at the same frequency. Even though velocity measurements occur more frequently, it does not effect the conclusion.)

If

$$\sigma_h = 40 \text{ m}$$

$$Q_B = 1.3 \times 10^4 \text{ m}^2$$

$$\sigma_v = 1 \text{ m/sec}$$

then

$$P_{hB_\infty} = 4560 \text{ m}^2$$

$$P_{AZ_\infty} = 7.1 \times 10^{-7} \text{ (m/sec}^2\text{)}^2$$

or

$$\sigma_{AZ} = \sqrt{P_{AZ_\infty}} = 8.4 \times 10^{-4} \text{ m/sec}^2$$

But δAZ values are expected to be on the order of 10 μg (9.8×10^{-5} m/sec^2). So filtering both δh and δV_Z measurements leads to a steady state uncertainty which is larger than the expected values of the quantity estimated δAZ which says that δAZ cannot be estimated with a white noise model for δh_B of this magnitude.

The second effect analyzed is the impact of modeling δh_B as an uncorrelated white noise when in fact it is a correlated process. Neglecting this correlation results in its effect biasing the estimate of δA_Z. This bias can be computed using a steady state analysis on the state estimates

$$\dot{x} = Fx + K(z - Hx)$$

$$K = P H^T R^{-1}$$

Then

$$H = \begin{bmatrix} 0 & b \\ c & d \end{bmatrix}$$

$$R^{-1} = \begin{bmatrix} \frac{1}{\sigma_h^2} & 0 \\ 0 & \frac{1}{\sigma_v^2} \end{bmatrix}$$

$$\underline{x} = \begin{bmatrix} \delta A_z \\ \delta h_B \end{bmatrix}$$

$$F = \begin{bmatrix} 0 & 0 \\ 0 & \beta \end{bmatrix}$$ where β is the correlation of δh_B

Then, setting $\dot{\underline{x}} = 0$ and solving for x results in

$$\delta A_z = \frac{V_z}{c} - \frac{d}{c} \delta h_B$$

$$\delta h_B = - \frac{P_{hB}\, b\, \delta h}{\sigma_h^2 \beta - P_{hB}\, b^2}$$

The difference in δA_z with δh_B correlated ($\beta \neq 0$) and δh_B uncorrelated ($\beta = 0$) is the bias

$$\Delta\delta A_z = - \frac{d}{cb} \frac{\sigma_h^2\, \beta\, \delta h}{(\sigma_h^2 \beta - P_{hB}\, b^2)}$$

If

$$\beta \approx 1/100$$

$$\delta h \approx 10 \text{ m}$$

$$\Delta\delta A_z \approx - \frac{d}{cb} \delta h = 2.5 \times 10^{-5}$$

which is a significant bias compared to the expected values of δA_z. Therefore considering the estimation accuracy and bias of δA_z with δh_B as a white noise, it can be concluded that this is an unacceptable model for δh_B. It is realized that this is a steady state analysis and the actual performance will differ from this, but this analysis is indicative of the performance expected and it is adequate to support the conclusion.

On the other hand, each element of Burns' model is separately estimated and as each parameter is observed, its uncertainty diminishes. The result being that the linear combination of parameters to form δh_B has a decreasing uncertainty that permits an accurate estimation of the δA_z term.

So the conclusion is that a single random walk state model for δh_B is inadequate here and the four state model proposed by Burns should be used. This conclusion assumes that the elements of the four state model are observable so that the covariance of the linear combination becomes less than that of the process noise covariance of w_B for the single state model. An alternative to estimating all four elements would be to retain only the e_{BA} and e_{CTP} terms and include the e_{CDL} and e_{CSP} term in the Q matrix for δh_b. This conclusion can be drawn from the relative magnitudes of the terms in $\sigma^2_{\delta h_b}$ above and the expected variation in each term (V will not change significantly over a flight).

The next subsystem addressed for state vector selection is the radar and its measurements. Several significant errors are identified which can be categorized as follows:

1) Errors in the orientation of the antenna in inertial space

2) Errors caused by electromagnetic propagation of the radar transmissions through a non-ideal medium, such as refraction and multipath

3) Inherent radar measurement errors

4) Survey errors in the checkpoint locations

These error sources can be modeled as follows.

The antenna orientation error in inertial space has three sources as identified in Refs. [31] and [49]. They are the tilt angles of the platform β_i, included as part of the INS error state; platform to case errors, μ, (or gimbal angle errors, e_i); and antenna/random errors, τ. These three error sources contribute to the velocity, elevation and azimuth measurements.

Two observations are made. First, note that the four gimbal angle errors, (e_1, e_2, e_3, e_4) cannot all be observed because one is redundant. Second, if the results of [31] and [50] are used where the angle errors have all been transformed to the navigation and inertial frames, respectively, the $\underline{\tau}$ and $\underline{\mu}$ terms cannot be separated if the same dynamic model is used for each. Recalling that the measurements have a term of the form ($\underline{\beta}^i + \underline{\tau}^i + \underline{\mu}^i$), this can readily be

seen from the standard definition of observability, i.e., $[H, H\Phi, H\Phi^2]^T$ has two identical columns. On the other hand, if either different dynamic models are used for $\underline{\tau}$ and $\underline{\mu}$ or $\underline{\tau}$ and $\underline{\mu}$ are defined in different coordinate frames with a time-dependent transformation between frames, $\underline{\tau}$ and $\underline{\mu}$ are separately observable. This is illustrated as follows. If μ is coordinatized in the platform frame and called $\underline{\mu}^P$ and τ is coordinatized in the case frame and called $\underline{\tau}^C$, the measurement term referred to above becomes

$$(\underline{\beta}^i + C_c^i \underline{\tau}^C + C_p^i \underline{\mu}^P)$$

where

$C_c^i = C_p^i C_c^P$ transformation from case to inertial

C_p^i = transformation from platform to inertial

C_c^P = transformation from case to platform

The transformation C_c^P contains the gimbal angles which will be time varying thus making $\underline{\tau}^C$ and $\underline{\mu}^P$ separately observable in the theoretical sense. In a practical sense, the azimuth component may be the only separable component of μ^P and τ^C because a heading angle will typically be held for a sufficient period of time to permit this component to be large relative to the smoothed measurement noise. The duration of pitch and roll will typically be short term, therefore making it difficult to observe and separate these components of τ^C and μ^P.

To get to the final selection of angular errors, it can be shown that the third component of $\underline{\tau}^C$ forms a non-separable linear combination with e4. Starting with the error in the transformation from antenna to inertial C_a^i from[49]leads to the term in the measurements

$$(\underline{\beta}^i + C_c^i \underline{\tau}^C + C_p^i \underline{\mu}^P)$$

referenced above.

This term is equal to

$$(\underline{\beta}^i + C_p^i(C_c^P \tau^C + \mu^P))$$

where we will work only with the term

$$C_c^p \tau^C + \mu^p$$

in platform frame since C_p^i is common to both.

Then from Ref. [31]

$$C_c^p = C_{g1}^p C_{g2}^{g1} C_{g3}^{g2} C_{g4}^{g3} C_c^{g4}$$

where

$$C_c^{g4} = \begin{bmatrix} c\Theta_4 & s\Theta_4 & 0 \\ -s\Theta_4 & c\Theta_4 & 0 \\ 0 & 0 & 1 \end{bmatrix}$$

Since the other transformations (C's) are defined in Ref. [49], they are not repeated here.

Then, from Ref. [49]

$$\underline{\mu}_p = C_{g1}^p \begin{bmatrix} 0 & s\Theta_1 & c\Theta_1 c\Theta_2 & s\Theta_1 s\Theta_3 - c\Theta_1 s\Theta_2 c\Theta_3 \\ 0 & c\Theta_1 & -c\Theta_2 s\Theta_1 & c\Theta_1 s\Theta_3 + s\Theta_1 c\Theta_3 s\Theta_2 \\ 1 & 0 & s\Theta_2 & c\Theta_2 c\Theta_3 \end{bmatrix} \underline{e}$$

or

$$\underline{\mu}_p = C_{g1}^p A\underline{e}$$

Then

$$C_c^p \tau_c + \mu^p = C_{g1}^p (C_{g2}^{g1} C_{g3}^{g2} C_{g4}^{g3} C_c^{g4} \tau_c + A\underline{e})$$

Working this out, one has

$$= C_{g1}^{P} \begin{bmatrix} (\ )\tau_1 + (\ )\tau_2 + (\ )e_1 + (\ )e_2 + (\ )e_3 + (s\Theta_1 s\Theta_3 - c\Theta_1 s\Theta_3 c\Theta_3)(\tau_3 + e_4) \\ (\ )\tau_1 + (\ )\tau_2 + (\ )e_1 + (\ )e_2 + (\ )e_3 + (c\Theta_1 s\Theta_3 + s\Theta_1 s\Theta_2 c\Theta_3)(\tau_3 + e_4) \\ (\ )\tau_1 + (\ )\tau_2 + (\ )e_1 + (\ )e_2 + (\ )e_3 + (c_2\ c_3)(\tau_3 + e_4) \end{bmatrix}$$

From this expression, one can see the nonseparable linear combination of $(\tau_3 + e_4)$. Redefine this sum to be

$$\tau_z = \tau_3 + e_4$$

Then

$$C_c^P\ \tau_c + \mu^P = C_{g1}^P (C_{g2}^{g1}\ C_{g3}^{g2}\ C_{g4}^{g3}\ C_c^{g4}\ \tau'^C + A'e')$$

where

$$\tau'^C = \begin{bmatrix} \tau_1 \\ \tau_2 \\ \tau_z \end{bmatrix}$$

$$e' = \begin{bmatrix} e_1 \\ e_2 \\ e_3 \end{bmatrix}$$

$$A' = \begin{bmatrix} 0 & s\Theta_1 & c\Theta_1 c\Theta_2 \\ 0 & c\Theta_1 & -c\Theta_2 s\Theta_1 \\ 1 & 0 & s\Theta_2 \end{bmatrix}$$

or

$$C_c^P \tau^C + \mu^P = C_c^P \tau'^C + B e'$$

where

$$B = \begin{bmatrix} 0 & \frac{c\Theta_1 + s\Theta_1}{\sqrt{2}} & \frac{(c\Theta_1 - s\Theta_1)c\Theta_2}{\sqrt{2}} \\ 0 & \frac{c\Theta_1 - s\Theta_1}{\sqrt{2}} & -\frac{(c\Theta_1 + s\Theta_1)c\Theta_2}{\sqrt{2}} \\ 1 & 0 & s\Theta_2 \end{bmatrix}$$

which is the first three columns from Figure 3 in Ref. [49].

So, the transformation error term becomes

$$(\beta^i + C_c^i \tau^C + C_p^i \mu^P) = (\beta^i + C_c^i \tau'^C + C_p^i B e')$$

τ'^C and e' will be included in the state vector to represent the case to antenna and gimbal angle errors respectively, keeping in mind that the third component of τ'^C includes the fourth gimbal angle error e_4. From Ref. [49] τ'^C and e' can be modeled as random constants

$$\dot{\tau}'^C = 0$$

$$\dot{e}' = 0$$

Initially, all six components will be included in the state vector, but the simulation studies may indicate that the roll and pitch related components are not separately observable, recalling the practical observability discussion above.

For the radar, range, range-rate, and monopulse azimuth and elevation measurement, errors are included. The radar errors on range δR and range rate $\delta \dot{R}$ are modeled as biases

$$\frac{d}{dt}\,\delta R = 0$$

$$\frac{d}{dt}\,\delta \dot{R} = 0$$

The residual propagation effects after compensation are not included as elements in the state vector but rather its effect should be treated as an additive white noise to the radar measurements.

The justification for this selection is as follows. It is assumed that at least the average propagation effects over a large geographic area will be removed by the compensation in the radar. The propagation error remaining then will be only the local variations from the average, primarily near each checkpoint. This residual should be small in magnitude assuming a reasonable compensation algorithm. Since the aircraft is moving relative to the checkpoint, the residual propagation error from measurement to measurement will probably uncorrelate making its estimation difficult. Therefore, they are included as a random additive noise to the measurements rather than states to be the estimated. On the other hand, the radar biases will remain constant independent of aircraft motion, location, or checkpoint. Therefore, these biases should be recoverable. The adequacy of the constant model proposed for δR and $\delta \dot{R}$ must be verified by test data.

The monopulse azimuth and elevation measurement errors included are a bias and scale factor error. The monopulse system assumes a linear relation between the ratio of difference to sum signal (Δ/Σ) and the measured angle which for measured elevation, E_m, is given by

$$E_m = K\left(\frac{\Delta}{\Sigma}\right)$$

A similar relationship holds for azimuth. This relationship is valid for small differences Δ. The error effects modeled in this process are that of a bias in this relationship which corresponds to Δ being zero but E_m not equaling zero and a scale factor error which corresponds to an error in the slope K.

The error in an elevation measurement can then be written as

$$\Delta K_E\, E_m + E_b$$

where

$$\Delta K_E = \frac{\Delta K_1}{K_E}$$

ΔK_1 = error in the elevation slope K_E

E_b = elevation bias

Similarly for the error in the azimuth measurement

$$\Delta K_A \, A_m + A_b$$

where

$$\Delta K_A = \frac{K_2}{K_A}$$

ΔK_2 = error in the azimuth slope K_A

A_b = azimuth bias

The models assumed for these error quantities are random constants

$$\dot{\Delta K_E} = 0$$

$$\dot{E}_b = 0$$

$$\dot{\Delta K_A} = 0$$

$$\dot{E}_A = 0$$

Again, the adequacy of these models must be verified by test data.

These error terms for range, range rate, azimuth and elevation add directly to the radar measurements for purposes of forming the H matrix and residuals in the filter.

The survey errors of the checkpoint can be modeled as random constants

$$\dot{\delta X} = 0$$

$$\dot{\delta Y} = 0$$

$$\dot{\delta Z} = 0$$

and δX, δY, and δZ represent the three cartesian components of a survey error. The ability to estimate survey errors depends on the number of measurements taken from the same checkpoint. A reasonable number of measurements from the same checkpoint and at different aircraft locations are required for the filter to estimate the survey error. If survey error states are included, either states for each checkpoint are included or filter rectification on checkpoint switching is required. Also, one checkpoint must always be chosen as a reference from which other checkpoint survey errors are measured. It is recommended that survey errors be included in the state only if frequent measurements to each checkpoint from different aircraft locations are taken.

This completes the filter state selection. The suboptimal filter state is summarized in Table 4.

Table 4
Suboptimal State Vector

δr_{ix}	x cartesian position error in inertial space
δr_{iy}	y cartesian position error in inertial space
δr_{iz}	z cartesian position error in inertial space
δV_{sx}	x velocity error
δV_{sy}	y velocity error
δV_{sz}	z velocity error
β_{ix}	platform angular error about x axis
β_{iy}	platform angular error about y axis
β_{iz}	platform angular error about z axis
ABX	x accelerometer bias
ABY	y accelerometer bias
ABZ	z accelerometer bias
ASFX	x accelerometer scale factor error
ASFY	y accelerometer scale factor error
ASFZ	z accelerometer scale factor error
AMX_z	x accelerometer misalignment about z axis
AMZ_x	z accelerometer misalignment about x axis
AMZ_y	z accelerometer misalignment about y axis
GBX	x gyro bias
GBY	y gyro bias
GZR	z gyro bias and torquing error

Table 4 (Contd.)

GFX_x	g sensitive drift of x gyro about x axis
GFX_z	g sensitive drift of x gyro about z axis
GFY_y	g sensitive drift of y gyro about y axis
GFY_z	g sensitive drift of y gyro about z axis
GFZ_y	g sensitive drift of z gyro about y axis
GFZ_z	g sensitive drift of z gyro about z axis
e_{BA}	blanchard algorithm error in baro altimeter
C_{DL}	dynamic lag coefficient in baro altimeter
C_{TP}	standard temperature error coefficient in baro altimeter
C_{SP}	standard pressure error coefficient in baro altimeter
τ_1^c	antenna misalignment about case x axis
τ_2^c	antenna misalignment about case y axis
τ_z^c	antenna misalignment about case z axis
e_1	angle error in gimbal #1
e_2	angle error in gimbal #2
e_3	angle error in gimbal #3
δR	radar range bias
$\delta \dot{R}$	radar range rate bias
ΔK_E	monopulse elevation scale factor error
E_b	monopulse elevation bias

Table 4 (Contd.)

ΔK_a	monopulse azimuth scale factor error
A_b	monopulse azimuth bias
δX	x axis survey error
δY	y axis survey error
δZ	z axis survey error

6.9.3 Process Noise Covariance Matrix

The process noise covariance matrix Q reflects the system driving noises and accounts for unmodeled and neglected effects. Unmodeled effects considered for inclusion in the Q matrix are the gyro misalignment terms and the gyro g^2-dependent drift terms. The gyro g^2-dependent drift terms are represented in general by

$$\dot{\beta}_i \alpha f_j f_k GFFI_{jk}$$

which exist only for $j \neq k$.

Starting with the general form

$$Q = \int \Phi N \Phi \, ds \qquad \text{let } \Phi \sim I$$

then

$$Q_{\beta_i} = \sigma^2_{GFFI_{jk}} \int f_j^2 f_k^2 \, ds \quad , \quad j \neq k$$

In particular, from Eqn. (6-21) of Ref. [29],

$$Q_{\beta_{ix}} \alpha \sigma^2_{GFFX_{xy}} \int f_x^2 f_y^2 + \sigma^2_{GFFX_{xz}} \int f_x^2 f_z^2 + \sigma^2_{GFFX_{yz}} \int f_y^2 f_z^2$$

$$Q_{\beta_{iy}} \alpha \sigma^2_{GFFY_{xy}} \int f_x^2 f_y^2 + \sigma^2_{GFFY_{xz}} \int f_x^2 f_z^2 + \sigma^2_{GFFY_{yz}} \int f_y^2 f_z^2$$

$$Q_{\beta_{iz}} \alpha \sigma^2_{GFFZ_{xy}} \int f_x^2 f_y^2 + \sigma^2_{GFFZ_{xz}} \int f_x^2 f_z^2 + \sigma^2_{GFFZ_{yz}} \int f_y^2 f_z^2$$

An expression is required for

$$\int f_a^2 f_b^2$$

where a and b take on the values x, y, and z, and $a \neq b$.

Let

$$f^2 = f_a^2 + f_b^2$$

then

$$f^4 \geq f_a^2 f_b^2$$

$$\int f_z^2 f_b^2 \leq \int f^4 \approx (2V_{ab}|\Delta V_{ab}|)^2$$

where

$$V_{ab} = \sqrt{V_a^2 + V_b^2}$$

$$\Delta V_{ab} = \sqrt{f_a^2 + f_b^2}\ \Delta t$$

Making this substitution in the equations above, one has

$$Q_{\beta_{ix}} \alpha \sigma^2_{GFFX_{xy}} C_{xy} + \sigma^2_{GFFX_{xz}} C_{xz} + \sigma^2_{GFFX_{yz}} C_{yz}$$

$$Q_{\beta_{iy}} \alpha \sigma^2_{GFFY_{xy}} C_{xy} + \sigma^2_{GFFY_{xz}} C_{xz} + \sigma^2_{GFFY_{yz}} C_{yz}$$

$$Q_{\beta_{iz}} \alpha \sigma^2_{GFFZ_{xy}} C_{xy} + \sigma^2_{GFFZ_{xz}} C_{xz} + \sigma^2_{GFFZ_{yz}} C_{yz}$$

where

$$C_{xy} = (2V_{xy}|\Delta V_{xy}|)^2$$

$$C_{xz} = (2V_{xz}|\Delta V_{xz}|)^2$$

$$C_{yz} = (2V_{yz}|\Delta V_{yz}|)^2$$

$$V_{xy} = \sqrt{V_x^2 + V_y^2}$$

$$V_{xz} = \sqrt{V_x^2 + V_z^2}$$

$$V_{yz} = \sqrt{V_y^2 + V_z^2}$$

$$\Delta V_{xz} = \Delta t \sqrt{f_x^2 + f_z^2}$$

$$\Delta V_{xy} = \Delta t \sqrt{f_x^2 + f_y^2}$$

$$\Delta V_{yz} = \Delta t \sqrt{f_x^2 + f_z^2}$$

The gyro misalignment terms which have also been neglected are given from Eqn. (6-15)[29] as

$$\dot{\beta}_i \alpha C_p^i \delta C_g^p \omega_p^g$$

which in general is given as

$$\delta C_g^p \omega_{ip}^g = \begin{bmatrix} GSF_x & -XG_y & XG_z \\ YG_x & GSF_y & -YG_z \\ -ZG_x & ZG_y & GSF_z \end{bmatrix} \omega_{ip}^g$$

where

$GSF_{x,y,z}$ are torquing scale factor errors and the other terms represent the misalignments

ω_{ip}^g is the angular velocity of the platform in inertial space

For the space stable system with no platform torquing $\omega_{ip}^g = 0$. The process noise matrix term becomes simply

$$Q_\beta = 0$$

6.9.4 Transition Matrix Evaluation

The transition matrix Φ can in general be represented as

$$\Phi = e^{\int F dt}$$

for a system described by $\dot{x} = F x + u$.

Φ can be approximated as a Taylor series retaining the first two terms,

$$\Phi \approx I + \int F\,dt$$

the second order terms are assumed neglectible.

The evaluation of $\int F\,dt$ depends on how rapidly F varies. The following forms are used

$$\int F\,dt = \begin{cases} F\,\Delta t & \text{for slowly varying F} \\ (F_{i+1} + F_i)\frac{\Delta t}{2} & \text{(trapezoidal integration) for rapidly varying F} \end{cases}$$

The rapidly varying terms are usually just the specific force related terms, for which the integrals $\Delta v = \int F\,dt$ are available from the IMU.

6.9.5 Initial State Vector and Covariance Matrix

The probability distributions of all elements of the state vector are symmetric about zero. Therefore, the expected value of the state vector, given no measurements, is zero

$$\hat{\underline{x}}_0 = E[\underline{x}_0] = 0$$

The variances of the horizontal components of position and velocity error can be initialized to sufficient accuracy by considering the simplistic error model

$$\delta p = \delta v_B \; t_{NAV} + (\delta v_s/\omega_s)\sin(\omega_s \; t_{NAV} + \phi)$$

$$\delta v = \delta v_B \quad + \quad \delta v_s \quad \cos(\omega_s \; t_{NAV} + \phi)$$

where

δv_B = bias velocity error

δv_s = amplitude of the Schuler oscillation

ω_s = Schuler radian frequency

t_{NAV} = time since INS was switched to nav mode

ϕ = random phase of Schuler oscillation

The variances of the errors are then given by

$$P_{\delta p_e} = (\sigma_{VB} \; t_{NAV})^2 + .5(\sigma_{VS}/\omega_s)^2$$

$$P_{\delta p_n} = P_{\delta p_e}$$

$$P_{\delta v_e} = \sigma_{VB}^2 + .5 \; \sigma_{VS}^2$$

$$P_{\delta v_n} = P_{\delta v_e}$$

where typical values, for a 1 n.mi./hr system, would be

$$\sigma_{VB} = 2 \text{ f/sec}$$

$$\sigma_{VS} = 5 \text{ f/sec}$$

The cross-correlation implied by this crude model is ignored on conservatism grounds.

The second order vertical channel will, in steady-state, drive the altitude error to the linear combination of baro-altitude error and vertical acceleration error, in order to zero the rate-of-change of vertical velocity. Additionally, in order to zero the rate-of-change of altitude, the vertical velocity will exhibit an error which is proportional to the vertical acceleration error and baro-altitude error as is illustrated in Ref.[23] and presented above. So, in the local level frame we have a four element vector which we can consider for this initial covariance definition given by

$$X = \begin{bmatrix} \delta h \\ \delta V_z \\ \delta h_B \\ \delta A_z \end{bmatrix}$$

$$\text{Cov } X = E[X X^T] = \begin{bmatrix} P_{\delta h}^2 & P_{\delta h \delta V_z} & P_{\delta h \delta h_B} & P_{\delta h \delta A_z} \\ & P_{\delta V_z}^2 & P_{\delta V_z \delta h_B} & P_{\delta V_z \delta A_z} \\ & & P_{\delta h_B}^2 & P_{\delta h_B \delta A_z} \\ & & & P_{\delta A_z}^2 \end{bmatrix}$$

where, assuming δh_B and δA_z are independent,

$$P_{\delta h}^2 = a^2 P_{\delta A_z}^2 + b^2 P_{\delta h_B}^2$$

$$P_{\delta V_z}^2 = c^2 P_{\delta A_z}^2 + d^2 P_{\delta h_B}^2$$

$$P_{\delta h_B}^2 = \sigma_{e_{BA}}^2 + \sigma_{C_{DC}}^2 v_h^2 + \sigma_{C_{TP}}^2 h^2 + \sigma_{C_{SP}}^2 |V|^4$$

(from Ref.[29], eq. 5-4)

$$P_{\delta A_z}^2 = K \sigma_{ABZ}^2$$

$$P_{\delta h \delta V_z} = a\, c\, P_{\delta A_z}^2 + bd\, P_{\delta h_B}^2$$

$$P_{\delta h \delta h_B} = b\, P_{\delta h_B}^2$$

$$P_{\delta h \delta A_z} = a\, P_{\delta A_z}^2$$

$$P_{\delta V_z \delta h_B} = d\, P_{\delta h_B}^2$$

$$P_{\delta V_z \delta A_z} = c\, P_{\delta A_z}^2$$

$$P_{\delta h_B \delta A_z} = 0$$

where, from Ref. [29], Eq. (3),

$$a = \frac{1+c_1\, c_4}{c_2 - 2w_s^2(1+c_1\, c_4)} \quad , \quad b = \frac{c_2}{c_2 - 2w_s^2(1+c_1\, c_4)}$$

$$c = \frac{c_1}{c_2 - 2w_s^2(1+c_1\, c_4)} \quad , \quad d = \frac{2w_s^2\, c_1}{c_2 - 2w_s^2(1+c_1\, c_4)}$$

where

c_1, c_2, c_3 = vertical channel gain parameters

w_s = Schuler frequency ($=\sqrt{g/R}$)

K = scale factor multiplier

This defines the initial uncertainties and correlations for the vertical channel related terms.

The platform tips may be assumed to be related to the Schuler oscillation δp given above as

$$\beta = \delta P/R$$

then

$$P_{\beta_e} = (\sigma_{VS}\ \omega_s/g)^2$$

$$P_{\beta_n} = P_{\beta_e}$$

The azimuth error is related to the initial gyro-compassing error, in addition to the subsequent azimuth gyro drift rate

$$P_{\beta_z} = (2\sigma_{GBX}/\Omega\cos L)^2 + (\sigma_{GBZ}\ t_{NAV})^2$$

where it has been assumed that the platform is aligned with the x axis east and Ω = earth rate, L = latitude. These initial covariance values for the position, velocities and tips are referenced to the local level frame which should be transformed to the inertial frame for use by the EIF.

The instrument error covariances (accelerometer and gyro) are initialized with

$$P_I = \sigma_I^2\ K$$

where

σ_I = instrument standard deviation (accelerometer and gyro)
e.g., I = GBX, GBY, GBZ,

K = scale factor multiplier

The same form is used for the gimbal angle error and antenna misalignment initial covariance.

The initial covariance for radar error states are defined in a similar manner.

$$P = \sigma^2 K_e$$

where σ^2 is taken as the system specification for each measurement type.

6.9.6 Conclusion

The filter has been formulated for the EAR/GEANS error isolation filter. This formulation has included the filter state vector selection, process noise covariance matrix definition, transition matrix evaluation, initial state vector and covariance matrix definitions. The state vector elements and models for the INS are well defined but the state vector elements and models for the radar are less well understood and will require validation using test data. Gravity errors have not been considered here since they are the topic of a separate memo. The filter algorithm and measurement matrices are also the topics of separate memos.

6.9.7 Subsequent Refinements

Subsequent to the initial definition of the EIF state vector presented in Ref. [48] and repeated in Section 6.9.2, a few instrument error states have been deleted, some modified, and others added. Those deleted are baro-altimeter dynamic lag error, monopulse elevation and azimuth scale factor errors, and radar checkpoint x,y,z survey errors. Those changed are monopulse elevation and azimuth angle biases to cosine biases. Those added are radar range-rate scale factor error, and three gravity perturbation components. The current EAR/GEANS EIF state vector is defined in Section 6.10, Table 6 of this report.

6.10 Feedback Correction Equations for EAR/GEANS EIF

This section and Appendix A comprise Intermetrics AFAL/GPS Memo #79-01, "Feedback Correction Equations for EAR/GEANS EIF," by Neai A. Carlson, dated 31 May 1979 [51].

6.10.1 Introduction and Summary

The EAR/GEANS onboard navigation filter can operate in either a feedback or feedforward mode. As described in Reference [52] the feedback mode is the normal operating mode; however, the system operator can switch from one option to the other as he chooses. A system status bit indicates which mode is being used at any given time.

In the feedback mode, all 13 onboard filter states are utilized to correct the INS, altimeter, and antenna subsystems. The feedback correction is completed on all 13 states within one 1/32 sec computation cycle, and so indicated by an event flag. This flag is recorded at 8 Hz on the flight data tape; hence, it is possible post-flight to determine the time of feedback correction to within $\pm$ 1/16 sec.

During post-flight data analysis, the Error Isolation Filter (EIF) determines running estimates of the errors in several components of the onboard-computed EAR/GEANS state, plus estimates of a sizeable number of system error sources. Certain EIF error-state estimates must be adjusted each time an onboard feedback correction is encountered, to account for the discrete jump in the onboard state.

The remainder of this memo describes the theoretical basis for feedback correction compensation in the EIF; the relationship between EAR/GEANS correction components and EIF error states; and the feedback compensation equations actually implemented in the EIF.

6.10.2 Theoretical Background

Certain EIF error-state elements must be adjusted each time an onboard feedback correction is encountered; other EIF error-state elements are independent of the onboard state, and require no adjustment. This section describes the general process whereby EAR/GEANS onboard state corrections are implemented and these corrections are compensated in the EIF. For purposes of discussion, the following definitions are convenient:

$\underline{x}$ = EAR/GEANS indicated state
$\delta\underline{x}$ = onboard filter computed error in $\underline{x}$
$\bar{\underline{s}}$ = EIF reference system state
$\underline{e}$ = EIF best estimate of error in $\bar{\underline{s}}$
$\underline{s}$ = $\bar{\underline{s}}$ - $\underline{e}$, EIF best estimate of system state
$()^-$ = value just before onboard correction
$()^+$ = value just after onboard correction

When the EAR/GEANS onboard navigation filter is operating in the feedback mode, it periodically corrects the indicated state as follows:

$$\underline{x}^+ = \underline{x}^- - \delta\underline{x}^- \qquad (6.10\text{-}1)$$
$$\delta\underline{x}^+ = \underline{0}$$

That is, the filter-computed error $\delta\underline{x}$ is subtracted from the indicated state $\underline{x}$, whereafter the error is reset to zero. For purposes of post-flight analysis, the onboard system records the correction as

$$\delta\underline{x} \equiv \delta\underline{x}^- \stackrel{\cdot}{\equiv} \underline{x}^- - \underline{x}^+ \qquad (6.10\text{-}2)$$

During post-flight processing, the EIF maintains a best estimate $\underline{s}$ of the true system state. This estimate is maintained in two parts, a reference or nominal value $\bar{\underline{s}}$ and a best estimate $\underline{e}$ of the error in that reference value:

$$\underline{s} = \bar{\underline{s}} - \underline{e} \qquad (6.10\text{-}3)$$

This relationship by definition remains unchanged when the onboard filter applies discrete corrections $\delta\underline{x}$ to the onboard state $\underline{x}$. Hence, the estimated error $\underline{e}$ must be adjusted to compensate for discrete changes in the reference state $\bar{\underline{s}}$, or in the estimated true state $\underline{s}$, resulting from the onboard correction $\delta\underline{x}$.

The adjustment $\delta\underline{e}$ to the EIF error state required to compensate for an onboard correction $\delta\underline{x}$ can be defined by

$$\underline{e}^{+} = \underline{e}^{-} - \delta\underline{e} \qquad (6.10\text{-}4)$$

$$\delta\underline{e} = \left(\frac{\partial\bar{\underline{s}}}{\partial\underline{x}} - \frac{\partial\underline{s}}{\partial\underline{x}}\right)\delta\underline{x} \overset{\Delta}{=} A\delta\underline{x} \qquad (6.10\text{-}5)$$

That is, an adjustment δe_i is required in any EIF error state element for which either i) the reference value $\bar{s}_i$ is derived directly from the current onboard state $\underline{x}$, or ii) the true value - estimated as s_i - is actively controlled by the onboard system as a function of $\underline{x}$ or $\delta\underline{x}$.* No adjustment is required in an error state for which iii) the reference value $\bar{s}_i$ is derived independently of the current onboard state, and the true value is unchanged by the onboard correction.

All three cases are possible in principle. For the EAR/GEANS EIF, most of the error states related to the onboard correction fall in category i), and a few fall in category iii). Careful examination of variable definitions, onboard correction mechanisms, and EIF reference data construction is necessary to determine the proper relationships. These factors are examined in detail in Section 6.10.3.

A potential further complexity arises when the EIF error state is available at some time t_e not identical to the feedback correction time t_f.

---

*Example: true attitude of an inertial platform actively torqued to correct for filter-computed tilts.

The compensation valid at t_f must be propagated from t_f to t_e via the EIF state transition matrix Φ before the EIF error state at t_e can be corrected:

$$\begin{aligned} \delta\underline{e}_f &= A\ \delta\underline{x}_f \\ \underline{e}_e^+ &= \underline{e}_e^- - \Phi(t_e,t_f)\delta\underline{e}_f \end{aligned} \qquad (6.10\text{-}6)$$

In the present mechanization of the EIF, the error state $\underline{e}$ is propagated explicitly to each EAR/GEANS feedback correction time, such that $t_e \equiv t_f$; hence, the compensation can be applied directly as per Eqs. (6.10-4,5).

3. Relationship of Feedback Correction States to EIF Error States

The EAR/GEANS feedback correction $\delta\underline{x}$ comprises 13 elements, defined in Table 5. The EIF error state $\underline{e}$ comprises 44 elements, defined in Table 6. The relationsnips between the elements of $\delta\underline{x}$ and the elements of e are represented by the 44 x 13 matrix A in Eq.(-5). To determine these relationships requires careful examination of the definitions of corresponding elements of each state space. Details of these relationships are presented in the following four subsections.

For sake of clarity, the specific coordinate frames in which vectors are represented are indicated by superscripts:

- $(\ )^i$ = inertial (space-stable) coordinates
- $(\ )^p$ = GEANS platform coordinates (nominal accelerometer and gyro input axes)
- $(\ )^r$ = GEANS rotated platform frame
- $(\ )^n$ = GEANS navigation frame
- $(\ )^c$ = GEANS gimbal case frame
- $(\ )^a$ = EAR antenna frame

Coordinate transformations C from one frame to another are indicated by corresponding subscript and superscript, e.g.,

Table 5
Definition of EAR/GEANS Feedback Correction States

Elements of $\delta\underline{x}$	Math Symbol	Description	Coord. Frame	Units
1-3	$\delta\underline{v}_s^i$	Corrected error[2] in onboard components of space-relative velocity $\underline{v}_s$	Inertial	m/s
4-6	$\delta\underline{r}^i$	Corrected error in onboard components of geocentric position $\underline{r}$	Inertial	m
7	δh_B	Corrected error in onboard Blanchard altimeter bias Δh_B	None	m
8-10	$\delta\underline{\phi}^i$	Corrected error in platform-to-inertial rotation vector[3] equivalent to C_p^i	Inertial	r
11-13	$\delta\underline{\alpha}^c$	Corrected error in case-to-antenna rotation vector equivalent to C_c^a	Case	r

Notes:
1. Definitions derived from [52], pp. 4-29 to 4-32
2. Corrected error is amount subtracted from the onboard state, i.e., minus the change in onboard state.
3. Rotation vector equivalent to coordinate rotation matrix (Appendix A).

Table 6
Definition of EAR/GEANS Error Isolation Filter States

Elements of $\underline{e}$	Math Symbol	Description	Coord. Frame	Units
1-3	$e\underline{r}^i$	Error[2] in onboard geocentric postion vector $\underline{r}$	Inertial	m
4-6	$e\underline{v}_s^{\,i}$	Error in onboard inertial (space-relative) velocity vector $\underline{v}_s$	Inertial	m/s
7-9	$\underline{\varepsilon}^i$	Error in onboard platform-to-inertial rotation vector[3] equivalent to C_p^i	Inertial	r
10-12	$\underline{AB}^p$	Accelerometer biases	Platform	m/s^2
13-15	$\underline{ASF}^p$	Accelerometer scale factor errors	Platform	ND
16-18	$\begin{Bmatrix} AMXz \\ AMzX \\ AMzY \end{Bmatrix}$	$\begin{Bmatrix} x \\ z \\ z \end{Bmatrix}$ accel'r misalign'ts about $\begin{Bmatrix} z \\ x \\ y \end{Bmatrix}$ axes	Platform	r
19-21	$\underline{GB}^g$	Gyro bias drift rates	Gyro	r/s
22-27	$\begin{Bmatrix} GFXX \\ GFXz \\ GFYY \\ GFYz \\ GFzY \\ GFzz \end{Bmatrix}$	$\begin{Bmatrix} x \\ x \\ y \\ y \\ z \\ z \end{Bmatrix}$ gyro drift sensitivities to specific force along $\begin{Bmatrix} x \\ z \\ y \\ z \\ y \\ z \end{Bmatrix}$ axes	Gyro	$\frac{r/s}{m/s^2}$
28-30	$\begin{Bmatrix} e_{BA} \\ c_{TP} \\ c_{sp} \end{Bmatrix}$	Error in onboard Blanchard algorithm bias Altimeter temp.-induced scale factor error Altimeter static pressure coef. error	None None None	m ND $\frac{m}{(m/s)^2}$
31-33	$\underline{\iota}^c$	Error in initial onboard antenna-to-case coord. rotation vector equiv. to C_{ao}^c	Case	r
34-36	$\underline{\epsilon}^g$	Errors in onboard gimbal angles $\theta_1, \theta_2, \theta_3$	Gimbal	r
37-39	$\begin{Bmatrix} RB \\ RRB \\ RRSF \end{Bmatrix}$	Radar range bias Radar range-rate bias Radar range-rate scale factor error	None None None	m m/s ND
40-41	$\begin{Bmatrix} eCA \\ eCE \end{Bmatrix}$	Monopulse $\begin{Bmatrix} \text{azimuth} \\ \text{elevation} \end{Bmatrix}$ cosine biases	None	ND
42-44	$e\underline{g}^e$	Error in onboard gravitational accel'n vector $\underline{g}^e$ at given postion	Earth-fixed	m/s^2

Notes: 1. Definitions derived from [53,54,55]
2. Error equals indicated value minus true value
3. Rotation vector equivalent to coordinate rotation matrix (Appendix A)

$$\underline{v}^i = C_p^i \underline{v}^p$$

C_p^i = coordinate transformation from frame p to i

6.10.3.1 Position and Velocity Corrections

Elements 1-3 and 4-6 of the feedback correction $\delta\underline{x}$ comprise corrections to the inertial components of space-relative velocity $\bar{\underline{v}}_S$ and geocentric position $\bar{\underline{r}}$ computed by the onboard system:

$$\begin{aligned} \delta x(1,2,3) &\triangleq \delta\bar{\underline{v}}_S^i = \bar{\underline{v}}_S^{i-} - \bar{\underline{v}}_S^{i+} \\ \delta x(4,5,6) &\triangleq \delta\bar{\underline{r}}^i = \bar{\underline{r}}^{i-} - \bar{\underline{r}}^{i+} \end{aligned} \qquad (6.10\text{-}7)$$

The EIF utilizes the onboard values of $\bar{\underline{r}}^i$ and $\bar{\underline{v}}_S{}^i$ as the reference values from which the best estimates $\underline{r}^i$ and $\underline{v}_S{}^i$ are determined:

$$\begin{aligned} \underline{r}^i &= \bar{\underline{r}}^i - e(1,2,3) \\ \underline{v}_S{}^i &= \bar{\underline{v}}_S{}^i - e(4,5,6) \end{aligned} \qquad (6.10\text{-}8)$$

These true-value estimates do not change when an onboard correction occurs. Hence, the corresponding EIF error state elements must be adjusted to compensate for jumps in the reference values $\bar{\underline{r}}^i$ and $\bar{\underline{v}}_S{}^i$:

$$\begin{aligned} \delta e(1,2,3) &= \delta\bar{\underline{r}}^i = \delta x(4,5,6) \\ \delta e(4,5,6) &= \delta\bar{\underline{v}}_S{}^i = \delta x(1,2,3) \end{aligned} \qquad (6.10\text{-}9)$$

6.10.3.2 Baro Altimeter Correction

Element 7 of the feedback correction $\delta\underline{x}$ comprises a correction to the Blanchard barometric altimeter reading $\bar{h}_B$[52, p.4-29]:

$$\delta x(7) \triangleq \delta\bar{h}_B = \bar{h}_B^- - \bar{h}_B^+ \qquad (6.10\text{-}10)$$

How this correction is implemented in the onboard system is not fully understood at this time[54]. For present purposes, we assume that the onboard filter maintains an altimeter bias term $\Delta\bar{h}_B$, used to generate corrected baro outputs $\bar{h}_B$ from the raw readings $\tilde{h}_B$ as

$$\bar{h}_B = \tilde{h}_B + \Delta\bar{h}_B \qquad (6.10\text{-}11)$$

We also assume that the filter-computed altimeter correction $\delta\bar{h}_B$ is applied to this bias term,

$$\Delta\bar{h}_B^+ = \Delta\bar{h}_B^- - \delta\bar{h}_B \qquad (6.10\text{-}12)$$

such that the corrected bias value can be applied to all raw baro outputs $\tilde{h}_B$ processed before the next filter cycle. Note the Eqs(6.10-11,12) are consistant with-10), if $\bar{h}_B^-$ is interpreted as the adjusted reading that would have been obtained with the old bias value $\Delta\bar{h}_B^-$, and $\bar{h}_B^+$ as the adjusted reading actually obtained with the new bias value $\Delta\bar{h}_B^+$. That is, $\delta\bar{h}_B$ is manifest as a jump in the sequence of adjusted baro readings $\bar{h}_B$.

We further assume that the onboard-adjusted baro reading $\bar{h}_B$ (rather than the unadjusted reading $\tilde{h}_B$) is recorded for post-processing purposes. The EIF, then, utilizes the onboard-adjusted value $\bar{h}_B$ as the reference value from which the best estimate of barometric altitude is computed as

$$h_B = \bar{h}_B - e(28) - \text{other EIF error terms} \qquad (6.10\text{-}13)$$

where e(28) represents the residual Blanchard algorithm bias error. The sequence of true baro altitude estimates h_B should not jump when an onboard correction occurs. Hence, the EIF altimeter bias error state must be adjusted to compensate for onboard corrections to the sequence of reference values $\bar{h}_B$:

$$\delta e(28) = \delta\bar{h}_B = \delta x(7) \qquad (6.10\text{-}14)$$

6.10.3.3 Platform Tilt Correction

Elements 8-10 of the feedback correction $\delta\underline{x}$ comprise small-angle corrections to the platform-to-inertial transformation matrix $\bar{C}_p^i$ computed by the onboard system. This transformation from GEANS platform to inertial coordinates is maintained as the product of two rotations [26, p.3]:

$$\bar{C}_p^i = \bar{C}_r^i \bar{C}_p^r \tag{6.10-15}$$

where $\bar{C}_r^i$ represents a rotation of approximately 90^o about z, and $\bar{C}_p^r$ is a very slowly varying, near-unit matrix. In the notation of [52, p.4-3]*,

$$\bar{C}_r^i \triangleq A_{ij} \simeq \begin{pmatrix} 0 & -1 & 0 \\ 1 & 0 & 0 \\ 0 & 0 & 1 \end{pmatrix}; \quad \bar{C}_p^r \triangleq D_{ij} \simeq I \tag{6.10-16}$$

The EAR/GEANS onboard filter corrects $\bar{C}_p^i$ in a fashion equivalent to the following procedure [52, p.4-30]:

$$\begin{aligned} \bar{C}_r^{i+} &= (I + \delta\bar{\underline{\Phi}}^{i}*)\bar{C}_r^{i-} \\ \bar{C}_p^{i+} &= \bar{C}_r^{i+}\,\bar{C}_p^r \end{aligned} \tag{6.10-17}$$

where * represents the cross-product operator, and $\delta\bar{\underline{\phi}}^i$ is the platform tilt correction in inertial coordinates. More specifically, $\delta\bar{\underline{\Phi}}$ is the rotation from the uncorrected (p-) to the corrected (p+) platform frame (see Appendix A). This correction angle comprises elements 8-10 of the feedback correction $\delta\underline{x}$:

$$\delta x(8,9,10) \triangleq \delta\bar{\underline{\phi}}^i \tag{6.10-18}$$

The EIF utilizes the onboard-computed value of $\bar{C}_p^i$ as the reference

---

* The order D_{ij} given in [52] is incorrect, and should be reversed [54].

value from which the true-value estimate C_p^i is computed [52, p.5-2]*:

$$C_p^i = (I+\underline{\beta}^{i}\star)\bar{C}_p^i \qquad (6.10\text{-}19)$$

where

$$\underline{\beta}^i \triangleq e(7,8,9) \qquad (6.10\text{-}20)$$

Here, $\underline{\beta}^i$ represents the inertial components of the angular error of the onboard-computed platform-to-inertial coordinate rotation $\bar{C}_p^i$. More specifically, $\underline{\beta}$ represents the rotation of the true platform frame p relative to the onboard-computed platform frame $\bar{p}$ (see Appendix A).

The true platform attitude does not change as the result of an onboard correction, since the GEANS platform is not physically torqued. Hence, the true-value estimate C_p^i remains unchanged, and a discrete jump in the reference value $\bar{C}_p^i$ must be compensated by a corresponding adjustment to $\underline{\beta}^i$. From Eqs. (-17)-(-20), this adjustment can be determined equal to

$$\delta e(7,8,9) = \delta\underline{\beta}^i = \delta\underline{\bar{\Phi}}^i = \delta x(8,9,10) \qquad (6.10\text{-}21)$$

6.10.3.4 Antenna Misalignment Correction

Elements 11-13 of the feedback correction $\delta\underline{x}$ comprise small-angle corrections to the onboard transformation $\bar{C}_n^a$ from navigation frame to EAR antenna coordinates. The onboard system maintains $\bar{C}_n^a$ as the product of two rotations relative to the gimbal case:

$$\bar{C}_n^a = \bar{C}_c^a\,\bar{C}_n^c \qquad (6.10\text{-}22)$$

The onboard system computes the antenna orientation $\bar{C}_c^a$ relative to the case in terms of a misalignment $\bar{\underline{\alpha}}$ relative to its nominal orientation $\bar{C}_{co}^a$. This misalignment, expressed in case-frame coordinates as $\bar{\underline{\alpha}}^c$, is used to compute

*Ref. [1] has error in sign of $\underline{\beta}$: should be plus not minus [55].

the case-to-antenna transformation as follows [52, p.4-31]:

$$\bar{C}^a_c = \bar{C}^a_{co}(I - \underline{\bar{\alpha}}^{c*}) \tag{6.10-23}$$

Here, $\underline{\bar{\alpha}}^c$ represents the rotation of the onboard-computed antenna relative to its nominal orientation, as viewed from the case (see Appendix A). The onboard filter maintains a cumulative estimate of $\underline{\bar{\alpha}}^c$, and periodically corrects it as

$$\underline{\bar{\alpha}}^{c+} = \underline{\bar{\alpha}}^{c-} - \delta\underline{\bar{\alpha}}^c \tag{6.10-24}$$

where $\delta\underline{\bar{\alpha}}^c$ is the antenna misalignment error (angle from corrected to uncorrected antenna frame) comprising elements 11-13 of the onboard correction $\delta\underline{x}$:

$$\delta x(11,12,13) \triangleq \delta\underline{\bar{\alpha}}^c \tag{6.10-25}$$

The EIF utilizes as its reference state the initial value $\bar{C}^c_{ao}$ of the onboard-computed antenna-to-case transformation [54]. The EIF best estimate of this transformation is computed as [52, p.5-2]*

$$C^c_a = (I + \underline{\tau}^{c*})\bar{C}^c_{ao} \tag{6.10-26}$$

where

$$\underline{\tau}^c \triangleq e(31,32,33) \tag{6.10-27}$$

Here, $\underline{\tau}^c$ represents the case-frame components of the angular error in the initial value of the onboard-computed antenna-to-case transformation $\bar{C}^c_{ao}$. Specifically, $\underline{\tau}$ represents the angular rotation of the true antenna frame relative to the initial onboard-computed antenna frame, as viewed from the case (see Appendix A).

The true antenna attitude does not change as the result of an onboard

---

*Ref. [52] has error in sign of $\underline{\tau}$: should be plus not minus [55].

correction, nor does the initial value of the onboard-computed antenna attitude. Since the onboard correction affects neither the true state nor the EIF reference state, no adjustment to the corresponding EIF error states is required:

$$\delta e(31,32,33) = \delta \underline{\tau}^c \equiv \underline{0} \qquad (6.10\text{-}28)$$

(Note that, if the current value of the onboard-computed transformation $\bar{C}_a^c$ were used as the EIF reference value, then the EIF error state $\underline{\tau}^c$ would require adjustment to compensate for each onboard correction $\delta\bar{\underline{\alpha}}^c$ to that sequence of reference values $\bar{C}_a^c$. In this event, the required adjustment would be $\delta\underline{\tau}^c = -\delta\bar{\underline{\alpha}}^c$.)

6.10.4 Feedback Correction Equations for EIF

The following equations summarize the adjustments in the EIF error state $\underline{e}$ required to compensate for feedback corrections $\delta\underline{x}$ introduced by the EAR/GEANS onboard filter:

Inertial velocity
$$e(4,5,6)^+ = e(4,5,6)^- - \delta x(1,2,3) \qquad (6.10\text{-}29)$$

Inertial position
$$e(1,2,3)^+ = e(1,2,3)^- - \delta x(4,5,6) \qquad (6.10\text{-}30)$$

Blanchard altimeter
$$e(28)^+ = e(28)^- - \delta x(7) \qquad (6.10\text{-}31)$$

Platform tilt
$$e(7,8,9)^+ = e(7,8,9)^- - \delta x(8,9,10) \qquad (6.10\text{-}32)$$

Antenna misalignment
$$e(31,32,33)^+ = e(31,32,33)^- \quad \text{[no change]} \qquad (6.10\text{-}33)$$

These adjustment equations form the basis for subroutine 'INSCNT' in the EAR/GEANS EIF. Subroutine 'INSCNT' is called by 'FPROP' to reset the appropriate EIF error state variables, to account for feedback corrections applied by the onboard filter.

6.11 Filter/Smoother Mechanization Equations for EAR/GEANS EIF

This section and Appendix B comprise Intermetrics AFAL/GPS Memo #79-02, "Filter/Smoother Mechanization Equations for EAR/GEANS EIF," by Neal. A. Carlson, dated 31 May 1979 [56].

6.11.1 Introduction

The forward pass of the EAR/GEANS Error Isolation Filter (EIF) implements an optimal filter, for forward-successive state estimates based on all past* data generated by the onboard system. The backward pass of the EAR/GEANS EIF implements both an optimal filter, for backward-successive state estimates based on all future* data generated by the onboard system, and an optimal smoother, for backward-successive state estimates based on all past and future data generated by the onboard system.

The forward and backward optimal filters are implemented as Kalman filters in triangular square root form [57,58] The optimal smoother is implemented as a Fraser two-filter smoother[59], also in triangular square root form [57].

This memo describes i) the conventional covariance formulation of the optimal filter and two-filter smoother; ii) the triangular square root formulations of the optimal filter and two-filter smoother actually implemented in the EIF; and iii) potential improvements based on more recent developments[60,61].

6.11.2 Notation

$\underline{b}$ unweighted optimal gain vector $P\underline{h}$

d_k kth diagonal element of D

D diagonal matrix factor of P

$\underline{e}$ vector $U^T\underline{h}$

E unitary triangular matrix factor of Q

*Relative to the time point for each state estimate

$\underline{f}$ vector $S^T\underline{h}$

$\underline{h}$ measurement gradient vector $\partial z/\partial \underline{x}^T$

k index

n dimension of filter/smoother state

P state error covariance matrix

Q process noise covariance matrix

r variance of random measurement noise

R inverse covariance square root matrix S^{-1}

S triangular matrix square root of P

$\underline{S}_k$ kth column of S

$\bar{S}$ propagated square root matrix ΦS

t time

U unitary triangular matrix factor of P

$\underline{U}_k$ kth column of U

$\bar{U}$ propagated unitary matrix factor ΦU

V unitary triangular matrix factor of Q

W triangular matrix square root of Q

$\underline{x}$ state vector estimate

$\tilde{z}$ actual measurement

$\hat{z}$ predicted value of measurement

Δz measurement residual, actual minus predicted

α variance of measurement residual, $\underline{h}^T P \underline{h} + r$

Φ state transition matrix

$()'$ values at time t', prior to time propagation

$()^+$ values after measurement incorporation

$()_b$ backward filter variables

$()_f$ forward filter variables

$()_s$ smoother variables

6.11.3 Conventional Covariance Formulation

The conventional covariance filter propagates the state estimate $\underline{x}$ and covariance P from time t' to $t = t' + \Delta t$ as follows:

$$\Phi = \Phi\,(t,t')$$
$$Q = Q\,(t,t') \qquad (6.11\text{-}1)$$

$$P = \Phi P' \Phi^T + Q$$
$$\underline{x} = \Phi \underline{x}' \qquad (6.11\text{-}2)$$

Scalar measurements $\tilde{z}$ at time t are processed as follows:

$$\hat{z} = z\,(\underline{x},\, t)$$
$$\underline{h}^T = \partial \hat{z} \,/\, \partial \underline{x}$$
$$r = r(t) \qquad (6.11\text{-}3)$$
$$\Delta z = \tilde{z} - \hat{z}$$

$$\underline{b} = P\underline{h}$$
$$\alpha = \underline{h}^T \underline{b} + r$$
$$P^+ = P - \underline{b}\, \alpha^{-1} \underline{b}^T \qquad (6.11\text{-}4)$$
$$\underline{x}^+ = \underline{x} + \underline{b} \alpha^{-1} \Delta z$$

The two-filter smoother combines the forward-filter covariance P_f and state $\underline{x}_f$ with the backward-filter values P_b and $\underline{x}_b$, to form the smoothed covariance P_s and state $\underline{x}_s$:

$$P_s = (P_f^{-1} + P_b^{-1})^{-1}$$
$$\underline{x}_s = P_s (P_f^{-1} \underline{x}_f + P_b^{-1} \underline{x}_b) \qquad (6.11\text{-}5)$$

6.11.4 Triangular Square Root Formulation

The EAR/GEANS EIF implements the triangular square root formulations of the optimal filter and two-filter smoother. These formulations provide excellent numerical precision and stability with near-optimum computational efficiency[57,58] They are based on the square-root factorization of the state error and process noise covariance matrices:

$$P = SS^T; \quad S = P^{1/2}$$
$$Q = WW^T; \quad W = Q^{1/2} \qquad (6.11\text{-}6)$$

where S and W are upper triangular (zero below main diagonal). The covariance square root S and state estimate $\underline{x}$ are propagated from time t' to $t = t' + \Delta t$ as follows.

$$\Phi = \Phi(t,t')$$
$$W = W(t,t') \qquad (6.11\text{-}7)$$

$$\bar{S} = \Phi S'$$
$$[S \; 0] = [\bar{S} \; W] \; R$$
$$\underline{x} = \Phi \underline{x}' \qquad (6.11\text{-}8)$$

where R represents the Householder triangularization procedure (Appendix B). Scalar measurements $\tilde{z}$ at time t are processed as:

$$\hat{z} = z(\underline{x},t)$$
$$\underline{h}^T = \partial z / \partial \underline{x}$$
$$r = r(t)$$
$$\Delta z = \tilde{z} - \hat{z} \qquad (6.11\text{-}9)$$

$$
\begin{aligned}
&\underline{f} = S^T \underline{h} \\
&\alpha_0 = r; \quad \underline{b}_0 = \underline{0} \\
&\left.\begin{aligned}
\alpha_k &= \alpha_{k-1} + f_k^2 \\
\underline{b}_k &= \underline{b}_{k-1} + \underline{S}_k f_k \\
\underline{S}_k^+ &= (\underline{S}_k - \underline{b}_{k-1} f_k / \alpha_{k-1}) \sqrt{\frac{\alpha_{k-1}}{\alpha_k}} \\
\underline{x}^+ &= \underline{x} + \underline{b}_n \alpha_n^{-1} \Delta z
\end{aligned}\right\} \quad k = 1 \rightarrow n
\end{aligned}
\tag{6.11-10}
$$

where $\underline{S}_k$ represents the kth column of S, and $\underline{S}_k$ and $\underline{b}_k$ contain zeros below the kth elements.

The two-filter smoother combines the forward-filter covariance square root S_f and state $\underline{x}_f$ with the backward-filter values S_b and $\underline{x}_b$, to form the smoothed covariance square root S_s and state $\underline{x}_s$:

$$
\begin{aligned}
&R_f = S_f^{-1}; \quad R_b = S_b^{-1} \\
&[R_s^T \; 0] = [R_f^T \; R_b^T] \, R \\
&S_s = R_s^{-1} \\
&\underline{x}_s = S_s S_s^T (R_f^T R_f \underline{x}_f + R_b^T R_b \underline{x}_b)
\end{aligned}
\tag{6.11-11}
$$

where again, R represents an orthonormal Householder triangularization matrix (Appendix B).

6.11.5 Potential Improvements

The triangular square root filter in factored form [60,61], is the most efficient yet stable formulation of the optimal linear filter currently available. The filter covariance matrix P, triangular square root matrix S, and matrix factors U,D are related as follows:

$$P = SS^T = U D U^T$$
$$P^{1/2} = S = U D^{1/2} \tag{6.11-12}$$

The triangular matrix U comprises a normalized version of S having unit diagonal elements, and the diagonal matrix D contains the squared normalization factors. The process noise covariance matrix can be similarly factored:

$$Q = WW^T = VEV^T$$
$$Q^{1/2} = W = VE^{1/2} \tag{6.11-13}$$

Time propagation of the covariance factors U, D and state estimate $\underline{x}$ from time t' to t = t' + Δt can be performed as follows:

$$\Phi = \Phi(t,t')$$
$$V = V(t,t') \tag{6.11-14}$$
$$E = E(t,t')$$

$$\bar{U} = \Phi U'$$
$$[UD^{1/2}\ 0] = [\bar{U}D'^{1/2}\ VE^{1/2}]\ R \tag{6.11-15}$$
$$\underline{x} = \Phi \underline{x}'$$

where, again, R represents the Householder triangularization procedure. (There is currently no existing Householder-like algorithm to perform the factored operation implied by (-15) such that square roots of D' and E are unnecessary. However, an algorithm of this type is under development [62].) Scalar measurements $\tilde{z}$ at time t are processed as:

$$
\begin{aligned}
\hat{z} &= z(\underline{x},t) \\
\underline{h}^T &= \partial\hat{z}/\partial\underline{x} \\
r &= r(t) \\
\Delta z &= \tilde{z} - \hat{z}
\end{aligned}
\tag{6.11-16}
$$

$$
\begin{aligned}
&\underline{e} = U^T\underline{m} \\
&\alpha_0 = r; \quad \underline{b}_0 = \underline{0} \\
&\left.\begin{aligned}
\alpha_k &= \alpha_{k-1} + e_k^2 d_k \\
\underline{b}_k^+ &= \underline{b}_{k-1} + \underline{U}_k e_k d_k \\
\underline{U}_k^+ &= \underline{U}_k - \underline{b}_{k-1} e_k / \alpha_{k-1} \\
d_k^+ &= d_k \alpha_{k-1} / \alpha_k
\end{aligned}\right\} \quad k = 1 \rightarrow n \\
&\underline{x}^+ = \underline{x} + \underline{b}_n \alpha_n^{-1} \Delta z
\end{aligned}
\tag{6.11-17}
$$

Note that Eqs. (-17) are very similar to Eqs. (-10), but provide a computational savings of n square roots and approximately $n^2/2$ multiplies per measurement incorporation.

The two-filter smoother in principle can be performed in factored square-root form. However , as in the filter time propagation phase, there is currently no Householder-like algorithm for performing the triangularization of Eqs. (-11) directly in factored form without square roots.

6.11.6 Recommendations

The triangluar square root filter and smoother algorithms currently implemented in the EAR/GEANS EIF constitute the recommended formulation. These algorithms are nearly the most efficient, and are the most stable, formulations of the optimal linear filter and smoother.

A modest increase in computational efficiency is possible by using the U,D factored form of the triangular measurement update algorithm. However,

this efficiency increase is not sufficient to warrant recoding and retesting the EIF measurement incorporation routines, Householder triangularization routine, and optimal smoother routines. Furthermore, the Householder triangularization and smoother algorithms are somewhat more complex and less efficient in factored form; no direct factored-form algorithms are currently available to perform those functions.

APPENDIX A:

COORDINATE ROTATION MATRICES, VECTORS, AND ERRORS

A rotation or transformation from one coordinate frame to another can be represented by several different but equivalent mathematical forms. Two of these forms, the coordinate rotation matrix and the coordinate rotation vector, are related as follows:

$$\begin{aligned} C_a^b &= \exp(-\underline{\theta}_{ab}^{a*}) \\ &= I - (\underline{\theta}_{ab}^{a*}) + \frac{1}{2!}(\underline{\theta}_{ab}^{a*})^2 - \frac{1}{3!}(\underline{\theta}_{ab}^{a*})^3 \pm \cdots \end{aligned} \tag{A-1}$$

where

$C_a^b \triangleq$ matrix coordinate rotation form frame a to b

$\underline{\theta}_{ab}^a \triangleq$ vector rotation from frame a to b, coordinatized in a

$* \triangleq$ vector cross-product operator

The elements of the matrix C_a^b are cosines of the angles between respective coordinate axes of frames a and b. The direction of the vector $\underline{\theta}_{ab}$ is the axis of rotation from frame a to b; the magnitude of $\underline{\theta}_{ab}$ is the angle of rotation from a to b. Note that the components of $\underline{\theta}_{ab}$ are the same in both frames a and b:

$$\underline{\theta}_{ab}^b = C_a^b \underline{\theta}_{ab}^a = \underline{\theta}_{ab}^a \tag{A-2}$$

For small rotation angles, the first-order approximation to C_a^b is

$$|\underline{\theta}_{ab}| \ll 1: \quad C_a^b \approx I - \underline{\theta}_{ab}^{a*} \approx I - \underline{\theta}_{ab}^{b*} \tag{A-3}$$

Consider next perturbed rotation variables denoted by ($\bar{}$), having errors $\delta(\ )$ relative to the true values ( ):

$$\bar{C}_a^b \equiv C_a^b + \delta C_a^b \tag{A-4}$$

$$\bar{\underline{\theta}}_{ab} \equiv \underline{\theta}_{ab} + \delta\underline{\theta}_{ab}$$

From Eq.(A-1), the following first-order relationships between the perturbed and true rotations are readily derived:

$$\bar{C}_a^b = (I - \delta\underline{\theta}_{ab}^{b*})C_a^b \approx C_a^b(I - \delta\underline{\theta}_{ab}^{a*})$$

$$\delta C_a^b = (-\delta\underline{\theta}_{ab}^{b*})C_a^b = C_a^b(-\delta\underline{\theta}_{ab}^{a*}) \tag{A-5}$$

$$C_a^b = (I + \delta\underline{\theta}_{ab}^{b*})\bar{C}_a^b \approx \bar{C}_a^b(I + \delta\underline{\theta}_{ab}^{a*})$$

If the a-to-b rotation error is associated with a perturbed final frame $\bar{b}$, the initial frame a being fixed, Eqs. (A-5) can be written as

$$C_a^{\bar{b}} = C_b^{\bar{b}} C_a^b = (I - \delta\underline{\theta}_b^{b*})C_a^b$$

$$\delta C_a^b = (C_b^{\bar{b}} - I)C_a^b = (-\delta\underline{\theta}_b^{b*})C_a^b \tag{A-6}$$

$$C_a^b = C_{\bar{b}}^b C_a^{\bar{b}} = (I + \delta\underline{\theta}_b^{b*})C_a^{\bar{b}}$$

where

$C_a^{\bar{b}} \triangleq$ perturbed coordinate rotation from frame a to $\bar{b}$

$\delta\underline{\theta}_b \triangleq$ vector rotation error from frame b to $\bar{b}$

Alternately, if the a-to-b rotation error is associated with a perturbed initial frame $\bar{a}$, the final frame b being fixed, Eqs. (A-5) can be written

as

$$C_{\bar{a}}^{b} = C_{a}^{b}\, C_{\bar{a}}^{a} = C_{a}^{b}\,(I + \delta\underline{\theta}_{a}^{a*})$$

$$\delta C_{a}^{b} = C_{a}^{b}(C_{\bar{a}}^{a} - I) = C_{a}^{b}(+\delta\underline{\theta}_{a}^{a*}) \qquad \text{(A-7)}$$

$$C_{a}^{b} = C_{\bar{a}}^{b}\, C_{a}^{\bar{a}} = C_{\bar{a}}^{b}\,(I - \delta\underline{\theta}_{a}^{a*})$$

where

$C_{\bar{a}}^{b} \overset{\Delta}{=}$ perturbed coordinate rotation from frame $\bar{a}$ to b

$\delta\underline{\theta}_{a} \overset{\Delta}{=}$ vector rotation error from frame a to $\bar{a}$

Note that

$$C_{a}^{\bar{b}} \equiv C_{a}^{\bar{b}} \equiv C_{\bar{a}}^{b}$$

$$\delta\underline{\theta}_{ab} \equiv \delta\underline{\theta}_{b} \equiv -\,\delta\underline{\theta}_{a} \qquad \text{(A-8)}$$

That is, $\delta\underline{\theta}_{ab}$ represents the general a-to-b rotation error, $\delta\underline{\theta}_{b}$ the forward rotation error of the final frame b to $\bar{b}$, and $\delta\underline{\theta}_{a}$ the backward rotation error of the initial frame a to $\bar{a}$.

APPENDIX B:

HOUSEHOLDER TRIANGULARIZATION PROCEDURE

The Householder procedure reduces a general nxm matrix A (where generally $m \geq n$) to nxn upper or lower triangular form A^+ via a sequence of n orthogonal rotations. To be specific, we will consider reduction to lower triangular form. (The procedure for upper triangular form simply reverses the order of computations.) The reduction procedure can be described as

$$A^{(n)} = A^{(0)}R^{(1)}R^{(2)}\ldots R^{(n)}$$
$$A^{(k)} = A^{(k-1)}R^{(k)} \qquad \text{(B-1)}$$

where

$A^{(0)}$ = original nxm matrix A
$A^{(n)}$ = final nxm matrix A^+ in lower triangular form
$A^{(k)}$ = intermediate matrix with first k rows in lower triangular form (zeroes to right of main diagonal)
$R^{(k)}$ = rotation matrix designed to rotate elements k to m of row k such that all but element k become zero

The kth step of this process, indicated by Eq.B-1 , can be described in partitioned form as follows:

$$\begin{matrix} k-1 \\ n-k+1 \end{matrix}\left\{\begin{bmatrix} A_{ii}^{+} & O_{ik} \\ A_{ki}^{+} & A_{kk}^{(k)} \end{bmatrix}\right. = \begin{bmatrix} A_{ii}^{+} & O_{ik} \\ A_{ki}^{+} & A_{kk}^{(k-1)} \end{bmatrix}\begin{bmatrix} I_{ii} & O_{ik} \\ O_{ki} & R_{kk} \end{bmatrix} = \begin{bmatrix} A_{ii}^{+} & O_{ik} \\ A_{ki}^{+} & A_{kk}^{(k-1)}R_{kk} \end{bmatrix} \qquad \text{(B-2)}$$

(k-1 and m-k+1 under the first matrix; k-1 and m-k+1 under the second matrix)

The first k-1 rows and columns of $A^{(k-1)}$ are already in lower triangular

form and are not affected at step k. Those elements below and to the right of element k,k are all affected at step k:

$$A_{kk}^{(k)} = A_{kk}^{(k-1)} R_{kk} \tag{B-3}$$

The Householder triangularization procedure at this step can be described in terms of the following orthogonal rotation matrix [62]:*

$$R = R(\underline{r}) = \begin{bmatrix} r_1/r_m & -(\underline{r}_2/r_m)^T \\ \underline{r}_2/r_m & I - \underline{r}_2(r_1+r_m)^{-1}(\underline{r}_2/r_m)^T \end{bmatrix} \tag{B-4}$$

where

$$\begin{aligned} \underline{r}^T &\equiv (r_1\ \underline{r}_2^T) \\ r_m &= \sqrt{\underline{r}^T\ \underline{r}}\ \ \mathrm{sgn}(r_1) = |\underline{r}|\ \mathrm{sgn}(r_1) \end{aligned} \tag{B-5}$$

The matrix R rotates the vector $\underline{r}$ such that all elements but the first become zero:

$$\begin{aligned} \underline{r}^{T+} &= \underline{r}^T R \\ r_1^+ &= (r_1^2 + \underline{r}_2^T\ \underline{r}_2)/r_m \equiv r_m \\ \underline{r}_2^{T+} &= \underline{r}_2^T - (r_1 r_m + r_1^2 + \underline{r}_2^T\underline{r}_2)\, r_m^{-1}\, (r_1+r_m)^{-1}\ \underline{r}_2^T \\ &= \underline{r}_2^T - (r_1+r_1^+)(r_1+r_m)^{-1}\ \underline{r}_2^T \equiv \underline{0}^T \end{aligned} \tag{B-6}$$

Step k of the triangularization process, Eq. (B-3), can be performed in terms of the rotation $R = R_{kk}$, generalized as follows:

---

*This form and the result, Eqs. (B-8), differ slightly from the standard Householder procedure [63]; the computation of $\underline{b}_1^+$ is somewhat more precise here.

$$\begin{bmatrix} a_1^+ & \underline{0}^T \\ \underline{b}_1^+ & B_2^+ \end{bmatrix} = \begin{bmatrix} a_1 & \underline{a}_2^T \\ \underline{b}_1 & B_2 \end{bmatrix} R(\underline{a}) \qquad \text{(B-7)}$$

$$\begin{aligned} a_1^+ &= \sqrt{a_1^2 + \underline{a}_2^T \underline{a}_2}\ \operatorname{sgn}(a_1) \equiv \sqrt{\underline{a}^T \underline{a}}\ \operatorname{sgn}(a_1) \\ \underline{a}_2^{T+} &= \underline{0}^T \\ \underline{b}_1^+ &= (\underline{b}_1 a_1 + B_2 \underline{a}_2)/a_1^+ \equiv B\,\underline{a}/a_1^+ \\ B_2^+ &= B_2 - (\underline{b}_1 + \underline{b}_1^+)(a_1 + a_1^+)^{-1}\ \underline{a}_2^T \end{aligned} \qquad \text{(B-8)}$$

For triangularization step k, Eqs. (B-8) can be rewritten in terms of elements of the matrix A as follows:

$$\begin{aligned} a_{kk}^+ &= \sqrt{a_{kk}^2 + \ldots + a_{km}^2}\ \operatorname{sgn}(a_{kk}) \\ a_{kj}^+ &= 0 \\ a_{ik}^+ &= (a_{ik}\, a_{kk} + \ldots + a_{im}\, a_{km})/a_{kk}^+ \\ a_{ij}^+ &= a_{ij} - (a_{ik} + a_{ik}^+)(a_{kk} + a_{kk}^+)^{-1}\ a_{kj} \end{aligned} \qquad \text{(B-9)}$$

where

$k = 1$ to n

$j = k+1$ to m

$i = k+1$ to n

Note that, in Eqs. (B-7) to (B-9), any column $j \geq k$ for which element a_{kj} is already zero can be bypassed in the step k calculations. This

column does not contribute to the updated elements of column k, nor do its own elements change. If a_{kk} itself is zero, the entire k^{th} step is bypassed. These facts can be used to effect significant computational savings when the nxm matrix A is already partially in triangular form. For example, in optimal filter and smoother formulations, A generally represents the combination of two nxn matrices W, V,

$$A = \underset{n}{[W} \quad \underset{n}{V]} \Big\} n \tag{B-10}$$

where one or both of W, V may already be in triangular form. The computational savings are rather dramatic in such cases:

Form of W, V	Approx. No. of Multiplications
Both square	$\frac{5}{3}n^3$
One square, one triang.	$\frac{3}{3}n^3$
Both triangular	$\frac{1}{3}n^3$
One square, one zero	$\frac{2}{3}n^3$

REFERENCES

1. Przyjemski, J.M., and Konop, P.L., "Limitations on GPS Receiver Performance Imposed by Crystal-Oscillator G-Sensitivity", NAECON '77 Record, 17-19 May 1977.

2. Computer Program Development Specification (B5) for Data Processor of the AFAL GDM, Spec. No. 6700173001, prepared by Collins, 22 October 1976.

3. Anon., "Critical Design Review of AFAL GDM/GPS User Equipment -- Navigation Design, Session 7", Collins, Cedar Rapids, Iowa, 7 December 1976.

4. Mickelson, W.A., "Stabilization of Closed Loop GPS/INS Kalman Filter during Rate Aiding", Collins Memo GDM-154, 25 January 1977.

5. Carroll, R.W., and Mickelson, W.A., "Velocity Aiding of Noncoherent GPS Receiver", presented at National Aerospace and Electronics Conference, Dayton, Ohio, 17-19 May 1977.

6. Widnall, W.S., "Modeling the Errors in the Rate-Aided GPS Measurements", Intermetrics Memo COLPFP #04-77, 5 July 1977.

7. Widnall, W.S., "Stability of Alternate Designs for Rate Aiding of Non-Coherent Mode of a GPS Receiver," IR-302, Intermetrics, Inc., Cambridge, MA, 25 September 1978.

8. Hemesath, N.B., and Hutchinson, W.M., "Anti-Jamming Characteristics of GPS/GDM", Collins Division of Rockwell, Cedar Rapids, Iowa, presented at the National Telecommunications Conference, Dallas, Texas, November 1976.

9. Anon., "Computer Program Development Specification (B5) for Data Processor of the AFAL GDM", Spec. 6700173001, Collins Division of Rockwell, Cedar Rapids, Iowa, 22 October 1976.

10. Myers, K.A., and Butler, R.R., "Simulation Results for an Integrated GPS/Inertial Aircraft Navigation System", presented at the National Aerospace Electronics Conference, 18-20 May 1976.

11. Sinha, P. K., "Integrated GPS/Inertial Simulator Computer Program," IR - 236, Intermetrics, Inc., Cambridge, MA., 26 August 1977.

12. Musick, S. H., "PROFGEN - A Computer Program for Generating Flight Profiles", Report No. AFAL-TR-76-247, November 1976.

13. Widnall, W. S. and Sinha, P. K., "Comparison of Three Vertical Channel Designs for an Integrated GPS/Inertial Navigation System", Report No. IR-234, Intermetrics, Inc., Cambridge, MA. 27 July 1977.

14. Widnall, W. S., and Grundy, P. A., "Inertial Navigation System Error Models", Report TR-03-73, Intermetrics, Inc., Cambridge, MA. 11 May 1973.

15. Sinha, P. K., and Widnall, W. S., "Some Effects of High Dynamic Trajectories on Strapdown Inertial Navigation System Performance," IR-255, Intermetrics, Inc., Cambridge, MA., 6 January 1978.

16. Sinha, P. K., "Integrated GPS/Strapdown Inertial Simulator Computer Program," IR-253, Intermetrics, Inc., Cambridge, MA., December 1977.

17. Widnall, W. S., "Clock Frequency G-Sensitivity Modeling and Compensaton," AFAL/GPS Analysis Memo # 03-77, Intermetrics, Inc., Cambridge, MA, 31 August 1977.

18. Widnall, W. S., "Azimuth Gyro G-Sensitivity Calibration and Compensation," AFAL/GPS Analysis Memo # 05-77, Intermetrics, Inc., Cambridge, MA., 31 August 1977.

19. Widnall, W.S., "Continuity of Kalman Filter Feedback to Receiver Aiding," AFAL/GPS Analysis Memo #04-77, Intermetrics, Inc., Cambridge, MA., 31 August 1977.

20. Widnall, W. S., "Stability of Receiver Aiding in Non-Coherent Mode," AFAL/GPS Analysis Memo #06-77, Intermetrics, Inc., Cambridge, MA., 16 September 1977.

21. Sinha, P. K., and Widnall, W. S., "C5A GPS/Inertial Simulation Results," AFAL/GPS Analysis Memo #02-77, Intermetrics, Inc., Cambridge, MS., 7 July 1977.

22. Widnall, W.S., and Sinha, P. K., "Comparison of Three Vertical Channel Designs for an Integrated GPS/Inertial Navigation System," IR-234, Intermetrics, Inc.,Cambridge, MA., 27 July 1977.

23. Grundy, P. A., "Review of AFAL Technical Memorandum 'A Vertical Channel Error Model for EAR/GEANS'," AFAL/GPS Analysis Memo #07-77, Intermetrics, Inc., Cambridge, MA., 22 September 1977.

24. Musick, S. H., "A Vertical Channel Error Model for EAR/GEANS," AFAL-TM-76-49, Air Force Avionics Laboratory, WPAFB, Ohio, October 1976.

25. Grundy, P. A., "Review of AFAL Technical Memorandum 'Fundamental Error Dynamics for a Space Stable Navigator'," AFAL/GPS Analysis Memo #08-77, Intermetrics, Inc., Cambridge, MA., 22 September 1977.

26. Burns, J. N., "Fundamental Error Dynamics for a Space Stable Navigator," AFAL-TM-76-50, Air Force Avionics Laboratory, WPAFB, Ohio, November 1976.

27. Britting, K. R., Inertial Navigation System Analysis, Wiley-Interscience, 1971.

28. Grundy, P.A., "Review of AFAL Technical Memorandum 'An Error Model for the Baro-Damped GEANS Inertial Navigator'," AFAL/GPS Analysis Memo #09-77, Intermetrics, Inc., Cambridge, MA, 18 October 1977.

29. Burns, J. N., "An Error Model for the Baro-Damped GEANS Inertial Navigator," AFAL-TM-77-15, Air Force Avionics Laboratory, WPAFB, Ohio, July 1977.

30. Grundy, P. A., "Review of AFAL Technical Memorandum 'Radar Measurements and Measurement Matrices for EAR'," AFAL/GPS Analysis Memo #10-77, Intermetrics, Inc., Cambridge, MA., 18 October 1977.

31. Musick, S. H., "Radar Measurements and Measurement Matrices for EAR," AFAL-TM-76-48, Air Force Avionics Laboratory, WPAFB, Ohio, 12 May 1976.

32. Wiederholt, L. F., "Review of AFAL Technical Memorandum 'EAR Flight Test Data to be Recorded on the CIRIS Recorder for Error Isolation Filter Processing'," AFAL/GPS Analysis Memo 78-01, Intermetrics, Inc., Cambridge, MA, 26 January 1978.

33. Musick, S. H., "EAR Flight Test Data to be Recorded on the CIRIS Recorder for Error Isolation Filter Processing," AFAL-TM- -77, Air Force Avionics Laboratory, Cambridge, MA, 9 January 1978.

34. Grundy, P. A., "Review of AFAL Technical Memorandum 'Geodetic Error Models for Simulating and Estimating INS Error Behavior'," AFAL/GPS Analysis Memo #78-02, Intermetrics, Inc., Cambridge, MA, 6 March 1978.

35. Musick, S. H., "Geodetic Error Models for Simulating and Estimating INS Error Behavior," AFAL-TM-77-44, Air Force Avionics Laboratory, WPAFB, Ohio, 1977.

36. Shaw, L., Paul, I., and Henrikson, P., "Statistical Models for the Vertical Deflections from Gravity-Anomaly Models", Journal of Geophysical Research, Vol. 74, No. 17, August 1969.

37. Kasper, J.F., "A Second-Order Markov Gravity Anomaly Model", Journal of Geophysical Research, Vol. 76, No. 32, November 1971.

38. Jordan, S.K., "Self-Consistent Statistical Models for the Gravity Anomaly, Vertical Deflections, and Undulation of the Geoid", Journal of Geophysical Research, Vol. 77, No. 20, July 1972.

39. Jordan, S.K., "Effects of Geodetic Uncertainties on a Damped Inertial Navigation System", IEEE Transactions on Aerospace and Electronic Systems, September 1973.

40. Nash, R.A., "Effect of Vertical Deflections and Ocean Currents on a Maneuvering Ship", IEEE Transactions on Aerospace and Electronic Systems, Vol. AES-4, No. 5, September 1968.

41. Bernstein, U., and Hess, R.I., "The Effects of Vertical Deflections on Aircraft Inertial Navigation Systems", AIAA Journal, Vol. 14, No. 10, October 1976.

42. Rose, R.C., and Nash, R.A., "Direct Recovery of Deflections of the Vertical Using an Inertial Navigator", IEEE Transactions on Geoscience Electronics, Vol. GE-10, No. 2, April 1972.

43. Chatfield, A.B., Bennett, M.M., and Chen, T., "Effect of Gravity Model Inaccuracy on Navigation Performance", AIAA Journal, Vol. 13, No. 11, November 1975.

44. Junkins, J.L., "Development of Finite Element Models for the Earth's Gravity Field, Phase I: Macro Gravity Model for Satellite Orbit Integration", UVA/525023/ESS77/103, Univ. of Virginia, March 1977.

45. Junkins, J.L., and Saunders, J.T., "Development of Finite Element Models for the Earth's Gravity Field, Phase II: Fine Structure Disturbance Gravity Representations", UVA/525023/ESS77/104, Univ. of Virginia, March 1977.

46. Heiskanen, W.A., and Vening Meinesz, F.A., The Earth and Its Gravity Field, McGraw-Hill, New York, 1958.

47. Widnall, W.S., Grundy, P.A., "Inertial Navigation System Test Methods", AFSWC-TR-73-35, Intermetrics, Inc., August 1973.

48. Wiederholt, L.F., "Filter Synthesis for the EAR/GEANS Error Isolation Filter", AFAL/GPS Analysis Memo #03-78, Intermetrics, Inc., Cambridge, MA, 10 May 1978.

49. Burns, J., "Platform to Antenna Attitude Error Models for EAR/GEANS", AFAL-TM-77-59, Air Force Avionics Laboratory, November 1977.

50. Burns, J., "EAR/GEANS H-Matrices in Inertial State Variables", AFAL-TM-77-67, Air Force Avionics Laboratory, December 1977.

51. Carlson, N.A., "Feedback Correction Equations for EAR/GEANS EIF", AFAL/GPS Analysis Memo #79-01, Intermetrics, Inc., Cambridge, MA, May 31, 1979.

52. Musick, S.H., "EAR/GEANS Error Isolation Filter (EIF): Specification of EIF Input from Flight Recorded Data," AFAL-TM-78-31, September 1978

53. Geier, G.J., unpublished notes defining EAR/GEANS Error Isolation Filter state vector, November 1978

54. Musick, S.H., telephone conversations with author, April 1979.

55. Musick, S.H., telephone conversations with author, May 1979.

56. Carlson, N.A., "Filter/Smoother Mechanization Equations for EAR/GEANS EIF", AFAL/GPS Analysis Memo #79-02, Intermetrics, Inc., Cambridge, MA, 31 May 1979.

57. Carlson, N.A., "PFP Filter and Smoother Formulations," CIRIS Memo #05-72 (Rev.), Intermetrics, Inc., Cambridge, MA, 13 November 1972.

58. Carlson, N.A., "Fast Triangular Formulation of the Square Root Filter", AIAA Journal, Vol. 11, No. 9, September 1973, pp. 1259-65.

59. Fraser, D.C., "A New Technique for the Optimal Smoothing of Data", M.I.T. Instrumentation Lab, Report T-474, Cambridge, Massachusetts, January 1967.

60. Bierman, G.J., "Measurement Updating Using the U-D Factorization", report for NASA under contract NAS 7-100, Jet Propulsion Laboratory, Pasadena, Cal., 1975.

61. Bierman, G.J., Factorization Methods for Discrete Sequential Estimation, Academic Press, New York, NY, 1977, pp. 53,78,107.

62. Carlson, N.A., unpublished notes on factored triangularization techniques, Intermetrics, Inc., Cambridge, MA, April 1979.

63. Kaminsky, P.G., "Square Root Filtering and Smoothing for Discrete Processes," SUDAAR No. 427, Ph.D. Thesis in Dept. of Aeronautics and Astronautics, Stanford University, Stanford, CA, July 1971.

*U.S.Government Printing Office: 1979 — 657-084/321